Molecular Biomarkers for Frailty as Prognostic Predictors of Postoperative Outcomes in Elderly Glioblastoma Patients

Dissertation

Zur Erlangung des Grades

Doktor der Naturwissenschaften

am Fachbereich Biologie

der Johannes Gutenberg-Universität Mainz

vorgelegt von

Wafa Abuhashem

geboren am 01.08.1994

in Berlin

Mainz, August 2025

Lizenzvermerk

Dekan:

1. Gutachter:

2. Gutachter:

Tag der mündlichen Prüfung: 13/10/2025

Dr.-Ing. Yasser Abuhashem & Dipl.-Ing. Mervat Abuhashem

gewidmet

Preface

Table of Contents

Zusammenfassung I

Abstract II

1 Introduction 1

1.1 Aging and Frailty 1

1.2 Classification and Pathological Context of Glioblastoma 4

1.2.1 Grading of Gliomas 4

1.2.2 Molecular Pathology 6

1.2.2.1 IDH1/2 6

1.2.2.2 ATRX 7

1.2.2.3 TERTp 7

1.2.2.4 1p/19q Codeletion 8

1.2.2.5 Chromosome +7/−10 9

1.2.2.6 EGFR 9

1.2.2.7 MGMT 9

1.3 Frailty Screening and Management in the Postoperative Setting 10

1.3.1 Screening- Concepts 10

1.3.1.1 Frailty Phenotype 10

1.3.1.2 Frailty Index 12

1.3.2 Stage-Based Approach to Frailty in the Perioperative Setting 15

1.3.3 Risks of Frailty 16

1.3.3.1 Functional dependency 17

1.3.3.2 Falls 17

1.3.3.3 Malnutrition 17

1.3.3.4 Comorbidity 18

1.3.3.5 Polypharmacy 18

1.3.3.6 Delirium 18

1.3.3.7 Depression and Social Isolation 19

1.4 Criteria for Molecular Biomarkers of Frailty 23
1.5 Telomere Length as a Candidate Biomarker 24
1.5.1 Structure and Function of Telomeres 24
1.5.1.1 Mechanisms of Telomere Maintenance: Telomerase and ALT 25
1.5.2 Telomere Dynamics in Aging 26
1.5.3 Epidemiological Perspectives on Telomere Length and Frailty 27
1.6 DNA Methylation-based Biomarkers as Candidate Biomarkers 28
1.6.1 DNA Methylation and Demethylation in Gene Regulation 29
1.6.2 Epigenetic Clocks 29
1.6.2.1 First-Generation Clocks 30
1.6.2.1.1 CpG Sites Integrated into the Horvath Clock 31
1.6.2.2 Second-Generation Clocks 31
1.6.2.3 Third-Generation Clock 32
1.7 Scope of the Thesis 33
2 Results 34
2.1 Characterization of the Primary Glioblastoma Study Cohort 34
2.2 Patient Characterization by GFI and G8 Frailty Screening 38
2.3 Correlation of Candidate Biomarkers with Frailty Scores 40
2.3.1 Correlation of Epigenetic Age Acceleration with Frailty Scores 40
2.3.2 Correlation of Telomere Length with Frailty Scores 43
2.3.2.1 Overview of Telomere Length Distribution (n = 28) 43
2.3.2.2 Correlation of Telomere Length with Frailty Scores 44
2.4 Impact of Frailty, Telomere Length, and Epigenetic Aging on Postoperative Outcomes 46
2.4.1 Correlation of GFI and G8 Frailty Scores with Postoperative Hospitalization Duration 47
2.4.2 Correlation of Epigenetic Age Acceleration and TL with Postoperative Hospitalization Duration 48
2.4.3 Impact of Frailty, Epigenetic Age Acceleration, and Telomere Length on Postoperative Hospitalization Duration 49

2.4.4 Impact of Postoperative Hospitalization Duration and Frailty Scores on Discharge Decision-Making 50
2.4.5 Impact of Epigenetic Age Acceleration and Telomere Length on 51
Discharge Decision-Making 51
2.5 Survival Analysis 53
2.5.1 Impact of MGMT Methylation and TERTp Mutation Status on Overall Survival (OS) and Progression-Free Survival (PFS) 53
2.5.2 GrimAge-Based Analysis of Slow Agers in MGMT-Methylated and Unmethylated Subgroups 56
3 Discussion 58
3.1 Study Design and Methodology 58
3.1.1.1 G8 and GFI for Risk Stratification 58
3.1.1.2 Predictive Value of G8 and GFI 58
3.1.1.3 Limitations and Considerations 59
3.1.2 Importance of Longitudinal Blood Analysis for Frailty Dynamics 59
3.2 Telomere Length Analysis: Biological and Methodological Considerations 60
3.2.1 Telomere Heterogeneity Across Cell Types 60
3.2.2 Limitations of Conventional Methods 62
3.3 Epigenetic Age Analysis: Biological and Methodological Considerations 64
3.3.1 Integrating Epigenetic Markers and Clinical Assessments in Frailty Evaluation 64
3.3.2 Methodological Considerations in Statistical Analysis of Epigenetic Age Acceleration ... 64
3.3.3 Age-Related Epigenetic Changes: Cause or Consequence? 65
3.3.3.1 Role of age-related CpGs 66
3.4 Linking Telomere Length, Epigenetic Aging, and Cellular Senescence 68
3.4.1 Epigenetic Aging and Cellular Senescence 68
3.4.2 Epigenetic Aging and Telomere Length 69
3.5 Conclusion and Future Directions 71
4 Materials und Methods 73
4.1 Ethical Approval and Data Collection 73

4.2 Pre-Screening Tools 74
4.3 Molecular Pathology and Imaging 76
4.3.1 TERT Promoter Sequencing 77
4.3.1.1 DNA Extraction from Fresh-Frozen GBM Tissue 77
4.3.1.2 Assessment of Tumor Cell Heterogeneity 81
4.3.1.2.1 Cryostat Microtomy 81
4.3.1.2.2 Hematoxylin and Eosin (H&E) Staining 81
4.3.1.3 DNA Extraction from FFPE GBM Tissue 82
4.3.1.4 PCR Amplification and Sanger Sequencing 83
4.4 Whole Blood Molecular Biomarker Analysis 86
4.4.1 Extraction of gDNA from Whole Blood 86
4.4.2 TRF Analysis 88
4.4.3 DNA Methylation Analysis 96
4.5 Acknowledgment of Conceptual Influences 98
5 Abbreviations 99
6 References 103
7 Acknowledgements 124
8 Curriculum Vitae 125

Zusammenfassung

Glioblastom-Patientinnen und -Patienten über 65 Jahre sind in klinischen Studien häufig unterrepräsentiert, sodass Therapieentscheidungen oft auf der subjektiven Einschätzung der körperlichen Belastbarkeit beruhen. Dabei wird das chronologische Alter häufig als Ersatzmaß verwendet, obwohl es die tatsächliche therapeutische Belastbarkeit nur unzureichend abbildet. Besonders im perioperativen Management kann dies problematisch sein, da Komorbiditäten und altersassoziierte physiologische Veränderungen zu einer verlängerten Genesungsdauer und einem erhöhten Komplikationsrisiko führen. Frailty wird daher zunehmend als präziserer Indikator für postoperative Risiken angesehen, bleibt in der klinischen Praxis jedoch bislang häufig subjektiv eingeschätzt und ohne standardisierte Verfahren.

Ziel dieser Studie war es zu untersuchen, inwiefern präoperative Frailty-Screenings und molekulare Biomarker zur Vorhersage postoperativer Verläufe beitragen können. Ein besonderer Fokus lag auf der Analyse der Telomerlänge und DNA-Methylierungsmarkern als Indikatoren des biologischen Alters. Die Patientinnen und Patienten wurden präoperativ mithilfe der G8- und GFI-Fragebögen gescreent. Parallel erfolgte die Analyse der Telomerlänge mittels Southern-Blot sowie der epigenetischen Alterungsmarker GrimAge, PhenoAge, Hannum und DunedinPACE. Primäre Endpunkte waren die Entlassungsmodalität, bestehend aus häuslicher Entlassung oder institutioneller Weiterversorgung, sowie die Dauer des stationären Aufenthalts.

Die Ergebnisse zeigten, dass kürzere Telomerlängen und eine erhöhte extrinsische Altersbeschleunigung, berechnet anhand der Hannum-Uhr, mit einem nicht signifikanten Trend zu einer längeren postoperativen Hospitalisierung und einer erhöhten Wahrscheinlichkeit für eine Entlassung in eine institutionelle Weiterversorgung einhergingen. Unter den Frailty-Screening-Tools zeigte der G8-Score eine leichte Tendenz zu einer verlängerten Aufenthaltsdauer, während der GFI dazu neigte, Frailty bei Hochrisikopatientinnen und -patienten zu unterschätzen. Für andere epigenetische Alterungsmaße ergab sich kein klarer prädiktiver Wert. Beide Screening-Instrumente identifizierten jedoch relevante Problembereiche, insbesondere Polypharmazie, psychosoziale Belastungen und funktionelle Einschränkungen im Alltag.

Zusammenfassend lässt sich festhalten, dass Frailty-Fragebögen wertvolle Zusatzinformationen für das Comprehensive Geriatric Assessment (CGA) in dieser Studie lieferten. Hochrisikopatientinnen und -patienten sollten im Rahmen des CGA gezielt auf entsprechende Problembereiche untersucht werden, beispielsweise mithilfe von Instrumenten wie den Instrumental Activities of Daily Living (IADL), der Cumulative Illness Rating Scale for Geriatrics (CIRS-G) und dem Timed Get-Up-and-Go Test (TGUG).

Abstract

Glioblastoma patients over the age of 65 are often underrepresented in clinical trials, which leads to treatment decisions frequently being based on subjective assessments of physical resilience. Chronological age is commonly used as a surrogate marker, although it inadequately reflects actual physiological capacity. This is particularly problematic in perioperative management, as comorbidities and age-related physiological changes can lead to prolonged recovery and increased risk of complications. Frailty is therefore increasingly recognized as a more accurate predictor of postoperative risk but is still often assessed subjectively and without standardized tools in clinical care.

The aim of this study was to investigate the extent to which preoperative frailty screenings and molecular biomarkers may help predict postoperative outcomes. A particular focus was placed on the analysis of telomere length and DNA methylation-based markers as indicators of biological age. Patients were screened preoperatively using the G8 frailty score and the Groningen Frailty Indicator (GFI). In parallel, telomere length was assessed via Southern blot analysis, and epigenetic age was estimated using the GrimAge, PhenoAge, Hannum, and DunedinPACE clocks. Primary endpoints included discharge modality, defined as discharge to home versus institutional care, and the duration of hospital stay.

The results showed that shorter telomere length and elevated extrinsic epigenetic age acceleration (EEAA), calculated using the Hannum clock, were associated with a non-significant trend toward longer postoperative hospitalization and a slightly increased likelihood of discharge to institutional care. Among the frailty screening tools, the G8 score showed a weak trend toward longer hospital stays, while the GFI tended to underestimate frailty in high-risk patients. No clear predictive value was observed for the other epigenetic aging measures. Nevertheless, both screening instruments identified relevant areas of concern, particularly polypharmacy, psychosocial burden, and functional limitations.

In conclusion, frailty questionnaires provided valuable additional information for the Comprehensive Geriatric Assessment (CGA) in this study. High-risk patients should be specifically evaluated for the respective problem domains within the CGA framework, for example using instruments such as the Instrumental Activities of Daily Living (IADL), Cumulative Illness Rating Scale for Geriatrics (CIRS-G), and Timed Get-Up-and-Go test (TGUG).

1 Introduction

1.1 Aging and Frailty

Aging is commonly defined as a continuous process characterized by the gradual accumulation of changes within an organism over time (Harman, 1981). These molecular alterations occur at both genetic and epigenetic levels and are shaped by environmental and stochastic factors (Fraga, 2009). This definition also supports the view that aging begins as early as conception, rather than only later in life (Panagiotou, 2025).

Currently, two main theories dominate the scientific discourse: the programmed theory, which suggests that aging follows a biological schedule governed by genetic mechanisms and is a continuation of early developmental processes; and the damage or error theory, which interprets aging as the result of cumulative damage to cells and tissues caused by harmful external factors that progressively worsen over time (Panagiotou, 2025).

From a gerontological perspective, aging research primarily focuses on the decline in functional capacity (Mitnitski & Rockwood, 2016), a process closely linked to a higher incidence of age-related diseases such as cancer, diabetes, and cardiovascular conditions (Niccoli & Partridge, 2012; Zenin et al., 2019), and can further contribute to disease-related mortality (Rockwood et al., 2017). With advancing age, these degenerative processes accelerate, following a trajectory that aligns with the Gompertzian law of mortality (Gompertz, 1820; Makeham, 1860).

However, the rate of age-related changes is not uniform across individuals. The inter-individual variability implies that, even among individuals of the same chronological age, biological aging may proceed at markedly different rates (Le Saux et al., 2017). Similarly, different organ systems within the same person may age at varying speeds, known as intra-individual variability (Le Saux et al., 2017).

In response to the need to clinically capture and quantify functional decline in aging, the concept of frailty has gained increasing prominence in the medical discourse for more than two decades (Fried et al., 2001; Rockwood et al., 1994; Rubenstein et al., 1984). Frailty is

described as a syndrome of reduced physiologic reserve and heightened vulnerability to stressors, resulting from a cumulative decline of multiple physiological systems that manifest in adverse health outcomes (Bortz, 2002; Campbell & Buchner, 1997; Fried et al., 2001; Hamerman, 1999; Rockwood et al., 2000) such as falls, hospitalizations, disability, and mortality (Fried et al., 2001). An important aspect is its increasing prevalence with age, making older adults a particularly vulnerable group. This trend is especially evident among women, who show a higher prevalence of frailty than men, yet have a greater life expectancy (Fried et al., 2001).

Frailty is best conceptualized when viewed alongside the construct of healthy aging (Fig. 1). While healthy aging is associated with a lower likelihood of disease, maintenance of physical and cognitive function, and continued participation in social life (Panagiotou, 2025), frailty marks the stage at which physiological decline increasingly threatens an individual's ability to maintain independence in daily living. It can therefore be understood as the transitional stage between healthy aging and the loss of functional independence.

Furthermore, it should be noted that historically rooted geriatric concepts such as "multimorbidity" and "disability" are neither exclusive to healthy aging nor synonymous with frailty, but may coexist with both phenomena to varying degrees. Instead of functioning as clear-cut diagnostic criteria, they should be understood as potentially overlapping clinical states that accompany the aging process. The critical factor is how effectively these stressors are managed. For example, well-controlled type 2 diabetes or hypertension can allow for a largely symptom-free life when properly treated. Likewise, in the case of disability, the diagnosis itself is not the primary concern, but rather the ability to manage daily life with appropriate aids. A patient who can safely use a walker, implanted hearing aids, or orthopedic shoes can maintain independence despite certain limitations.

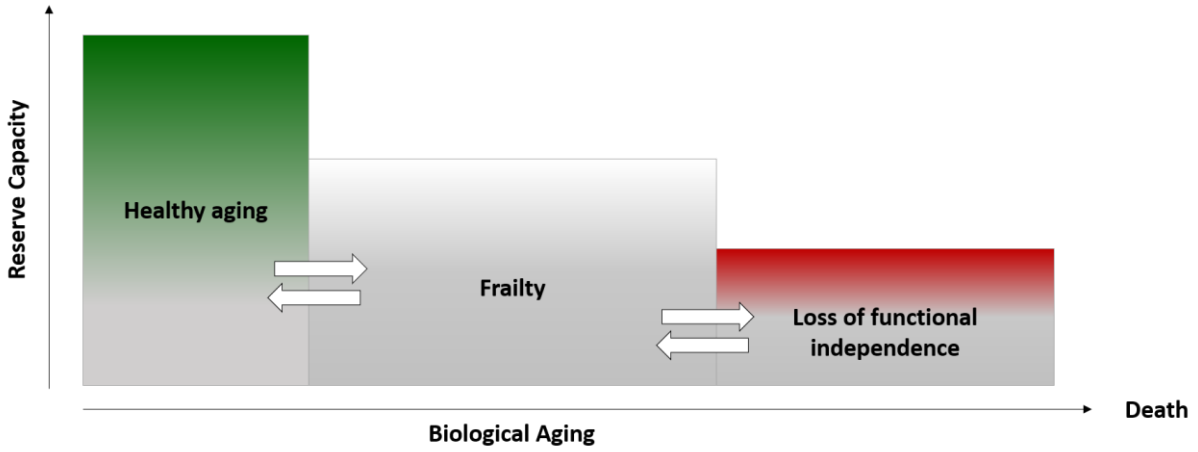

Fig. 1. *Frailty* as an intermediate stage between *healthy aging* and *loss of functional independence*; the illustration reflects a conceptual model grounded in biological aging and the deficit accumulation theory (Mitnitski & Rockwood, 2016). Although it suggests a gradual progression, this trajectory does not preclude alternative models in which frailty may emerge suddenly, for instance, following acute events.

In the context of glioblastoma treatment in elderly patients, median survival remains approximately 12 months, regardless of the multimodal therapy applied (Hertler et al., 2023). Given this limited prognosis, the primary goal is not to prevent frailty, but to slow its progression, as full functional recovery is unlikely at this stage of the disease. The emphasis shifts toward tertiary prevention measures aimed at minimizing complications, preserving quality of life, and maintaining the highest possible degree of autonomy. Equally important is quaternary prevention, which seeks to avoid burdensome or non-beneficial therapeutic interventions that add to the frailty of a patient. If the progression of frailty can no longer be slowed, its assessment may still provide a rationale for initiating palliative care at an earlier stage, rather than postponing it until the terminal phase of life.

1.2 Classification and Pathological Context of Glioblastoma

1.2.1 Grading of Gliomas

In recent decades, the classification of brain tumors has been continuously refined. Historically, glioma diagnosis relied on the microscopic evaluation of hematoxylin- and eosin-stained tissue sections and immunohistochemical analyses (Louis et al., 2016). The 2016 World Health Organization (WHO) classification was the first to systematically integrate molecular information into brain tumor diagnostics (Louis et al., 2016), enabling the grading of gliomas based on their degree of malignancy and prognosis. The 2021 WHO classification further built on this approach, offering an even more precise categorization (Louis et al., 2021).

Most adult gliomas are characterized by diffuse infiltration of the grey and white matter of the brain, which prevents clear separation from the surrounding tissue and makes complete surgical removal challenging (Sulangi et al., 2024). Due to this infiltrative nature (Louis et al., 2016), histological specimens often contain a mixture of tumor cells and non-neoplastic brain tissue, which complicates accurate diagnosis.

A notable exception is WHO grade 1 glioma, such as pilocytic astrocytoma (Louis et al., 2016), which predominantly occurs in childhood (Theeler et al., 2014). This tumor type typically forms a well-defined, solid mass that displaces rather than infiltrates adjacent tissue (Louis et al., 2016). Accordingly, these tumors are regarded as a distinct entity, in contrast to WHO grade 2–4 diffuse astrocytomas (Louis et al., 2016), which are characterized as follows:

Grade 2 gliomas are more challenging to remove completely given their tendency for diffuse infiltration (Sulangi et al., 2024). Although they show a low proliferation rate and slower tumor progression, they retain the capacity to develop into higher-grade forms (Tom et al., 2019). They are typically classified into diffuse astrocytomas and oligodendrogliomas (Louis et al., 2021; Weller et al., 2022). Although astrocytomas and oligodendrogliomas contain cells that morphologically resemble astrocytes and oligodendrocytes, they are thought to originate not from these cell types, but from undifferentiated or partially differentiated neural precursor or stem cells (Modrek et al., 2014).

When examining their molecular characteristics in greater detail (Fig. 2), astrocytomas almost invariably show ATRX loss in addition to an IDH mutation. A WHO 2021 grade 2 astrocytoma may progress to grade 3 or grade 4 IDH-mutant forms. In such cases, WHO guidelines recommend evaluation of homozygous deletion of CDKN2A/B. A diagnosis of WHO grade 4 is established when this deletion is identified in combination with necrosis or microvascular proliferation. By contrast, oligodendrogliomas typically display an IDH mutation accompanied by a 1p/19q co-deletion, frequently along with a TERT promoter mutation. These molecular alterations are associated with a more favorable prognosis and enhanced chemosensitivity. A WHO grade 2 oligodendroglioma (IDH-mutant, 1p/19q co-deleted) may progress to a grade 3 oligodendroglioma with the same molecular profile (Louis et al., 2021; Weller et al., 2022).

Grade 3 gliomas of both astrocytic and oligodendroglial origin demonstrate higher mitotic activity than grade 2 gliomas (Louis et al., 2021; Weller et al., 2022). These include grade 3 astrocytomas (IDH-mutant) and grade 3 oligodendrogliomas (IDH-mutant, 1p/19q co-deleted) (Louis et al., 2021; Weller et al., 2022). Although the distinction between CNS WHO grade 2 and 3 is based on mitotic activity, a clearly defined threshold remains lacking, as robust clinical prognostic associations have not yet been established (Brat et al., 2020).

Grade 4 gliomas represent the highest level of malignancy and are characterized by necrosis and/or microvascular proliferation, typically in combination (Louis et al., 2021; Weller et al., 2022). The most common form is glioblastoma with IDH-wildtype, which is frequently linked to TERT promoter mutations, EGFR gene amplification, gain of chromosome 7 and loss of chromosome 10 (Louis et al., 2021; Weller et al., 2022).

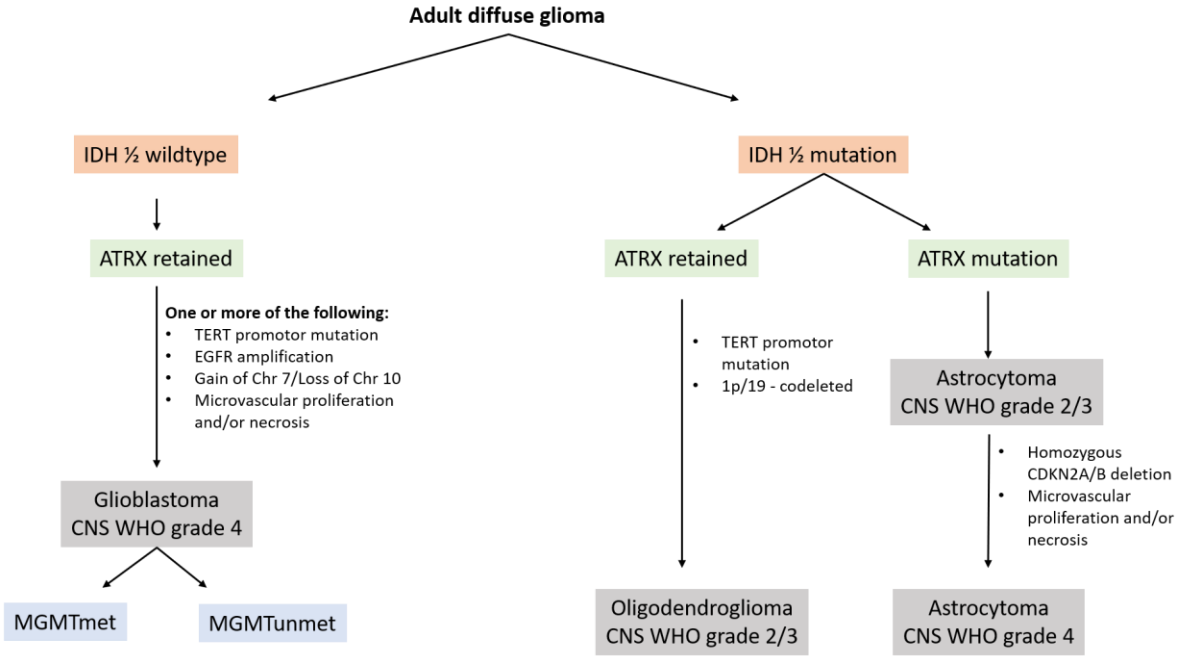

Fig. 2. A simplified schematic overview of adult diffuse glioma classification, based on IDH mutation status and key molecular markers, aligned with the 2021 WHO guidelines. Adapted from Torp et al. (2022), which was conceptually inspired by Gritsch et al. (2022), and supplemented with information from the WHO CNS tumor classification from Weller et al. (2022).

1.2.2 Molecular Pathology

1.2.2.1 IDH1/2

Isocitrate dehydrogenase (IDH) 1 and 2 are enzymes of the citric acid cycle that catalyze the conversion of isocitrate to α-ketoglutarate (Waitkus et al., 2016). Mutations in IDH1, most commonly affecting codon 132, and in IDH2, typically affecting codon 172, modify the enzyme's function, resulting in the conversion of α-ketoglutarate into 2-hydroxyglutarate, which then strongly accumulates in tumor cells (Dang et al., 2009; Ward et al., 2010). This oncometabolite competes with α-ketoglutarate for α-ketoglutarate-dependent dioxygenases, particularly TET2, and thereby induces global hypermethylation (Figueroa et al., 2010; Xu et al., 2011). In addition, these mutations promote angiogenesis by upregulating VEGF (Veganzones et al., 2017; Yalaza et al., 2017) and stabilizing HIF-1α (Yalaza et al., 2017), thereby supporting tumor microvessel formation.

IDH mutations frequently arise early during tumor development and often precede other genetic alterations such as ATRX or TP53 mutations (Johnson et al., 2014). Evidence suggests that IDH1 mutation in IDH-mutant astrocytoma is retained both at initial diagnosis and upon recurrence (Johnson et al., 2014). Consequently, IDH mutation is recognized as a driver mutation that helps distinguish lower-grade from higher-grade gliomas (Louis et al., 2021).

1.2.2.2 ATRX

ATRX mutations represent a relevant marker for further subclassification of IDH-mutant gliomas (Louis et al., 2021). The ATRX gene encodes the protein "Alpha-Thalassemia/Mental Retardation X-linked" (Gibbons et al., 1995), which under physiological conditions forms a protein complex together with DAXX (death-associated protein 6) and HP1 (heterochromatin protein 1) (Eustermann et al., 2011; Nan et al., 2007; Tang et al., 2004). This complex plays a crucial role in the deposition of H3 histones in telomeric and pericentromeric DNA regions (Lewis et al., 2010; Wong et al., 2010). The simultaneous presence of ATRX and TP53 mutations leads to the dissociation of these protein complexes from the telomeric DNA, thereby resulting in a loss of their stabilizing function (Gulve et al., 2022). As a consequence, DNA polymerase is no longer able to accurately replicate the repetitive telomeric sequences.

This results in structurally abnormal and excessively elongated telomeric sequences, which may be associated with the activation of the alternative lengthening of telomeres (ALT) mechanism, provided that additional genetic alterations are involved (Flynn et al., 2015). IDH-mutant astrocytomas with ATRX mutation show a better prognosis than those without ATRX loss, but a worse prognosis compared to oligodendrogliomas (Leeper et al., 2015; Wiestler et al., 2013).

1.2.2.3 TERTp

TERT, the catalytic subunit of telomerase, is essential for telomere maintenance (see Section 1.5.1.1). In gliomas, TERT promoter mutations (TERTp) are known to initiate increased telomerase activity and lead to telomere elongation in gliomas of both high and low malignancy (Eckel-Passow et al., 2015).

TERTp reactivation is typically induced by somatic point mutations at specific hotspot regions located –124 bp and –146 bp upstream of the TERTp translation start site. These mutations, referred to as C228T and C250T, result in the substitution of cytosine (C) with thymine (T) at the corresponding positions within the TERT promoter (Rubiano et al., 2023).

They typically occur in a heterozygous state, with either the C228T or the C250T mutation present (Rubiano et al., 2023), and create a de novo DNA sequence of 11 base pairs ('CCCGGAAGGGG') that forms a specific binding site for transcription factors of the ETS family. This newly formed binding site enables enhanced recruitment of ETS transcription factors, leading to increased TERT transcription and, consequently, elevated telomerase activity and telomere elongation (Bell et al., 2015).

A better prognosis can be observed in oligodendroglioma that simultaneously harbors a TERTp mutation, an IDH mutation, and a 1p/19q codeletion. In IDH-wildtype gliomas, the presence of a TERTp mutation is associated with a worse prognosis compared to IDH-wildtype gliomas without a TERTp mutation (Eckel-Passow et al., 2015).

1.2.2.4 1p/19q Codeletion

The 1p/19q loss arises from an imbalanced chromosome rearrangement involving the exchange of entire chromosomal arms (Griffin et al., 2006), and is predominantly found in IDH-mutant oligodendrogliomas (Louis et al., 2021). During this process, the aberrant chromosome carrying the chromosomal arms 1p and 19q is lost, while the newly formed chromosome containing the remaining arms 1q and 19p is retained (Griffin et al., 2006).

The mechanisms underlying the association between 1p/19q codeletion and improved therapeutic outcomes are not yet fully understood. It is thought that the tumor retains intact signaling pathways for apoptosis, making it more susceptible to chemotherapy. Another possible effect is the loss of genes that normally contribute to chemoresistance or tumor suppression (Pinkham et al., 2015).

1.2.2.5 Chromosome +7/−10

The loss of one copy of chromosome 10 and the gain of an additional copy of chromosome 7 are among the characteristic chromosomal alterations associated with glioblastoma (Lopez-Gines et al., 2005). According to the 2021 WHO classification, these changes, together with EGFR amplification and TERT promoter mutation, are considered defining features of IDH wildtype glioblastoma (Louis et al., 2021). In this context, the loss of chromosome 10 leads to the deletion of important tumor suppressor genes, particularly the phosphatase and tensin homolog (PTEN) (Liu et al., 1997; Steck et al., 1997), while the gain of chromosome 7 is thought to promote the overexpression of oncogenes such as EGFR (Libermann et al., 1985).

1.2.2.6 EGFR

Epidermal Growth Factor Receptor (EGFR) is a transmembrane cellular tyrosine kinase receptor that mediates signals promoting cell division. Its gene is located on chromosome 7, in the chromosomal band 7p12.1 (Saadeh et al., 2018). The simultaneous amplification and overexpression of EGFR is predominantly observed in glioblastomas (Biernat et al., 2004). This particularly activates the RAS/RAF/MEK/MAPK and PI3K/Akt signaling pathways, which suppress apoptosis and stimulate cell proliferation (Saadeh et al., 2018). As reviewed in Saadeh et al. (2018), some studies suggest that EGFR amplification promotes resistance to radio- and chemotherapy.

1.2.2.7 MGMT

O^6-methylguanine-DNA methyltransferase (MGMT) is a DNA repair enzyme that, under physiological conditions, removes incorrectly attached methyl groups from damaged O^6-methylguanine bases in DNA (Pegg et al., 1995). In the treatment of brain tumors with alkylating agents, these drugs work by alkylating guanine residues, ultimately causing double-strand breaks in tumor DNA (Christmann et al., 2011). However, when MGMT is active, it repairs this damage by removing the methyl groups, thereby reducing the intended therapeutic effect of chemotherapy (Christmann et al., 2011).

When the MGMT promoter becomes methylated (Costello et al., 1994), its affinity for transcription factors decreases, leading to reduced transcription of the MGMT gene and consequently lower levels of MGMT protein (Everhard et al., 2009; Pieper et al., 1999; Watt & Molloy, 1988). As a result, patients whose tumors exhibit MGMT promoter methylation derive greater survival benefit from treatment with the alkylating agent temozolomide compared to those without MGMT methylation (Drexler et al., 2023; Malmström et al., 2012b; Uno et al., 2011). This applies to approximately 40% of all patients with glioblastoma, while nearly all patients with an IDH mutation show a methylated MGMT promoter (Christians et al., 2019).

1.3 Frailty Screening and Management in the Postoperative Setting

1.3.1 Screening- Concepts

Currently, there is no unified consensus on how to define frailty or which instruments to use for its assessment in clinical settings (Shafiee Hanjani et al., 2024; Taylor et al., 2017; Theou et al., 2018; Van Damme et al., 2020).

Over the years, two main models have been established. The first is the Fried Frailty Phenotype (Fried et al., 2001), which defines frailty using five physical components, with any three indicating a frail status. The second is the frailty index (FI), also known as the deficit accumulation model (Mitnitski et al., 2001), which focuses less on the type of elements and more on the total number of accumulated deficits over time.

1.3.1.1 Frailty Phenotype

The Fried Frailty Phenotype (Fried et al., 2001) includes five criteria (Table 1): unintentional weight loss, reduced grip strength, slow gait speed, exhaustion, and low physical activity. These criteria are dichotomized as either “present” or “not present.” Based on the total score, individuals are classified into three categories: not frail (0 points), prefrail (1–2 points), or frail (3 or more points). Weight, grip strength, and gait speed are measured through

in-person tests conducted by a physician or study staff, whereas exhaustion and low physical activity are assessed subjectively through patient self-reports (Fried et al., 2001).

Table 1. Fried Frailty Phenotype

Criterion	Method	Yes	No
Weight Loss	***Self-reported*** *If >10% in one year or >5% in six months, mark as "yes"*		
Exhaustion	***Self-reported*** *If the patient reports exhaustion on a minimum of three days per week, mark as "yes"*		
Grip Strength	***Measurement-based*** *Assessment of grip strength via dynamometer with sex- and BMI-specific thresholds.*		
Gait Speed	***Measurement-based*** *Assessment of time to walk 15 feet, using sex- and BMI-specific thresholds.*		
Physical Activity	***Self-reported*** *Assessment of weekly activities, with sex-specific thresholds.* *Total Score:* *0 Points = "Not frail"* *1-2 Points = "Prefrail"* *≥ 3 Points = "Frail"*		

Adapted from Fried et al. (2001). Frailty in older adults: evidence for a phenotype. J Gerontol a Biol Sci Med Sci, 56(3): M146–M156.

Due to its ability to predict mobility limitations and mortality (Fried et al., 2001), it has been widely implemented in various research settings. Specifically in oncology, there is a deliberate focus on physical aspects such as exhaustion and slow gait speed, since surgery represents only the initial step in a demanding treatment sequence. The following cycles of systemic therapies, including radiotherapy and chemotherapy, can progressively increase a patient's risk of exhaustion and muscle weakness.

However, despite its utility, the Fried Frailty Phenotype does not account for cognitive impairments. For example, depression can cause psychomotor slowing, which may introduce bias in assessing low physical activity (Drey et al., 2011). As a result, patients with neurological or psychiatric conditions may be inadequately represented. Additionally, the model does not address the aspect of multimorbidity.

1.3.1.2 Frailty Index

The deficit accumulation model, further developed by Rockwood et al. (2005), considers 70 potential deficits spanning multiple physiological domains, including chronic diseases, physical disabilities, cognitive and sensory impairments, psychosocial dysfunctions, symptoms, and laboratory values (Fig. 3). By dividing the number of present deficits by the total number of possible deficits, a frailty index score is generated between 0 (no frailty) and 1 (maximum frailty). To make this abstract numerical value more practical in clinical settings, the Clinical Frailty Scale was introduced as part of the Canadian Study of Health and Aging (Rockwood et al., 2005). This scale ranges from 1 (very fit) to 7 (severely frail) and offers clinicians a straightforward way to assess the degree of frailty (Rockwood et al., 2005).

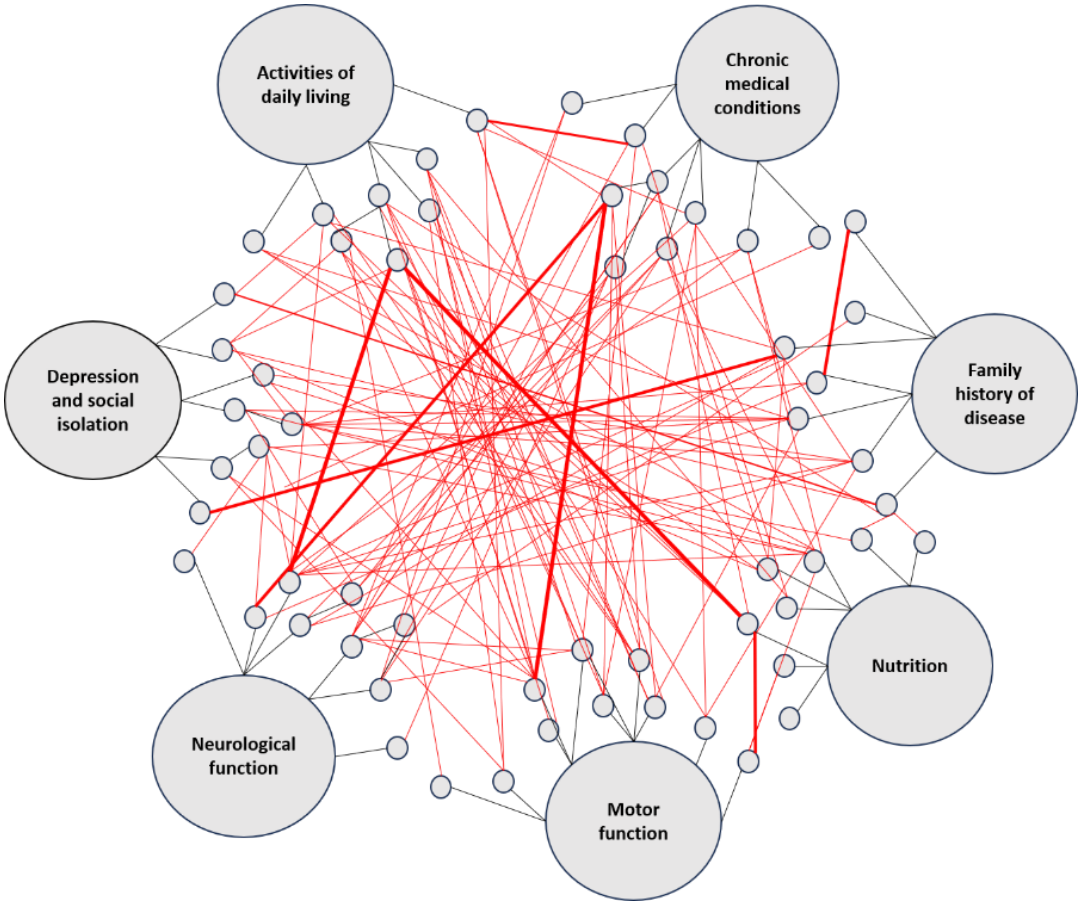

Fig. 3. Abstract illustration of the deficit accumulation theory described by Rockwood et al. (2005). Deficits (small circles) can be assigned to broader domains (large circles). All small circles are of equal size, illustrating the equal weighting of each deficit. Red lines represent interactions between deficits, with increasing line thickness indicating stronger interactions and thinner lines indicating weaker interactions. Which deficits interact, how they interact, and the strength of these interactions differ from one individual to another.

A distinctive feature of the deficit accumulation model is that it describes frailty as a process of “stochastic dynamics” (Mitnitski & Rockwood, 2015). Song et al. (2011) showed that a history of diarrhea, the use of dentures, or foot problems is a stronger predictor of cognitive decline in later life than traditional risk factors, underscoring the need to view deficit accumulation as a systemic rather than an organ-specific phenomenon.

Another key aspect of the frailty index is that all deficits are given equal weight (Mitnitski & Rockwood, 2019). This may seem paradoxical at first glance, for example when a skin condition is considered equivalent to a heart attack. Yet when one takes into account that a heart attack is not always lethal, just as a rash is not always harmless, both may pose significant risks (Mitnitski & Rockwood, 2019). In practice, however, the equivalence of seemingly minor and major deficits does not persist over time, since deficits can lead to functional limitations which in turn trigger a cascade of additional deficits. These added deficits make it possible for the frailty index to account for their varying impact throughout the progression of frailty (Mitnitski & Rockwood, 2019).

When examining the development of frailty, longitudinal data from the Canadian National Health Survey indicate that the rate of deficit accumulation is approximately 4.5% per year (Mitnitski & Rockwood, 2016), and this rate remains relatively stable throughout adulthood (Mitnitski & Rockwood, 2019). Over time, such steady growth results in the total number of deficits doubling roughly every 12.6 years, as demonstrated by Hoogendijk et al. (2018). This trajectory highlights that frailty is primarily the outcome of a continuous and partly irreversible biological process. However, it is also important to recognize that frailty can sometimes worsen or emerge more abruptly, for example, due to acute events such as accidents or severe illnesses, adding another dimension to its progression.

Another frequently discussed aspect in clinical practice is the link between frailty and mortality. Rockwood’s model explains that the accumulation of health deficits leads to an increased risk of mortality (Rockwood et al., 2017; Rockwood & Mitnitski, 2007). In oncology, frailty is not intended to be used as a direct prognostic tool for mortality, since prognosis is primarily driven by the underlying malignancy. Instead, frailty serves as an important indicator associated with increased mortality risk. Even patients with a high frailty index can often survive beyond one year, according to Rockwood & Mitnitski (2007).

In conclusion, the main practical challenge remains that implementation requires time, which is not always feasible in every clinical setting. While the frailty index captures the complexity of aging, its methodology often appears to contradict the principle of “Occam’s razor”. This principle is a core concept in clinical practice favoring the simplest and most plausible explanation for a diagnosis, one that consistently and comprehensively accounts for all known facts while avoiding unnecessary complexity. However, in the context of describing frailty, complexity is not a limitation but rather a marker of diagnostic precision (Mitnitski & Rockwood, 2019).

1.3.2 Stage-Based Approach to Frailty in the Perioperative Setting

The main goal of frailty assessment in surgical settings is to identify older patients at increased risk of postoperative complications such as infections, delirium, or prolonged hospital stays (Theodorakis et al., 2024). It supports both risk stratification and personalized perioperative planning. For risk assessment, it helps guide preoperative decisions, including evaluating the appropriateness of surgery and identifying patients who may benefit from enhanced perioperative care. For personalized care, it informs strategies such as selecting patients for prehabilitation, tailoring anesthesia plans, implementing delirium prevention strategies, and planning supportive care (Robinson et al., 2015). Figure 4 illustrates how this stepwise approach can be implemented, as originally outlined by Extermann (2012).

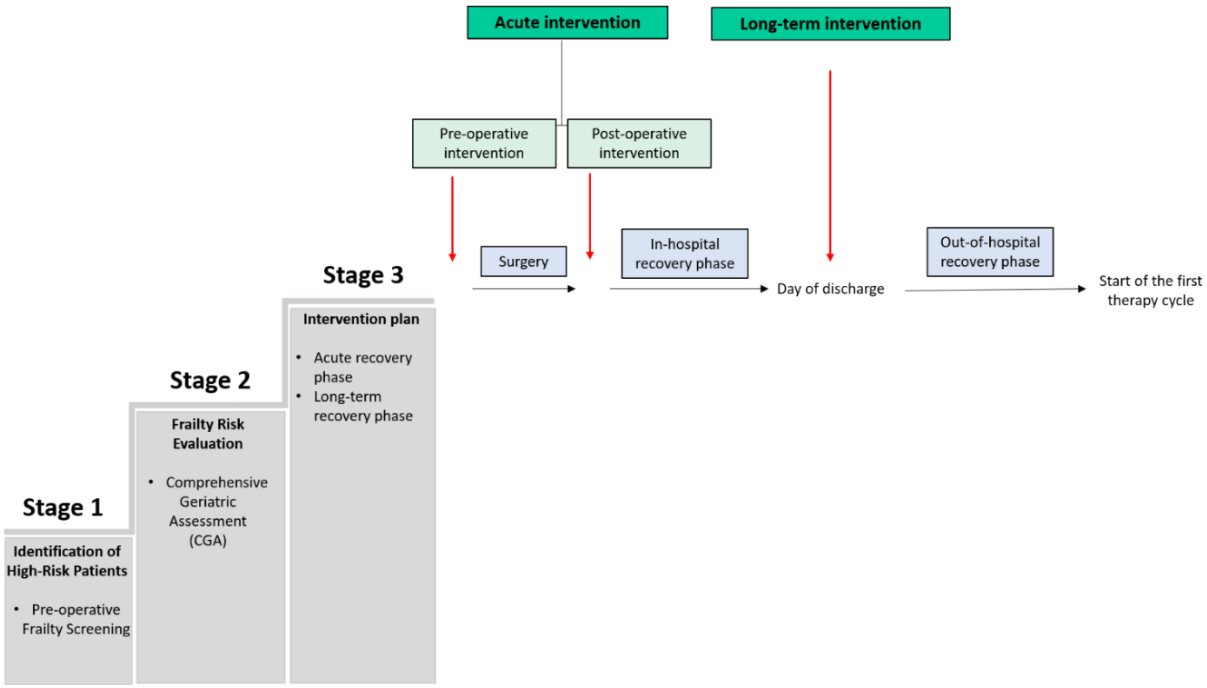

Fig. 4. Frailty management strategy in the context of surgical oncology. The figure is based on the widely used *two-step approach* (pre-operative screening and CGA) as described by Extermann (2012) and recommended by the International Society of Geriatric Oncology (n.d.). Here, this established model is illustrated in *three stages*, adding an explicit intervention planning step (Stage 3) to highlight practical implementation in both inpatient and outpatient care for geriatric patients.

Stage 1 involves preoperative screening to quickly identify patients at higher risk (Extermann, 2012; International Society of Geriatric Oncology, n.d.). This brief assessment can

be completed in 5 to 10 minutes by non-geriatric health care professionals (Soubeyran et al., 2014). The International Society of Geriatric Oncology (n.d.) specifically recommends the Geriatric-8 (G8), Triage Risk Screening Tool (TRST), and Vulnerable Elders Survey–13 (VES-13) for this purpose, as these are among the most studied tools and have shown high sensitivity (Decoster et al., 2015). These questionnaires blend counts of health deficits with phenotypic indicators such as weight loss, thereby capturing overlapping aspects of both the frailty phenotype and frailty index.

In Stage 2, high-risk patients undergo a Comprehensive Geriatric Assessment (CGA) aimed at uncovering hidden yet urgent risks (Wildiers et al., 2014), thus enabling timely acute and longer-term interventions. The CGA addresses key geriatric domains, including “functional status, fatigue, comorbidity, cognition, mental health, social support, nutrition, and geriatric syndromes” (Wildiers et al., 2014), with further screening tool details provided in Table 2.

Following this, the results should be discussed within a multidisciplinary team (Wildiers et al., 2014) composed of professionals whose expertise matches the patient's relevant problem domains (Stage 3). Life-threatening issues, such as malnutrition or imminent organ failure, should be prioritized before addressing aspects affecting quality of life.

It is also important to emphasize that discharge from the hospital does not mark the end of frailty management. Rather, the measures identified through the CGA should guide both discharge planning and ongoing reassessment before each treatment cycle. Long-term care may also include one-on-one discussions with the patient about specialized housing options or planning for palliative care (Ko, 2011). The latter marks the final stage of life, aiming to preserve dignity and ensure comfort through pain relief and emotional support (Ko, 2011).

1.3.3 Risks of Frailty

The following sections discuss frailty risks in the postoperative setting and outline CGA assessments used to identify them. These are summarized in Table 2, which presents the International Society of Geriatric Oncology guidelines recommending validated screening methods.

1.3.3.1 *Functional dependency*

Functional dependency refers to the diminished ability to live independently and carry out essential daily tasks (Rostoft & Rønning, 2017). Assessing functional status is especially important in older cancer patients, as age-related organic degeneration can lead to its decline, making it a key indicator of overall health (Rostoft & Rønning, 2017). For many patients, preserving independence holds greater therapeutic value than simply prolonging survival (Rostoft & Rønning, 2017). In this context, two types of questionnaires can support clinicians in providing more tailored care: those assessing basic activities of daily living (ADLs) and those assessing instrumental activities of daily living (IADLs) (Wildiers et al., 2014). Evidence from Natsume et al. (2024) further suggests that a structured 50-day postoperative rehabilitation program can lead to significant improvements in daily functioning among older glioblastoma patients.

1.3.3.2 *Falls*

Older adults with cancer and frailty have an increased risk of falling in the postoperative period (Meckstroth et al., 2024). Such falls can result in both fatal and non-fatal injuries (Bergen, 2016), complicating recovery. However, Meckstroth et al. (2024) found that although frailty was associated with both an increased risk of falls and higher rates of 30-day readmission or 90-day mortality, the occurrence of falls themselves was not independently associated with these outcomes after adjusting for frailty. Given that this heightened vulnerability may result from intrinsic factors such as cognitive deficits, circulatory instability, and reduced muscle strength, as well as extrinsic influences like hazardous environments and polypharmacy (Kim & Korc-Grodzicki, 2017), it is important to identify at-risk patients preoperatively, for example by using the Timed Get-Up-and-Go test (TGUG) (Wildiers et al., 2014).

1.3.3.3 *Malnutrition*

Malnutrition diminishes the patient's physiological reserve and may consequently impair the response to surgical stress (Gillis & Wischmeyer, 2019), increasing the risk of hospital readmissions, postoperative complications, and prolonged length of stay (Sandrucci et al.,

2018). To address this, the Mini Nutritional Assessment (MNA) offers a non-invasive and validated approach for detecting early risk of malnutrition in elderly patients (Guigoz et al., 2002).

1.3.3.4 *Comorbidity*

On average, older adults have three to four coexisting medical conditions (Friedrich et al., 2012), which can diminish or even outweigh the potential benefits of surgery (Griffiths et al., 2015). The Cumulative Illness Rating Scale for Geriatrics (CIRS-G) offers a structured, organ-based approach to evaluating comorbidities, supporting more informed treatment planning in older cancer patients (Friedrich et al., 2012).

1.3.3.5 *Polypharmacy*

Polypharmacy is defined as the concurrent use of five or more medications (Masnoon et al., 2017), encompassing both prescription and over-the-counter drugs (Montamat & Cusack, 1992). The involvement of multiple specialties in patient care (Clyne et al., 2016) and so-called "prescribing cascades" (Rochon & Gurwitz, 2017) can further increase the risk of patients receiving "potentially inappropriate medications" (Cannon et al., 2006). In this context, concern extends beyond the side effects of individual drugs to include complex drug interactions, cumulative or synergistic effects, and the risk of nonadherence. The most common adverse outcomes are delirium, falls, and incontinence, all of which warrant particular attention in clinical practice (Nightingale et al., 2017). This risk can be reduced through the specialized expertise of pharmacists, who perform thorough, individualized medication reviews to proactively identify risks and ensure safe, effective, and appropriate pharmacotherapy.

1.3.3.6 *Delirium*

In contrast to dementia, delirium is an acute and often reversible confusional state that commonly arises in the postoperative setting. Defined by the WHO as a disturbance of consciousness and attention, it may also involve perceptual abnormalities, psychomotor changes, and language impairments (World Health Organization, 2016). Key predictors of

postoperative delirium include pre-existing cognitive impairment, alcohol and medication use, intubation, extended ICU stays, and the use of physical restraints (Van Rompaey et al., 2009). To support early identification, the Montreal Cognitive Assessment (MoCA) provides a practical tool for assessing relevant cognitive domains and recognizing patients at increased risk (Wildiers et al., 2014).

1.3.3.7 *Depression and Social Isolation*

In the elderly population, depression is often accompanied by a pronounced decline in overall quality of life, reflected in reduced physical activity, chronic pain, and difficulties in sustaining social relationships (Deckx et al., 2015; Hopko et al., 2008). In this regard, tools such as the EORTC QLQ-C30 offer valuable insights into patients' quality of life, while the Geriatric Depression Scale (GDS) provides a robust means of evaluating depressive symptoms (Wildiers et al., 2014).

Table 2, Part 1: Comprehensive Geriatric Assessment (CGA) based on the guidelines of the International Society of Geriatric Oncology, 2015

Screening	Method	Content	Risk Score	Primary Source
Activities of Daily Living **(ADL)**	Questionnaire	• Bathing • Dressing • Toileting • Continence • Transferring • Feeding	**Score 4:** Moderate impairment **Score ≤ 2:** Severe functional impairment [1]	Katz et al., 1963, 1970*
Instrumental Activities of Daily Living **(IADL)**	Questionnaire	• Using the phone • Shopping • Food preparation • Housekeeping • Laundry • Mode of transportation • Responsibility for own medications • Ability to handle finances	**Score 0:** Complete dependence **Score of 8:** Complete independence [2]	Lawton, 1969 *
Montreal Cognitive Assessment **(MoCA)**	Functional Test	• Orientation • Naming • Memory • Attention • Language • Abstraction • Recall • Drawing	Normal if score **≥ 26** / 30 [3]	Nasreddine et al., 2005
Geriatric Depression Scale **(GDS)**	Questionnaire	• Energy and Activity • Social Engagement • Cognitive Symptoms • Emotional Symptoms • Physical Symptoms • Self-Perception	*GDS-15 [4]:* **Score 5-8:** Mild depression **Score 9-11:** Moderate depression **Score 12-15:** Severe depression	*GDS-30 *:* Yesavage & Sheikh, 1986 *GDS-15 *:* Almeida & Almeida, 1999; Arthur et al., 1999

***** Original authors as referenced in the International Society of Geriatric Oncology, n.d.

Table 2, Part 2: Comprehensive Geriatric Assessment (CGA) based on the guidelines of the International Society of Geriatric Oncology, 2015

Screening	Method	Content	Score for Risk	Primary Source
Mini Nutritional Assessment **(MNA)**	Questionnaire	**Screening Part** • Appetite • Weight loss • Mobility • Acute disease/stress • Dementia/depression • BMI **Assessment Part** • Independence • Medication • Pressure sores • Meals per day • Protein intake • Fruits/vegetables • Fluid intake • Mode of feeding • Self-view of health • Self-view of nutrition • Mid-arm circumference • Calf circumference	Score 17-23.5: Malnutrition risk Score < 17: Malnutrition [5]	Guigoz, 2006; Rubenstein et al., 2001; Vellas et al., 1999, 2006
Timed Get up and Go **(TGUG)**	Functional Test	The physician instructs the patient to rise from an armchair, walk a short distance of approximately three meters, turn around, and sit down again.	Score under 14 sec: Low falls risk Score over 14 sec: Increased falls risk [6]	Mathias et al., 1986; Podsiadlo & Richardson, 1991*
Cumulative Illness Rating Scale for Geriatrics **(CIRS-G)**	Questionnaire	• Cardiovascular • Hematopoietic • Respiratory • Sensory • GI • Hepatic • Renal • Urogenital • Musculoskeletal • Neurological • Endocrine • Psychiatric	For each system [7]: **Score 0-4:** **0:** No issue **1:** Mild disability **2:** Moderate disability, needs basic therapy **3:** Severe disability or chronic uncontrolled issues **4:** Critical, life-threatening, or end-organ failure	Extermann, 2000 *; Miller et al., 1992; Miller & Towers, 1991; Parmelee et al., 1995 *

***** Original authors as referenced in the International Society of Geriatric Oncology, n.d.

Table 2, Part 3: Comprehensive Geriatric Assessment (CGA) based on the guidelines of the International Society of Geriatric Oncology, 2015

Screening	Method	Content	Score for Risk	Primary Source
European Organization for Research and Treatment of Cancer Quality of Life Questionnaire - Core 30 **(EORTC QLQ-C30)**	Questionnaire	Assesses quality of life using the following items **Functional Scales:** • Physical • Role • Cognitive • Emotional • Social **Symptom Scales:** • Fatigue • Pain • Nausea and vomiting **Global Scale:** • Global Health and Quality of Life	All item responses were linearly transformed to a 0–100 scale using EORTC's standard linear transformation. [8]	Aaronson et al., 1993

***** Original authors as referenced in the International Society of Geriatric Oncology, n.d.

Notes: Table 2, Parts 1-3 are based on guidelines referenced in Decoster et al. (2015) and the International Society of Geriatric Oncology (n.d.); [1] Wallace & Shelkey, 2007; [2] Graf, 2009; [3] Nasreddine et al., 2005; [4] Greenberg, 2012; [5] Nestlé Nutrition Institute, 2009; [6] Calderdale & Huddersfield NHS Foundation Trust, n.d.; [7] Miller & Towers, 1991; [8] Fayers et al., 2002

1.4 Criteria for Molecular Biomarkers of Frailty

The selection of molecular biomarkers should be based on the following criteria:

based on Miller (2001) [1] and Johnson (2006) [2]

1) Outperforming Chronological Age [1]

Biomarkers that correlate too strongly with chronological age are of limited value, as they fail to differentiate between individuals (Mitnitski et al., 2016). Nonetheless, chronological age remains an essential covariate. While it cannot fully capture individual health status, it defines the timeframe over which physiological deficits accumulate and serves as a clinically meaningful reference point (Mitnitski & Rockwood, 2016, 2019). Informative biomarkers should therefore correlate only partially with chronological age while adding independent and health relevant information (Mitnitski & Rockwood, 2019). If this covariate is not taken into account, extremely high biological age estimates such as values above 120 years may occur, which challenge clinical interpretability (Mitnitski et al., 2016).

2) Prediction at the 90% Survival Threshold [1]

The biomarker should enable accurate prediction of an individual's remaining lifespan at an early stage, specifically at an age when 90% of the population is still alive.

This criterion ensures that the biomarker is capable of providing prognostic information when individuals are still in a relatively healthy state, prior to the onset of advanced age-related diseases or significant frailty (Miller, 2001).

3) Non-Interference with Physiological Outcomes [1]

The process of biomarker assessment must not affect life expectancy or influence the measurement of age-related parameters (Miller, 2001).

4) Assessment of the Biological Aging Rate [2]

The biomarker should provide precise insights into the rate of biological aging, as the goal is to determine the impaired recovery time before and after a given event (Johnson, 2006).

5) **Tissue Material Representative of Non-Pathological Aging [2]**

The biomarker must accurately reflect the underlying biological processes of physiological aging, excluding factors associated with the pathogenesis of specific diseases. This distinction ensures its relevance to aging itself rather than disease states (Johnson, 2006).

6) **Reproducibility [2]**

To facilitate repeated use in both research and clinical settings, the biomarker must be highly reproducible and non-invasive, ensuring that it is safe and harmless for individuals undergoing multiple assessments over time (Johnson, 2006).

A biomarker for biological aging should be part of a broader biomarker panel to reflect the multidimensional nature of aging. Rather than capturing isolated signals, it should contribute to a dynamic and interconnected profile. This aligns with Rattan's framework (2013), which highlights multidimensionality, dynamics, and interdependence as core features of health and aging.

1.5 Telomere Length as a Candidate Biomarker

1.5.1 Structure and Function of Telomeres

Telomeres are non-coding regions located at the ends of linear chromosomes, characterized by repetitive DNA elements. In mammals, they consist of the hexanucleotide sequence TTAGGG (O'sullivan & Karlseder, 2010). These sequences can range between 9–15 kb in humans (O'sullivan & Karlseder, 2010) and are repeated thousands of times. Their integrity is maintained by a specialized set of proteins known as the shelterin complex (O'sullivan & Karlseder, 2010). The six main proteins in mammals include: telomeric repeat-binding factor 1 (TRF1), telomeric repeat-binding factor 2 (TRF2), TRF2-interacting protein (RAP1), TRF1-interacting nuclear factor 2 (TIN2), adrenocortical dysplasia protein homolog

(TPP1, also known as ACD), and protection of telomeres 1 (POT1), as originally identified in key studies (Abreu et al., 2010; Baumann & Cech, 2001; Bianchi, 1999; Broccoli et al., 1997; Court et al., 2005; Lei et al., 2004; Loayza & de Lange, 2003; Martinez et al., 2010; Tejera et al., 2010; Teo et al., 2010; Zaug et al., 2010).

The telomeric terminus is characterized by the single-stranded G-rich overhang (Makarov et al., 1997), ranging from approximately 50 to 300 nucleotides in length (O'sullivan & Karlseder, 2010). The free 3'-OH group of this overhang functions as the initiation site for telomerase-driven telomere elongation (Wu et al., 2017) and is furthermore capable of folding back into a telomere loop (T-loop), thereby providing structural protection by preventing recognition of the chromosome end as a DNA double-strand break (Griffith et al., 1999; Lin et al., 2014).

During DNA replication, the ends of linear chromosomes cannot be fully replicated due to the inability of DNA polymerase to completely synthesize the terminal region of the lagging strand, resulting in the progressive shortening of telomeres in somatic cells with each cell division (Ohki et al., 2001). This phenomenon, first proposed theoretically by Watson (1972), is referred to as the end-replication problem. Once a critical telomere length is reached, cells enter a state of permanent growth arrest known as replicative senescence (Hayflick & Moorhead, 1961; Kaul et al., 2012) or alternatively, undergo apoptosis (Blasco, 2007). These outcomes contribute to cellular attrition and impair tissue integrity (Blasco, 2007). The latter is associated with age-related diseases (Zhu et al., 2011), which has led to telomere length becoming a central focus in aging research (Vaiserman & Krasnienkov, 2021).

1.5.1.1 *Mechanisms of Telomere Maintenance: Telomerase and ALT*

Telomerase, discovered by Greider & Blackburn (1985), resolves the end-replication problem by extending the guanine-rich overhang at the 3' end of chromosomes. Its catalytic subunit, hTERT (human telomerase reverse transcriptase), uses the RNA component hTERC (human telomerase RNA component) as a template to synthesize the repetitive TTAGGG sequence (Blackburn, 2001). Telomerase is primarily active in stem cells and tumor cells but it is absent in most somatic cells, leading to progressive telomere shortening (Martínez & Blasco, 2015).

In addition, an alternative mechanism for telomere elongation exists, termed alternative lengthening of telomeres (ALT), in which telomeres are extended independently of telomerase (Bryan & Reddel, 1997; Henson et al., 2002). This mechanism accounts for 10–15% of tumors (Heaphy et al., 2011) and relies on the transfer of telomeric DNA from one telomere to another via homologous recombination, where it serves as a template for elongation (Dunham et al., 2000).

1.5.2 Telomere Dynamics in Aging

Typically, telomere length declines with age, though the rate of shortening varies across the life span (Vaiserman & Krasnienkov, 2021). In humans, telomeres span several kilobases and vary between different cell types (Demanelis et al., 2020).

In newborns, leukocyte telomere length (LTL) in blood ranges from 8.55 to 13.32 kilobases (Okuda et al., 2002), and shortens by an average of 30 to 35 bp per year (Herrmann et al., 2018). In older individuals over the age of 60, it reaches values of 5 to 6 kb (Calado & Dumitriu, 2013). The rate of shortening is particularly high during the first four years of life due to rapid somatic growth (Frenck Jr et al., 1998). Studies further indicate that individuals who exhibit shorter or longer telomeres in childhood generally retain this relative ranking throughout their lifespan (Benetos et al., 2013). This early imprint suggests that telomere length in childhood plays a crucial role in determining the course of later life (Factor-Litvak & Susser, 2015).

However, there is ongoing debate regarding the critical threshold of telomere length. Steenstrup et al. (2017) describe a threshold of 5 kb, which is associated with increased mortality. Other studies on centenarians, however, report telomere lengths of around 3.0 to 3.4 kb, which remain stable in supercentenarians and, in some cases, even increase slightly beyond age 100 (Arai et al., 2015). This discrepancy could be explained by a survival effect, in which individuals with shorter telomeres die earlier, leaving only those with longer telomeres available for study (Mather et al., 2011).

Telomeres represent an interface between genetic stability, environmental influences, and lifestyle factors (Vaiserman & Krasnienkov, 2021). External factors such as chronic

psychological stress accelerate their shortening (Epel et al., 2006). A study involving women aged 20 to 50 found that increased psychological stress correlated with shorter telomeres and lower telomerase activity, and these were further associated with elevated stress hormones and established cardiovascular risk factors (Epel et al., 2006). In line with these findings, smoking and other factors of oxidative stress have also been shown to significantly contribute to telomere attrition (Babizhayev et al., 2011).

In addition, studies show that healthy lifestyle habits such as regular physical activity can have a positive impact on telomere length. According to Werner et al. (2009), athletes with long-term endurance training have significantly longer telomeres compared to their less active counterparts.

1.5.3 Epidemiological Perspectives on Telomere Length and Frailty

When examining the association between telomere length and frailty, data from the large-scale UK Biobank study by Bountziouka et al. (2022) show a significant link based on the Fried Frailty Index.

Among approximately 472,000 predominantly healthy adults aged 40 to 69 years, individuals with very short telomeres (–2SD) exhibited a 33% higher frailty rate compared to those with long telomeres (+2SD), consistently across all age groups. To rule out the possibility that this association is solely attributable to pre-existing conditions, Bountziouka et al. (2022) regressed telomere length on 123 disease indicators. The residual analysis demonstrated that the association with frailty remained significant even after adjusting for multimorbidity. These findings underscore that frailty can be regarded as a distinct clinical construct, independent of comorbidity.

1.6 DNA Methylation-based Biomarkers as Candidate Biomarkers

Pal and Tyler (2016) report that genetic predisposition accounts for only 20–30% of the aging process, whereas epigenetic mechanisms are thought to govern the remaining 70–80%. Epigenetic regulation modulates gene expression without altering the nucleotide sequence and involves several mechanisms, including DNA methylation (Schübeler, 2015), histone modifications (Chen et al., 2015), noncoding RNAs (Holoch & Moazed, 2015), and the structural organization of chromatin (Venkatesh & Workman, 2015).

Among these mechanisms, DNA methylation has become a central focus in aging research, particularly with respect to alterations in the methylome at CpG sites (Florath, Butterbach, Muller, et al., 2014; Johansson et al., 2013; Rakyan et al., 2010). CpG dinucleotides consist of a cytosine base that is connected in the 5′→3′ direction via a phosphate group to a guanine base, and are distributed throughout the genome (Larsen et al., 1992). DNA methylation is defined as the covalent addition of a methyl group ($–CH_3$) to the C5 atom of the cytosine, resulting in 5-methylcytosine, and is catalyzed by DNA methyltransferases (DNMTs) (Bestor, 2000). It is primarily concentrated in CpG islands, which are defined as genomic regions with a high CpG density, specifically regions that are at least 200 base pairs in length and have a CG content greater than 50% (Gardiner-Garden & Frommer, 1987). Outside CpG islands, methylated CpG sites can also be found throughout the genome (Bird, 2002).

Due to its mitotic stability, this epigenetic mark is considered a particularly robust biomarker of cellular aging (A. Bird, 2002; Horvath, 2013). The symmetrical nature of CpG methylation enables accurate replication of methylation patterns during cell division, ensuring consistent transmission to daughter cells (Holliday & Pugh, 1975; Riggs, 1975). However, these patterns remain dynamic over the lifespan and undergo substantial changes throughout human development, from the embryonic stage to old age (Jones et al., 2015; Razin & Kafri, 1994; Smith et al., 2014).

1.6.1 DNA Methylation and Demethylation in Gene Regulation

DNA methylation typically leads to transcriptional silencing, either by directly preventing transcription factor binding to DNA or by indirectly recruiting methyl-binding proteins that alter chromatin structure (Bird & Wolffe, 1999; Hashimshony et al., 2003; Nan et al., 1998).

In the direct mechanism, the addition of methyl groups narrows the major groove of DNA, thereby hindering transcription sites and impairing the binding of essential transcription factors (Tate & Bird, 1993; Watt & Molloy, 1988). Indirectly, specific methylation patterns recruit methyl-CpG-binding proteins, which can interfere with the binding of other regulatory proteins or modify DNA-bound histones. These histone modifications promote chromatin condensation and ultimately lead to transcriptional repression (Bird & Wolffe, 1999; Hashimshony et al., 2003; Nan et al., 1998).

As part of its dynamic regulation, DNA methylation can be reversed through either passive or active demethylation. Passive demethylation occurs during DNA replication, when methylation marks are not maintained on the newly synthesized strand, typically due to reduced activity of DNA methyltransferases (Monk et al., 1991; Rougier et al., 1998). In contrast, active demethylation involves the enzymatic removal of methyl groups by ten-eleven translocation (TET) enzymes, which oxidize 5-methylcytosine. This oxidation initiates a multistep process that ultimately results in demethylation and may facilitate gene expression (Guo et al., 2011; Ito et al., 2010; Tahiliani et al., 2009).

The biological relevance of this dynamic regulation becomes particularly evident in the context of aging, as promoter-associated hypermethylation within CpG islands is often accompanied by global hypomethylation across the genome (Levine, 2019).

1.6.2 Epigenetic Clocks

An epigenetic clock can be defined as the prediction of age-associated outcomes derived from consistent epigenetic changes using statistical modeling (Horvath & Raj, 2018). It is typically constructed from DNA methylation data obtained through array-based technologies (Horvath, 2013). These clocks are designed either to predict chronological age and/or to

estimate biological age by incorporating phenotypic age-related traits. In the latter case, epigenetic age is calculated and compared to chronological age: an epigenetic age exceeding chronological age indicates accelerated aging, whereas a lower epigenetic age suggests decelerated aging (Levine, 2019). However, since these clocks are developed from cross-sectional data, the terms “acceleration” and “deceleration” refer specifically to the difference between epigenetic and chronological age at a given point in time, rather than reflecting the actual pace of aging over time (Levine, 2019).

1.6.2.1 *First-Generation Clocks*

The first epigenetic clocks were developed by Hannum et al. (2013) and Horvath (2013). Both models used penalized regression methods (Elastic Net), which are based on the principle of identifying CpG sites that systematically change with age (Levine, 2019). In this process, CpG sites may be included in the model even if they lack a direct causal role in biological aging. Some appear age-associated merely because they reflect random patterns within the specific sample (Podolskiy & Gladyshev, 2019).

The Hannum clock was developed using Illumina 450k Infinium array data from whole blood samples (Hannum et al., 2013a). The sample included 656 individuals aged 19 to 101 years (Hannum et al., 2013a). In contrast, the Horvath clock was designed as a pan-tissue clock and was trained on approximately 8,000 samples from 82 datasets, encompassing a total of 51 different non-cancerous tissues and cell types (Horvath, 2013). Both clocks show an extremely high correlation with chronological age, with an r-value exceeding 0.95 (Levine, 2019).

Although both models demonstrate high predictive accuracy, their ability to reflect functional age-related changes is limited (Mangélinck & Mann, 2021). According to Horvath, no significant association between age-related methylation and mRNA expression across various tissues could be detected in the Horvath clock, whereas the Hannum clock shows a stronger association with changes in gene expression (Mangélinck & Mann, 2021).

1.6.2.1.1 *CpG Sites Integrated into the Horvath Clock*

Considering that the methylation difference with age at most CpG sites measured by epigenetic clocks is only 0.2 to 0.3% per year (Mangélinck & Mann, 2021), it becomes evident that minimal changes are sufficient to construct a robust model for estimating biological age (Mangélinck & Mann, 2021). Building on Horvath's findings in mesenchymal stem cells (2013), Raj (2018) hypothesizes that the minimal methylation change observed with age may be due to the contribution of long-lived adult tissue stem cells, whose proliferation is closely associated with epigenetic aging.

Given this background, a central question concerns the functional characteristics of the CpG sites included in the Horvath clock. This model is based on 353 CpG sites, of which 193 are positively correlated with age and 160 are negatively correlated (Horvath, 2013). The hypermethylated sites tend to be located in quiescent promoter CpG islands marked by bivalent chromatin modifications (H3K27me3 and H3K4me3) (Horvath, 2013). Such regions are typically involved in regulating genes that control differentiation and tissue specification (Harikumar & Meshorer, 2015). Conversely, the hypomethylated sites are often found within strong enhancer regions or weakly active promoter regions associated with tissue-specific transcriptional regulation (Horvath, 2013).

1.6.2.2 *Second-Generation Clocks*

Clocks that incorporate lifestyle factors and health conditions alongside chronological age belong to the second generation of epigenetic clocks. A prominent example is the DNAm PhenoAge clock (Levine et al., 2018), which selects 513 specific CpG sites associated with health-related factors using an Elastic Net regression model. The clock integrates nine clinical blood biomarkers that reflect key organ functions and inflammatory processes, including albumin, creatinine, glucose, C-reactive protein (CRP), lymphocyte percentage, mean corpuscular volume (MCV), red cell distribution width (RDW), alkaline phosphatase (ALP), and white blood cell count (Levine et al., 2018).

DNAm PhenoAge has been shown to correlate significantly with increased risk of coronary heart disease ($p = 3.35 \times 10^{-11}$), multimorbidity ($p = 1.95 \times 10^{-20}$), physical limitations

($p = 2.05 \times 10^{-13}$), and reduced disease-free survival ($p = 2.10 \times 10^{-10}$) (Levine et al., 2018). Although DNAm PhenoAge correlates with chronological age at approximately 75%, it exhibits superior predictive power for mortality and morbidity compared to earlier epigenetic clocks (Levine et al., 2018).

Another widely used clock, the so-called GrimAge clock (Lu et al., 2019), was designed to predict remaining lifespan. DNA methylation data from blood were regressed against the plasma concentrations of seven protein biomarkers, including PAI-1 (plasminogen activator inhibitor-1), GDF-15 (growth differentiation factor 15), leptin, TIMP-1 (tissue inhibitor of metalloproteinases 1), B2M (beta-2-microglobulin), adrenomedullin, and cystatin C (Lu et al., 2019). Additionally, self-reported smoking pack-years, chronological age, and sex were incorporated into the model (Lu et al., 2019). GrimAge has been shown to outperform PhenoAge and earlier clocks, particularly in predicting all-cause mortality and various age-related diseases (McCrory et al., 2021).

1.6.2.3 *Third-Generation Clock*

DunedinPACE is an epigenetic biomarker that measures the pace of human aging. According to Belsky et al. (2022), the clock quantifies biological aging as “years of aging per chronological year”, with values above 1 indicating accelerated aging and values below 1 indicating decelerated aging. The development of DunedinPACE was based on 19 biomarkers that were measured longitudinally at ages 26, 32, 38, and 45. By repeatedly measuring these biomarkers over several decades, age-related changes were tracked with high precision.

A key advantage of DunedinPACE is that its measurements are based on data from healthy middle-aged adults, collected prior to the onset of age-related diseases such as diabetes or cardiovascular conditions (Belsky et al., 2022). This enables the representation of the “true aging process” and minimizes distortion caused by age-related diseases.

Another distinctive feature of DunedinPACE is that all participants were born in the same year and city, namely Dunedin, New Zealand, forming a single-year birth cohort (Belsky et al., 2022). This allows for a clearer distinction between the true aging process and so-called cohort effects, which occur when individuals from different generations experience varying

environmental conditions that influence DNA methylation patterns but are unrelated to aging itself (Belsky et al., 2022).

1.7 Scope of the Thesis

This dissertation examines the role of frailty in predicting postoperative outcomes in glioblastoma patients aged 65 years and older. The primary objective is to assess the prognostic value of preoperative frailty assessments in combination with molecular aging markers, specifically telomere length and second- and third-generation epigenetic clocks. The clocks analyzed include GrimAge, PhenoAge, the Hannum clock, and DunedinPACE, each derived from blood samples collected prior to tumor resection. Clinical frailty was assessed using two standardized instruments, the G8 score and the Groningen Frailty Indicator.

The study retrospectively examined associations with hospital stay duration and discharge modality, defined as discharge to home or institutional care. Survival data were also analyzed to better contextualize frailty within the overall patient prognosis.

The overarching aim is to explore how molecular biomarkers may be integrated into preoperative risk stratification to enhance individualized treatment planning. By identifying high risk patients at an early stage, targeted short- and long-term interventions may help support recovery and preserve independence following surgery.

2 Results

2.1 Characterization of the Primary Glioblastoma Study Cohort

Table 3. Molecular Profile of the Primary GBM Study Cohort

	All primary glioblastomas (n = 40)
Male/female ratio	1.17 (21/18)
Age at diagnosis (mean ± SD)	75.43 ± 5.58
Genetic alterations	
IDH1 R132H mutation	0/40 (0%)
ATRX mutation	1/40 (3%)
TERT C228T mutation	29/40 (73%)
TERT C250T mutation	7/40 (18%)
TERT wildtype	4/40 (10%)
MGMT methylation	20/40 (50%)
Ki67 ≤ 20%	12/40 (30%)
Ki67 > 20% and ≤ 50%	25/39 (64%)
Ki67 > 50%	3/41 (7%)

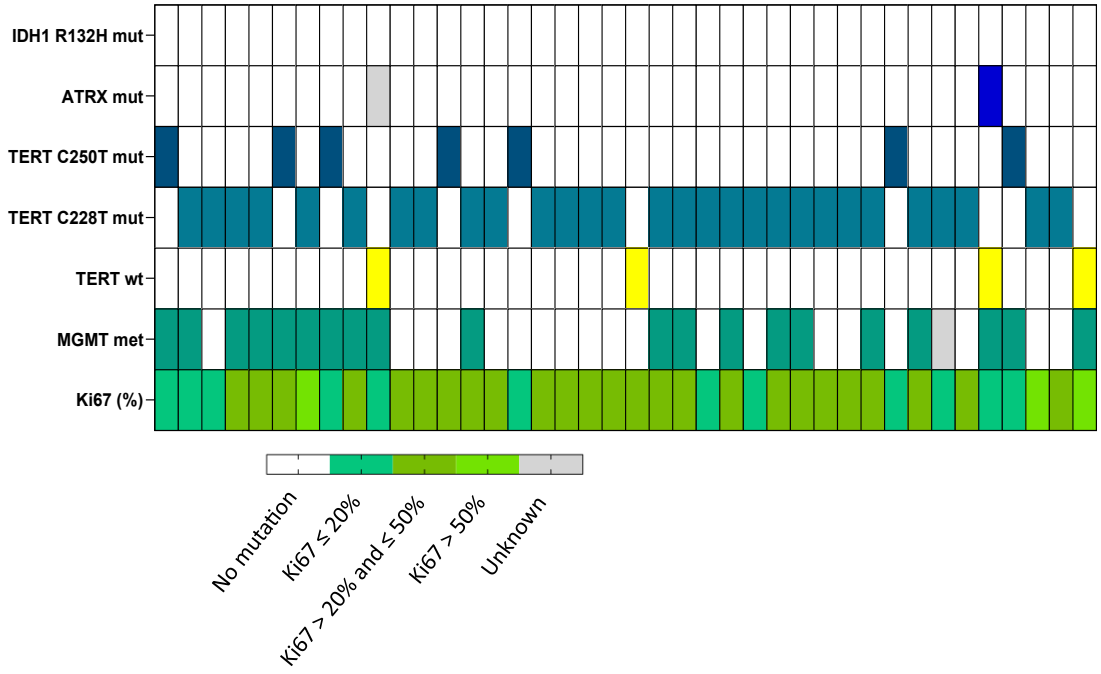

Fig. 5. Genetic alterations in all primary GBM patients (n = 40): *IDH1 R132H mut* = isocitrate dehydrogenase 1 (IDH1) R132H mutation; *ATRX mut* = alpha-thalassemia/mental retardation syndrome X-linked (ATRX) mutation; *TERT C228T mut* = telomerase reverse transcriptase (TERT) C228T mutation; *TERT C250T mut* = telomerase reverse transcriptase (TERT) C250T mutation; *TERT wt* = telomerase reverse transcriptase (TERT) wild-type; *MGMT met* = O6-methylguanine-DNA methyltransferase (MGMT) methylation; *Ki67* = Ki-67 proliferation index.

Morphological Features (a-d)

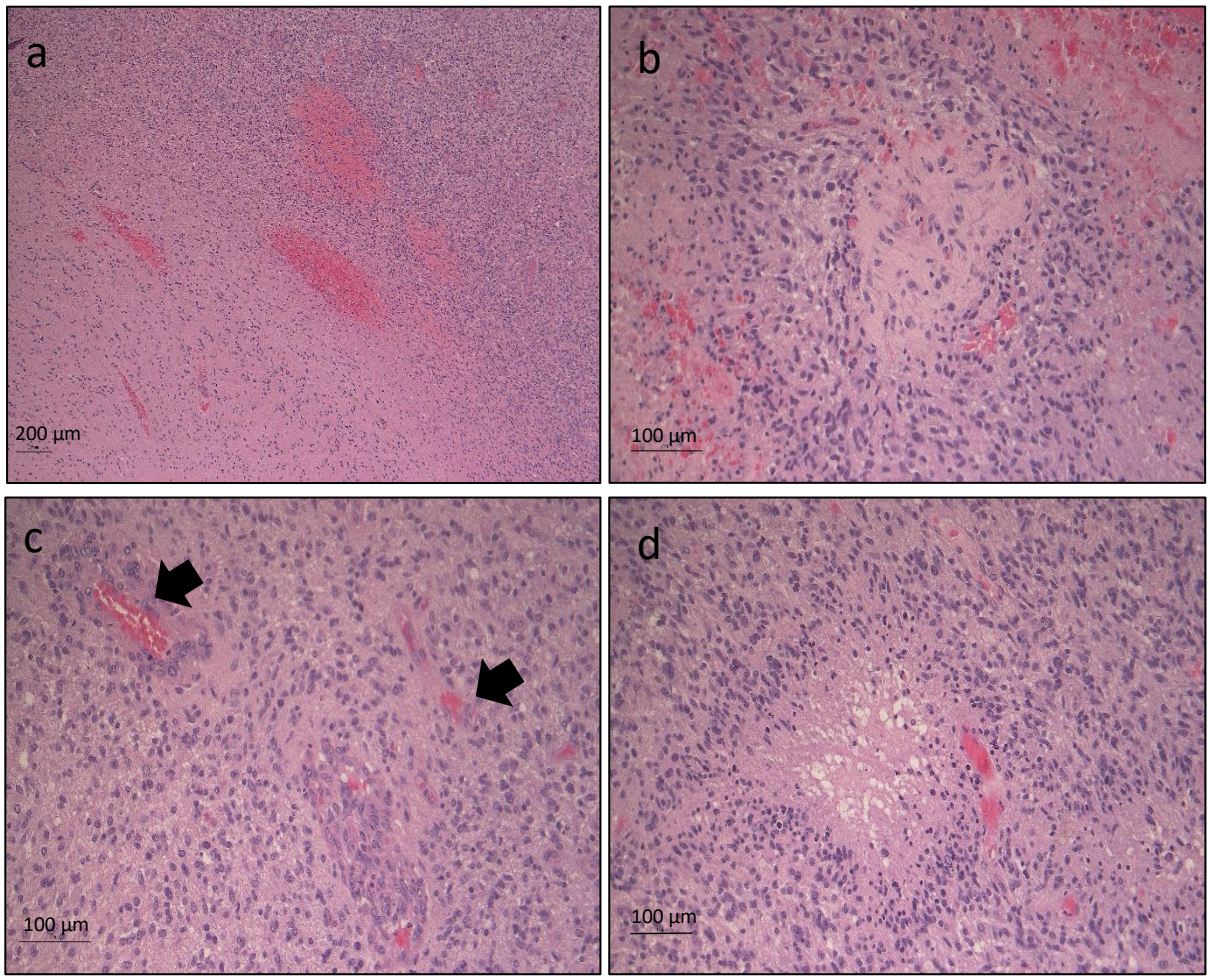

Fig. 6. Histological characteristics of glioblastoma multiforme:
(a) The diffuse nature of glioblastoma: an increase in mitotic activity and cell density from left to right.
(b) & (d) A classic feature of glioblastoma is necrosis, resulting from tumor cell death. Necrotic areas are often surrounded by a high density of viable tumor cells, a phenomenon known as palisading necrosis.
(b) Illustrates the process of how cells gradually align around the necrotic area, eventually forming the necrotic core.
(d) Depicts the final stage of necrosis, where the surrounding tumor cells are arranged in parallel.
(c) The proliferation and expansion of blood vessels in the tumor leads to new structures (some indicated by arrows). This process is known as microvascular proliferation.

Molecular Features (e-j)

IDH1 R132H mutation

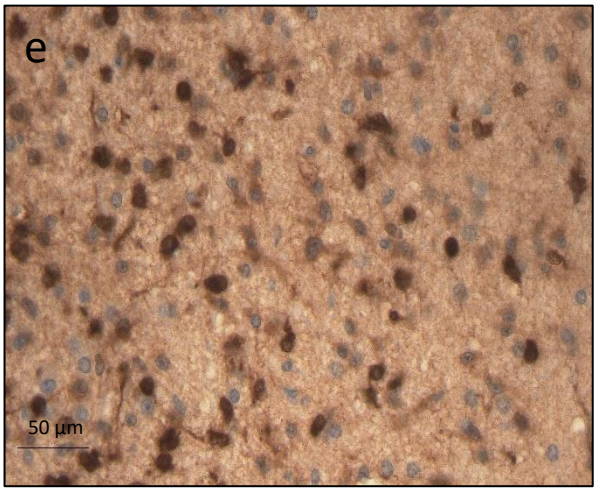

IDH1 R132H wildtype

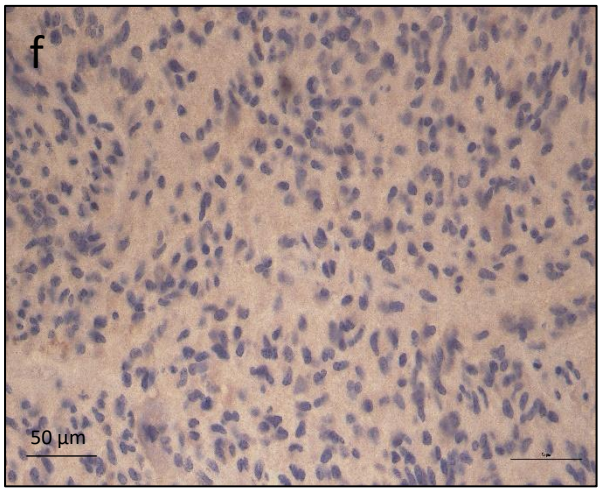

ATRX mutation

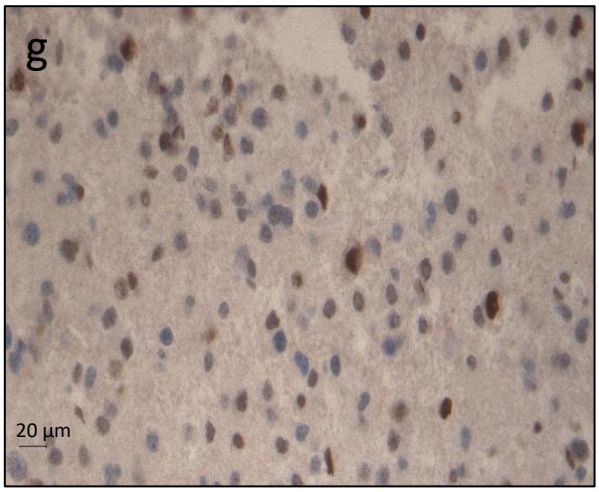

ATRX wildtype

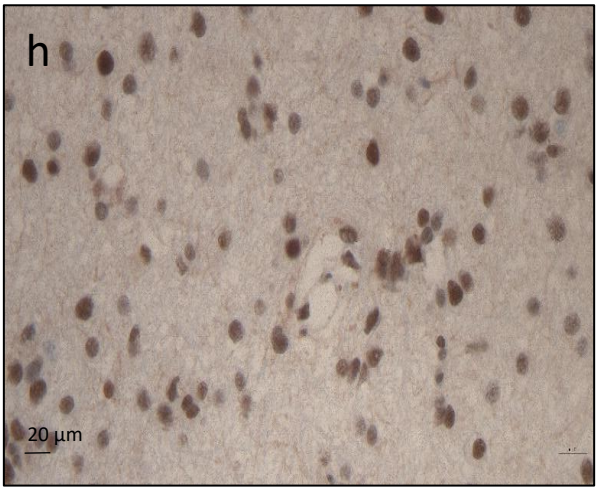

TERT C228T mutation

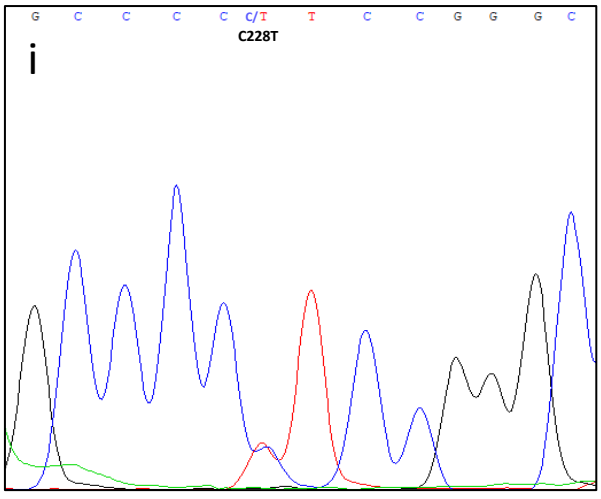

TERT C250T mutation

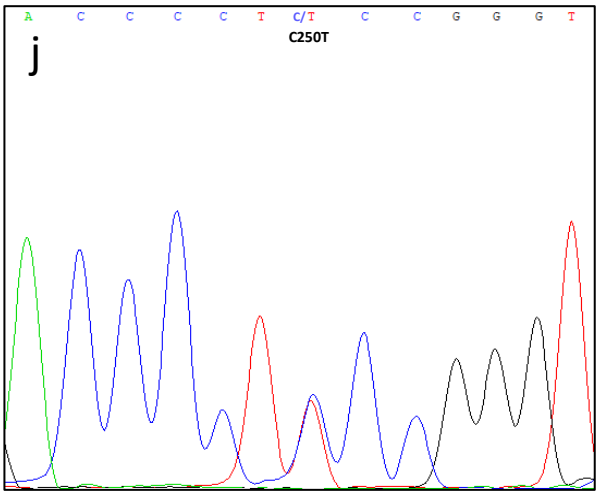

Fig. 7.
(e) *IDH1 R132H mutation*: Tumor cells with the IDH1 R132H mutation exhibit brown cytoplasmic staining (DAB reaction) due to the binding of the anti-IDH1 antibody, while nuclei are counterstained blue with hematoxylin.
(f) *IDH1 R132H wildtype*: IDH1 R132H wild-type cells show no brown cytoplasmic staining, but only blue nuclei due to hematoxylin counterstaining.
(g) *ATRX mutation*: ATRX-mutated cells (ATRX loss) show no brown nuclear staining, appearing exclusively blue due to hematoxylin counterstaining, indicating the absence of ATRX expression.
(h) *ATRX wildtype*: Tumor cells with intact ATRX expression exhibit brown nuclear staining due to the DAB reaction, while nuclei are counterstained blue with hematoxylin.
(i) *TERT C228T mutation*: The sequencing chromatogram shows overlapping peaks (C/T) at position 228, indicating a heterozygous C→T transition mutation in the TERT promoter; the majority of C228T mutations were found to be heterozygous.
(j) *TERT C250T mutation*: The sequencing chromatogram reveals overlapping peaks (C/T) at position 250, consistent with a heterozygous C→T transition mutation in the TERT promoter; the majority of C250T mutations were identified as heterozygous.

In line with the WHO 2021 classification for CNS tumors, selected molecular markers were used to guide both the classification and prognostic evaluation of glioblastoma (Table 3, Fig. 5–7). The IDH mutation status defines whether a tumor is classified as glioblastoma or IDH-mutant astrocytoma, whereas alterations such as TERT promoter mutations, MGMT promoter methylation and the Ki67 proliferation index offer clinically relevant insights into tumor behavior and response to therapy.

Morphological evaluation focused on key features such as necrosis and microvascular or macrovascular proliferation as illustrated in Fig. 6. All glioblastoma patients showed IDH wild type status and predominantly ATRX loss, assessed via immunohistochemistry. Notably, the TERT C228T mutation, determined by Sanger sequencing, was present in 73% of glioblastoma cases (Table 3, Fig. 5 and Fig. 7).

To gain insight into tumor aggressiveness, the proliferative activity was measured using the Ki67 index, reflecting the growth dynamics of malignant cells (Table 3, Fig. 5). Additionally, MGMT promoter methylation status, a critical factor guiding temozolomide therapy, was determined by methylation-specific PCR following bisulfite treatment, revealing methylation in 50% of patients within the cohort (Table 3, Fig. 5).

While these molecular features are not directly related to postoperative frailty, they provide an overview of the malignant potential and expected survival of the cohort (see Section 1.2), thereby offering the clinical context in which frailty-related biomarkers should be interpreted.

2.2 Patient Characterization by GFI and G8 Frailty Screening

A detailed analysis of how individual questions are weighted is crucial for determining which domains should be included in the Comprehensive Geriatric Assessment (CGA).

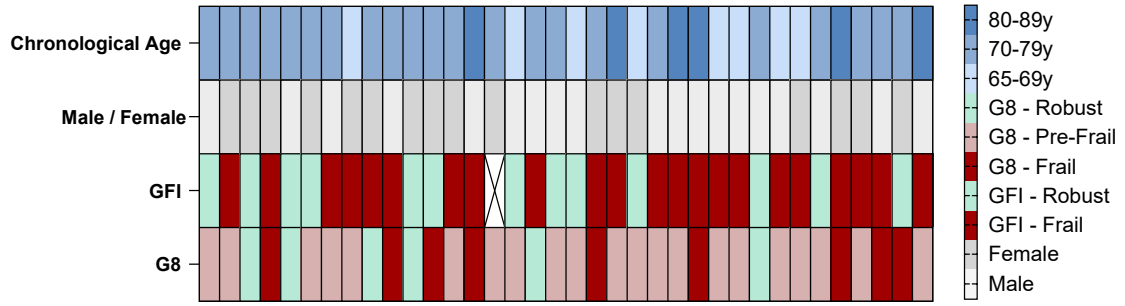

Fig. 8. Classification of patients as GFI-frail, GFI-robust (n = 35) & G8-frail, G8-pre-frail, or G8-robust (n = 36). *GFI* = Groningen Frailty Index; *G8* = Geriatric 8 Screening Tool.

Fig. 9. *Contributing to frailty*: A response of "1" increases the GFI frailty score; a higher score indicates greater frailty. *Not contributing to frailty*: A response of "0" decreases the GFI frailty score; a lower score indicates greater robustness. *Distribution of GFI scores (%)*: Percentage of responses relative to the total number recorded in the respective questionnaire.

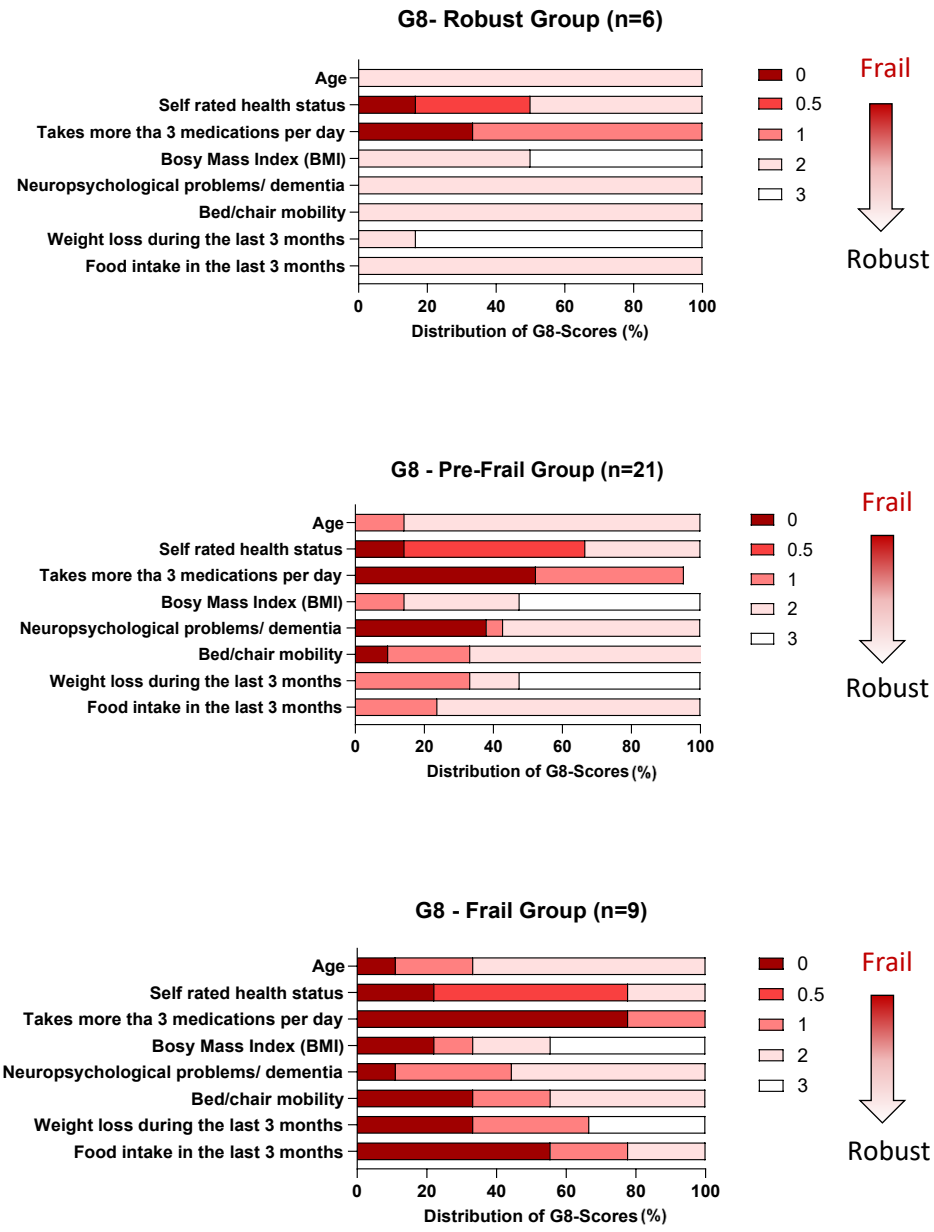

Fig. 10. Response options include the values 0, 0.5, 1, 2, or 3, depending on the question. Lower response values correspond to greater frailty, resulting in a lower G8 score. Conversely, higher response values increase the G8 score, indicating greater robustness. Distribution of G8 scores (%): Percentage of responses relative to the total number recorded in the respective questionnaire.

In summary, the frailty screening results indicate that frailty in this patient group is primarily driven by a combination of psychosocial, functional, and pharmacological factors. The GFI data indicate that psychosocial well-being accounted for more than 50% of frailty-related responses in the frail group, and still 30–45% in the robust group, underscoring its central role across the cohort (Fig. 9).

Functional impairments were also common: 40–45% of frail patients required assistance with daily tasks such as dressing and shopping (Fig. 9). Polypharmacy emerged as a strong correlate of frailty in both screening tools (Fig. 9, Fig. 10).

In the GFI-based assessment, 70% of frail patients reported taking more than four medications daily, compared to 40% among robust patients. The G8 tool confirmed this trend, showing that the proportion of patients taking more than three medications rose from one-third in the robust group to 50% in the pre-frail group and 80% in the frail group (Fig. 10).

These findings underscore the importance of expanding frailty assessments beyond physical function to include mental health, social support, and medication burden, thereby enabling a broader understanding of the origins of frailty.

2.3 Correlation of Candidate Biomarkers with Frailty Scores

To evaluate the potential of molecular biomarkers as complementary tools in frailty assessment, it is important to examine their correlation with established screening instruments. This comparison can reveal whether the biomarkers capture aspects of aging that are also reflected in the questionnaires.

2.3.1 Correlation of Epigenetic Age Acceleration with Frailty Scores

Table 4. Correlations of EAA, EEAA, and DunedinPACE with Frailty Scores (n = 25)

	GFI - Score			***G8 - Score***		
Correlation	***r^2***	***95% CI***	***p Value****	***r^2***	***95% CI***	***p Value****
EAA - GrimAge	*0.04497*	*-0.2751 to 0.8323*	*0.3088*	*4.713×10^{-5}*	*-0.5581 - 0.5762*	*0.9740*
EAA - PhenoAge	*0.01114*	*-1.809 to 1.094*	*0.6157*	*0.04158*	*-0.7397 - 2.121*	*0.3282*
EEAA	*0.001590*	*-1.242 to 1.032*	*0.8499*	*0.08260*	*-0.3321 - 1.850*	*0.1636*
DunedinPACE	*0.04626*	*-0.011 to 0.034*	*0.3019*	*0.002732*	*-0.020 - 0.026*	*0.8040*

Notes: CI = confidence interval*; EAA =* epigenetic age acceleration*; EEAA =* extrinsic epigenetic age acceleration*; GFI =* Groningen Frailty Index*; G8 =* Geriatric 8 Screening Tool*. Statistically significant correlations (p < 0.05) are marked with an asterisk (*).*

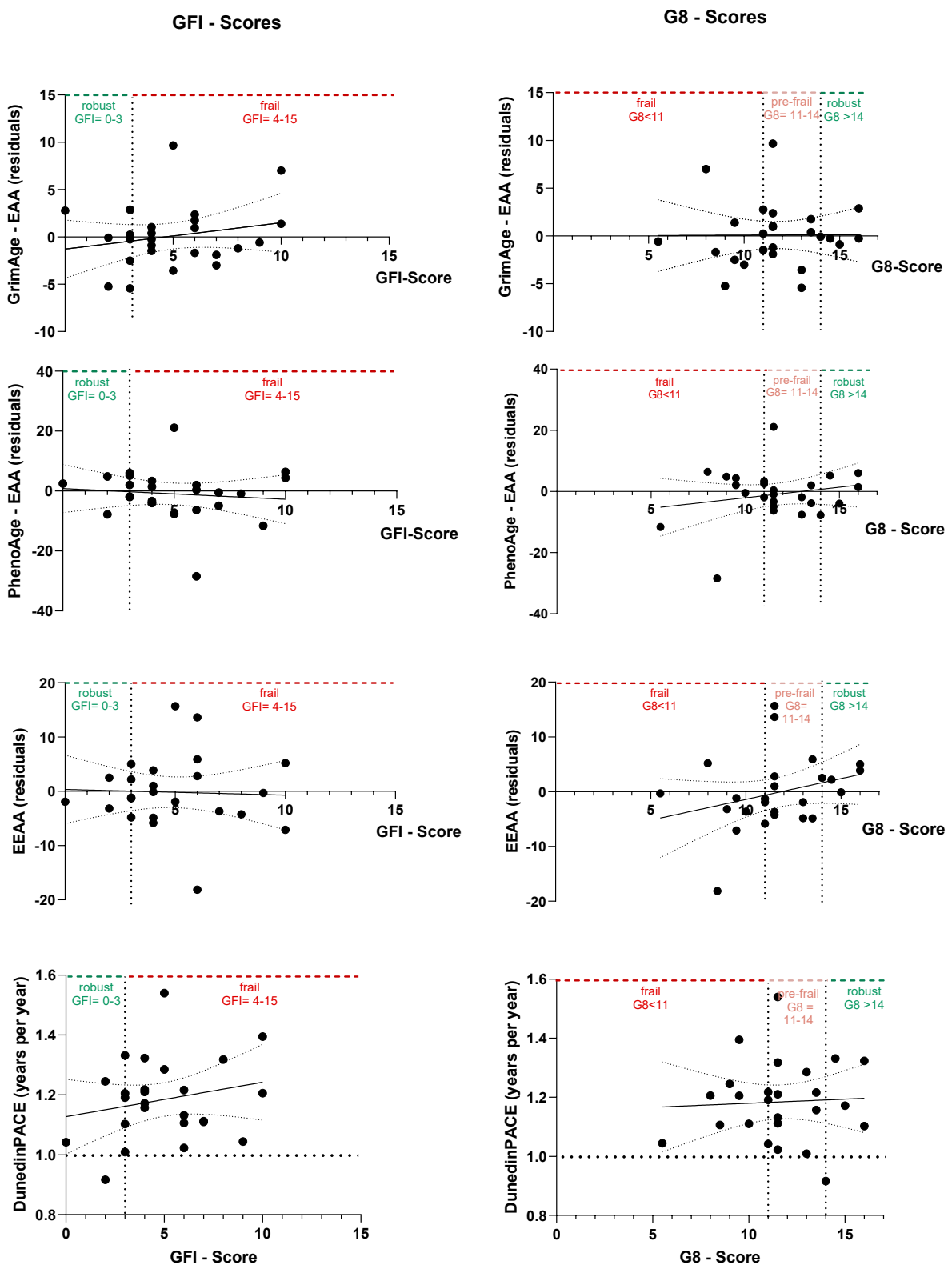

Fig. 11. *EAA* = epigenetic age acceleration (residual method); *EEAA* = extrinsic epigenetic age acceleration (residual method); *G8* = Geriatric 8 Screening Tool; *GFI* = Groningen Frailty Index.

The correlations of epigenetic age acceleration as measured by GrimAge, PhenoAge, extrinsic epigenetic age acceleration (EEAA), and DunedinPACE showed no significant

associations with GFI and G8 scores. However, GrimAge and DunedinPACE showed a trend toward higher age acceleration with increasing GFI scores, whereas no such trend was observed for the G8 screening tool (Table 4, Fig. 11).

This may be explained by the conceptual differences between the two frailty instruments. The G8 focuses on more physical clinical items and likely fails to capture the broader psychosocial and functional aspects of aging reflected in the GFI. Considering that GrimAge and DunedinPACE were developed in large, clinically and demographically heterogeneous population samples, incorporating systemic biological signals such as inflammation, metabolic stress, and cumulative life exposures (Belsky et al., 2022; Lu et al., 2019), it is plausible that these features align more closely with the multidimensional nature of the GFI, potentially accounting for the observed trends. Although these associations did not reach statistical significance, they warrant further investigation in larger and more age homogeneous cohorts.

2.3.2 Correlation of Telomere Length with Frailty Scores

2.3.2.1 Overview of Telomere Length Distribution (n = 28)

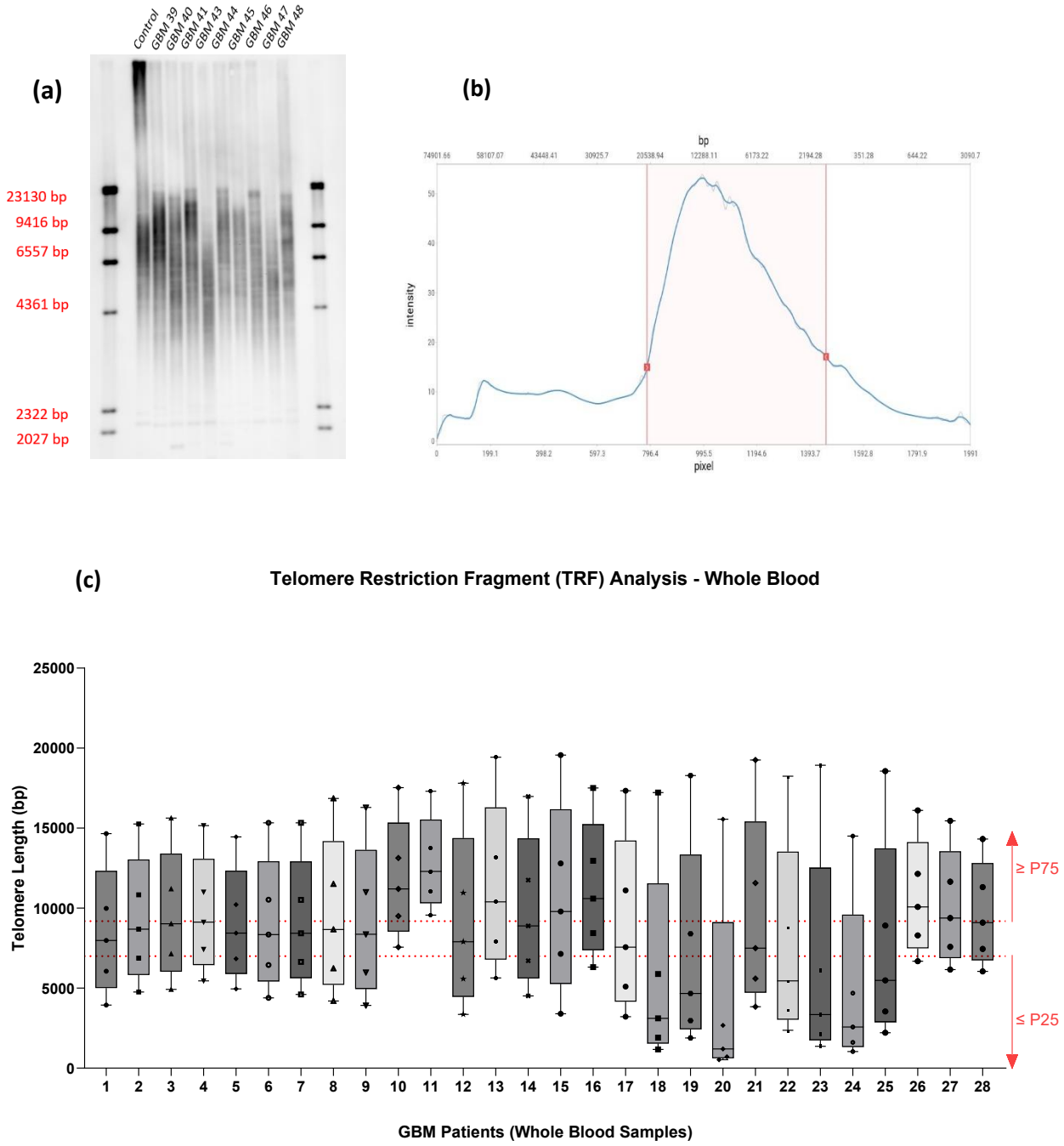

Fig. 12. (a) Southern blot analysis for TRF values were normalized to the respective gel-internal controls to allow comparability across samples. **(b)** Visualization of telomere length equilibrium, represented by a Gaussian distribution, generated using the WALTER online tool (Lyčka et al., 2021). The tool determines telomere length by analyzing intensity profiles and the pixel-based spatial distribution along the x- and y-axes. **(c)** Box plot showing telomere length distribution derived from TRF gel intensity profiles. Statistical parameters include the weighted median, interquartile range (P25 = 25th percentile, P75 = 75th percentile), and whiskers indicating minimum and maximum values. Dashed red lines represent the cohort's 75th (= P75) and 25th (= P25) percentiles.

2.3.2.2 *Correlation of Telomere Length with Frailty Scores*

Table 5. Correlation of TL parameters with Frailty Scores (n = 25)

	GFI - Score			G8 - Score		
Correlation	r^2	**95% CI**	***p* Value***	r^2	**95% CI**	***p* Value***
Mean TL	0.1268	-674.4 to 41.78	0.0807	0.2043	59.80 - 744.2	0.0233*
Median TL	0.1157	-716.5 to 62.86	0.0961	0.1965	54.50 - 798.2	0.0264*
First Quartile TL	0.09933	-641.8 to 83.44	0.1249	0.1413	-21.10 - 687.7	0.0640
Third Quartile TL	0.1380	-719.0 to 26.99	0.0675	0.2509	118.9 - 815.0	0.0108*

Notes: CI = confidence interval; *TL* = telomere length (bp*); G8* = Geriatric 8 Screening Tool; *GFI* = Groningen Frailty Index. Correlations were derived from simple linear regression analyses. Statistically significant correlations ($p < 0.05$) are marked with an asterisk (*).

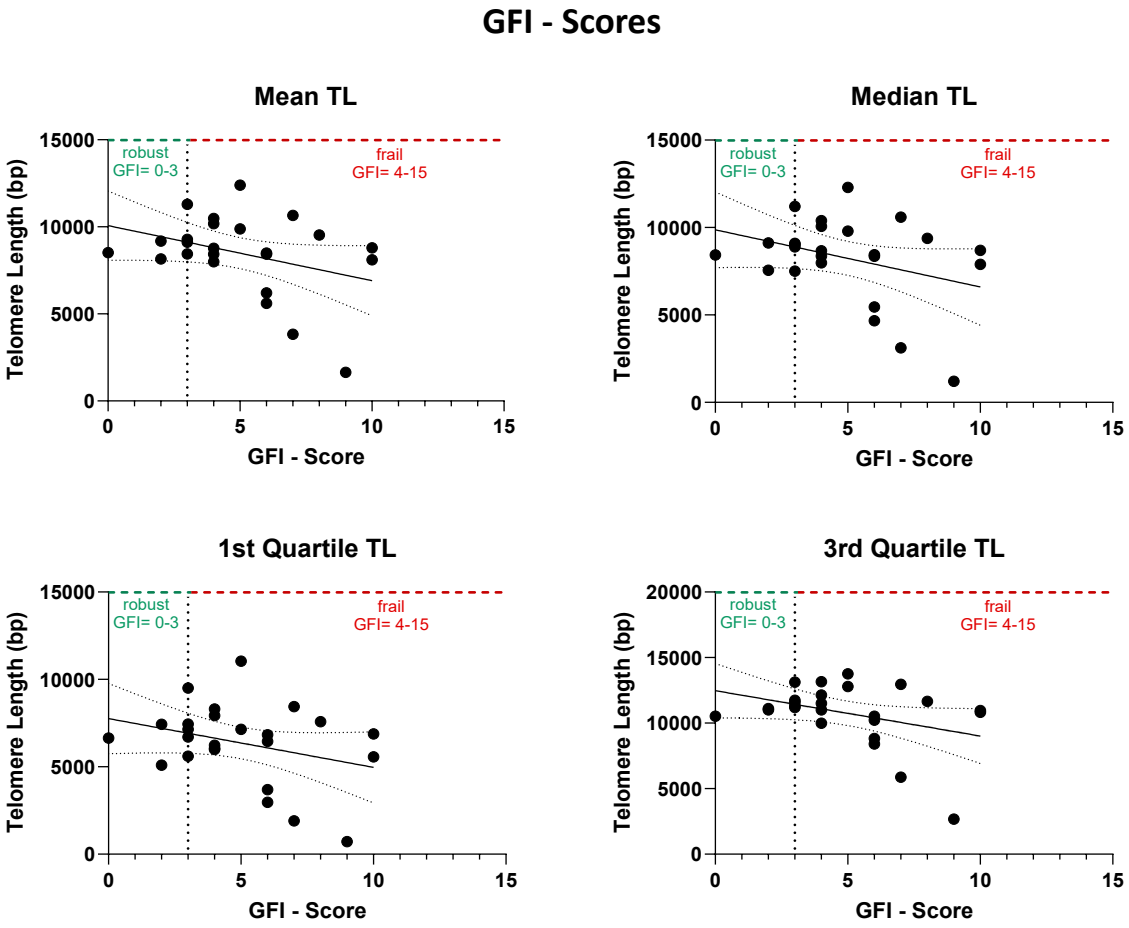

Fig. 13. *G8* = Geriatric 8 Screening Tool; *GFI* = Groningen Frailty Index; telomere length (TL) values were obtained from the analysis illustrated in Fig. 12c.

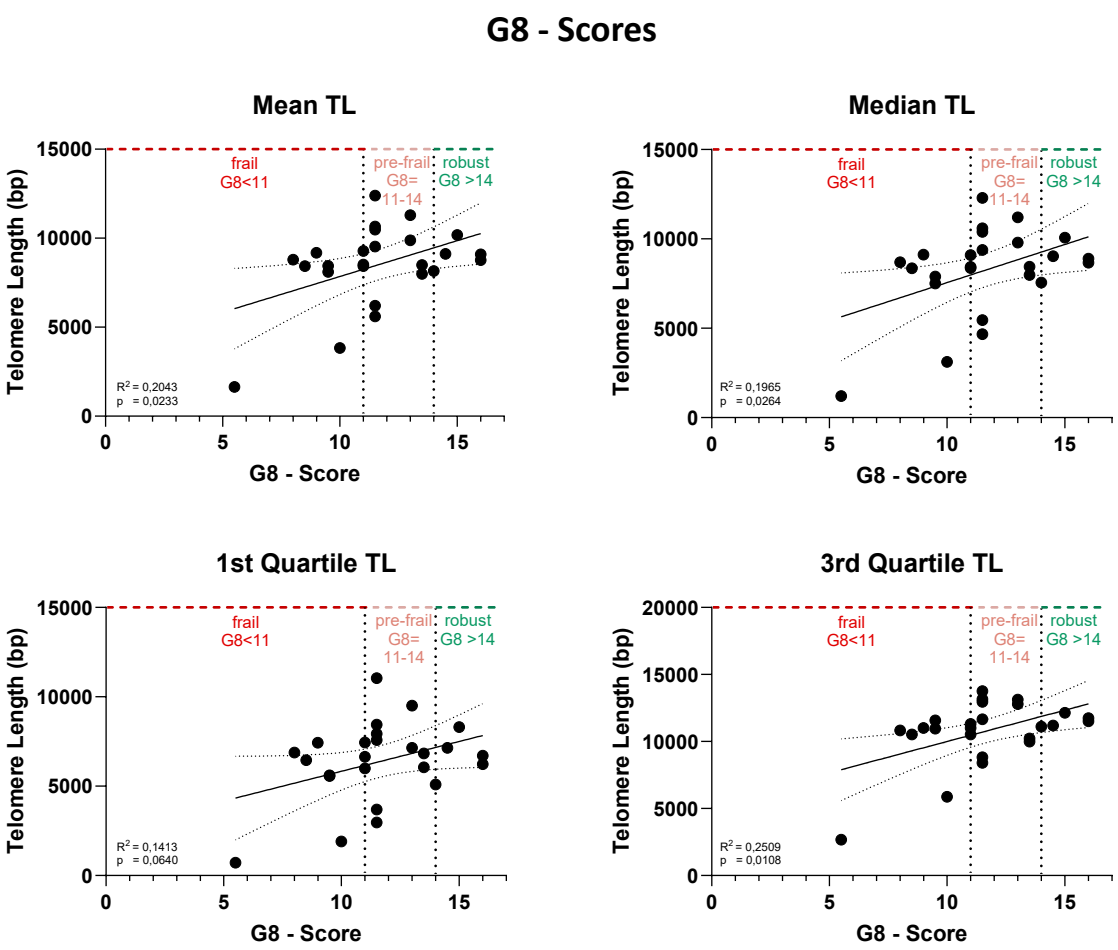

Fig. 14. *G8* = Geriatric 8 Screening Tool; *GFI* = Groningen Frailty Index; telomere length was obtained from the analysis illustrated in *Fig. 12c*.

In contrast to the epigenetic clocks, telomere length showed a significant negative correlation with the G8 score (mean TL: p = 0.0233; median TL: p = 0.0264; third quartile TL: p = 0.0108; Table 5, Fig. 14) and a non-significant trend with the GFI (Table 5, Fig. 13). Higher G8 scores were associated with longer telomeres. This may suggest that telomere attrition is more strongly related to physical aspects of frailty, as captured by the G8, which might also be more sensitive in detecting such associations in smaller cohorts. Nevertheless, the observed trend with the GFI indicates that telomere length may also reflect broader functional impairments beyond purely physical domains.

Previous studies have consistently linked telomere length with physical parameters such as mobility and weight loss (Njajou et al., 2012; Shin, 2019; Vieira et al., 2024) as well as with psychosocial factors like mood and perceived social support (Wilson et al., 2019). However, psychosocial assessments tend to be more subjective, variable, and context dependent, which

can increase response variability in instruments like the GFI. This greater variability might explain why larger sample sizes are necessary to detect significant correlations with the GFI compared to the G8 screening tool.

2.4 Impact of Frailty, Telomere Length, and Epigenetic Aging on Postoperative Outcomes

For the assessment of postoperative outcomes, both hospitalization duration and discharge decision making are used as key correlation parameters. Hospitalization duration refers to the total length of a patient's stay in the hospital following surgery and serves as a continuous clinical endpoint reflecting the patient's recovery speed. Analyzing how biological and clinical markers relate to hospitalization duration can provide insights into factors predicting prolonged recovery and support the optimization of individualized patient care (Fig.15-17).

In contrast, discharge decision making is a categorical clinical assessment based on the physician's evaluation of whether a patient is deemed capable of returning to their home environment, which is typically the preferred outcome or if they require further medical supervision and support after discharge. In some cases, this may involve permanent institutional care due to a lack of functional independence.

In the following analyses, discharge pathways are generally divided into Home Discharge (HD) and Post-Surgery Institutional Care (PSIC). The latter includes follow-up rehabilitation clinics, nursing home placements, and acute inpatient care such as intensive or palliative care (Fig. 18b–20).

2.4.1 Correlation of GFI and G8 Frailty Scores with Postoperative Hospitalization Duration

Table 6. Correlation of Frailty Scores with Postoperative Hospitalization Duration (n = 25)

	GFI - Score			G8 - Score		
Correlation	r^2	**95% CI**	***p* Value***	r^2	**95% CI**	***p* Value***
Mean TL (n=27)	0.06865	-1.617 to 0.3323	0.1868	0.01115	-1.262 – 0.7445	0.6001

Notes: CI = confidence interval; *G8* = Geriatric 8 Screening Tool; *GFI* = Groningen Frailty Index. Correlations were derived from simple linear regression analyses. Statistically significant correlations ($p < 0.05$) are marked with an asterisk (*).

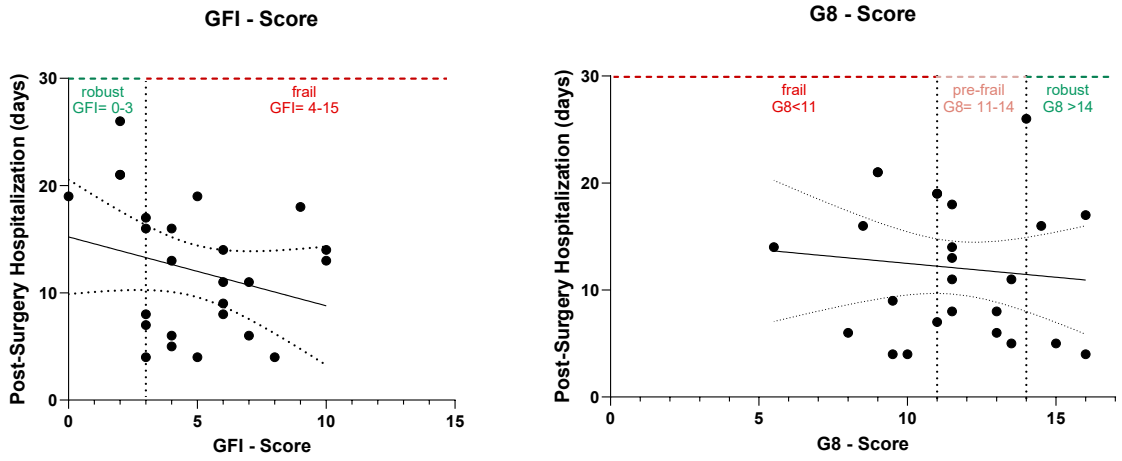

Fig. 15. *G8* = Geriatric 8 Screening Tool; *GFI* = Groningen Frailty Index.

No significant association was observed between either the GFI or the G8 scores and post-surgery hospitalization duration. Nonetheless, the G8 score exhibited a decreasing trend, suggesting that patients with higher robustness tend to experience shorter hospital stays (Table 6, Fig. 15). This observation may again reflect the G8's greater sensitivity in smaller cohorts, owing to its focused and standardized assessment of physical health. Alternatively, it may indicate that physical functioning plays a more direct role in discharge decision-making than psychosocial deficits, as it can be more readily assessed by clinicians.

2.4.2 Correlation of Epigenetic Age Acceleration and TL with Postoperative Hospitalization Duration

Table 7. Correlations of EAA, EEAA, and DunedinPACE with Postoperative Hospitalization Duration (n = 28)

Correlation	*r^2*	*95% CI*	*p Value**
EAA - GrimAge	*0.003098*	*-0.8304 - 0.6286*	*0.7785*
EAA - PhenoAge	*0.01664*	*-0.3657 - 0.1873*	*0.5129*
EEAA	*0.001479*	*-0.3156 - 0.3822*	*0.8459*
DunedinPACE	*0.1420*	*-31.33 - 0.1408*	*0.0481*
Mean TL (bp)	*0.01147*	*-0.001202 - 0.0006953*	*0.5875*

Notes: CI = confidence interval; *EAA =* epigenetic age acceleration*; EEAA =* extrinsic epigenetic age acceleration; TL = Telomere Length; Correlations were derived from simple linear regression analyses. Statistically significant correlations ($p < 0.05$) are marked with an asterisk (*).

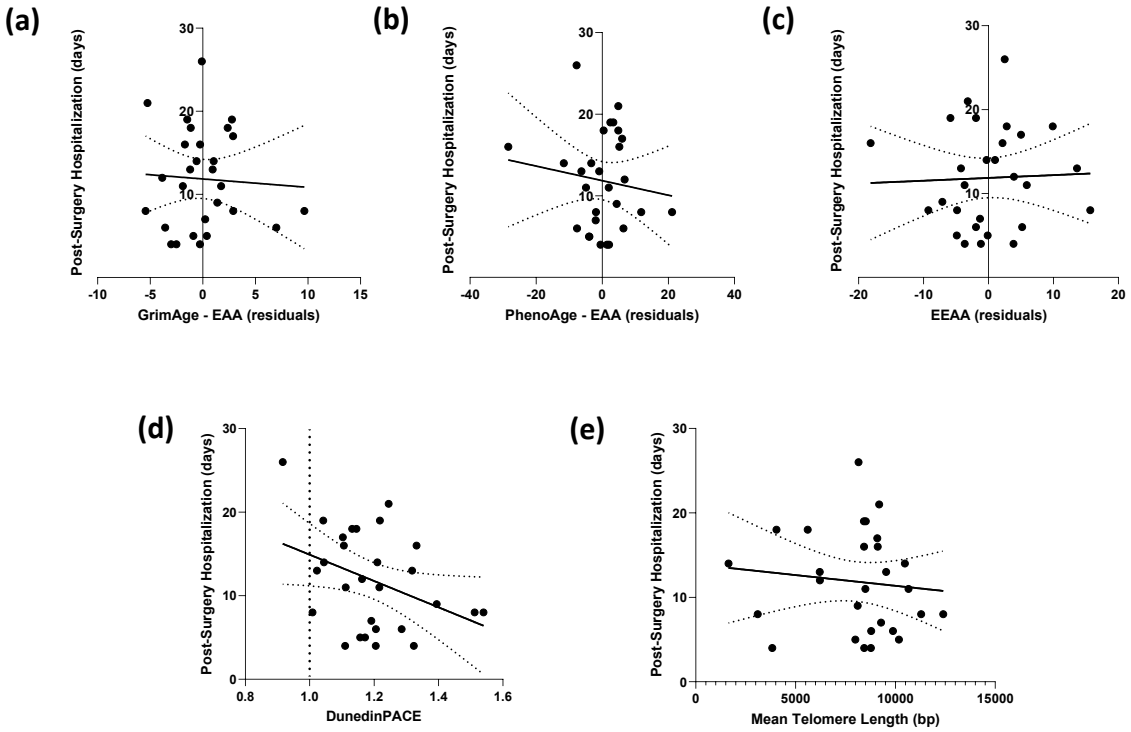

Fig. 16. EAA, EEAA, and TL vs. postoperative hospitalization duration

Shorter telomere length showed a non-significant trend toward longer postoperative hospital stays (Fig. 16e). Similarly, higher extrinsic epigenetic age acceleration (EEAA) was associated with a tendency toward prolonged hospitalization and discharge to institutional care. Both measures may reflect aspects of cellular and immune senescence relevant to postoperative recovery.

2.4.3 Impact of Frailty, Epigenetic Age Acceleration, and Telomere Length on Postoperative Hospitalization Duration

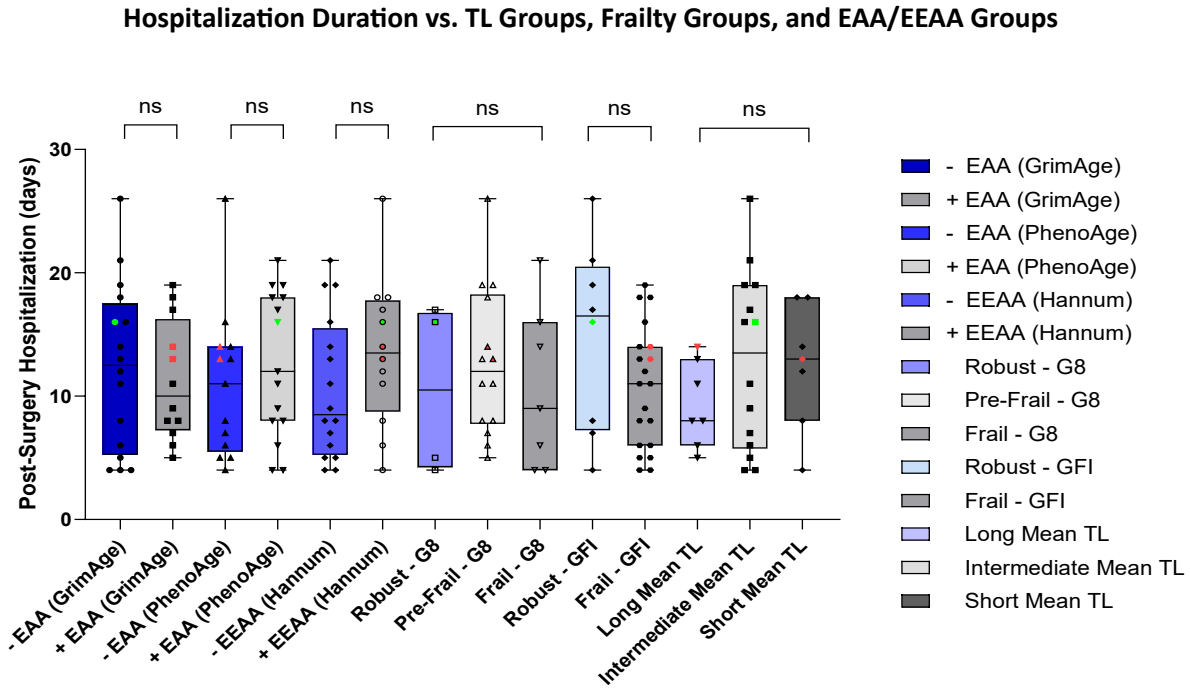

Fig. 17. *G8* = Geriatric 8 Screening Tool; *GFI* = Groningen Frailty Index; *-EAA/EEAA* = slower-than-expected age acceleration (residual method); *+EAA/EEAA* = faster-than-expected age acceleration (residual method*); Long Mean TL* = mean telomere length (TL) ≥ 75th percentile*; Intermediate Mean TL* = mean TL between the 25th and 75th percentiles; *Short Mean TL* = mean TL ≤ 25th percentile; Hospitalization duration: Mean TL = Median TL; *Red dots* = transfer to other hospital units, such as the intensive care unit or palliative care unit; *Green dots* = transfer to a nursing home.

Fig. 17 presents boxplots illustrating the distribution of postoperative hospitalization duration across subgroups defined by molecular biomarkers and frailty assessments. Patients were classified into slow and fast agers based on GrimAge, PhenoAge, and EEAA (Hannum) epigenetic clocks, stratified by frailty status according to GFI and G8 scores, and grouped by

telomere length categories. This allows for comparison of hospitalization durations between molecular biomarker and frailty subgroups.

Overall, no notable differences were observed in hospitalization duration between the groups. However, the +EEAA-PhenoAge group had a higher median hospitalization duration (12 days) compared to the -EAA-PhenoAge group (11 days), without reaching conventional levels of significance. Similarly, the median length of hospital stay in the +EEAA-Hannum group (13.5 days) was longer than in the -EEAA-Hannum group (8.5 days).

Regarding frailty screenings, the G8-Pre-Frail group had a longer median hospital stay (12 days) compared to the G8-Robust group (10.5 days), but the difference was not statistically confirmed. Likewise, in the group with short telomeres, a longer hospital stay (13 days) was observed compared to the group with long telomeres (8 days), without reaching statistical thresholds.

2.4.4 Impact of Postoperative Hospitalization Duration and Frailty Scores on Discharge Decision-Making

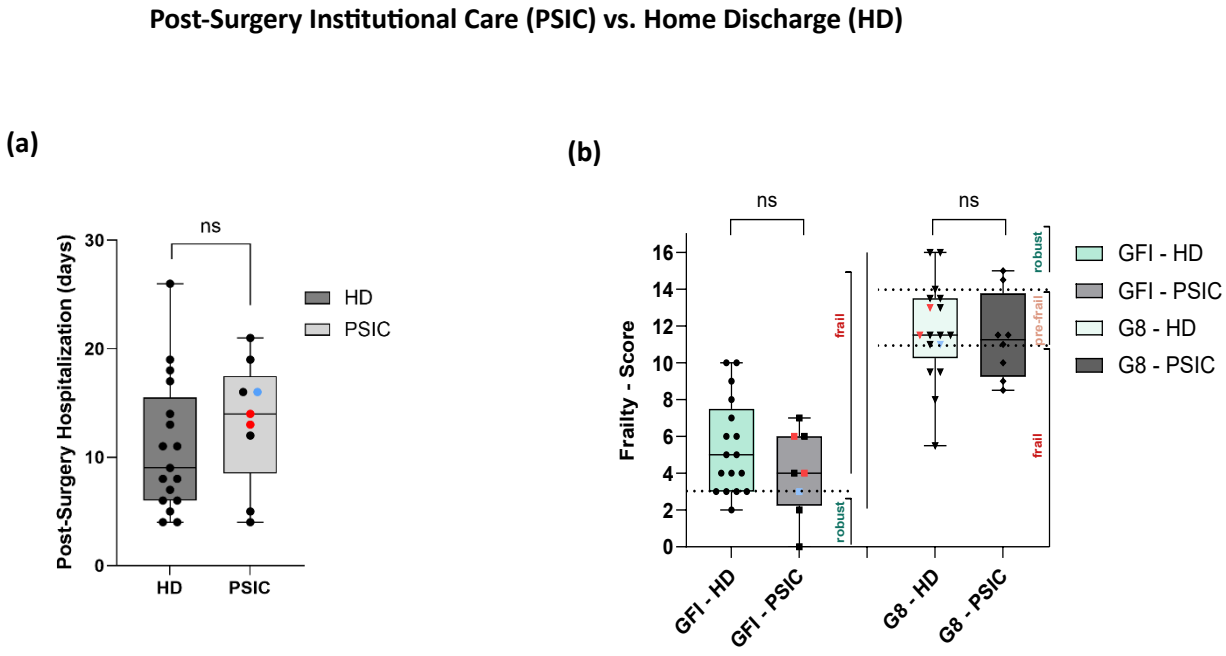

Fig. 18. *G8* = Geriatric 8 Screening Tool; *GFI* = Groningen Frailty Index; *HD* = home discharge; *PSIC* = post-surgery institutional care, which includes the following: *Black dots* = Transfer to an external rehabilitation clinic for follow-up treatment; *Red dots* = transfer to other hospital units, such as the intensive care unit or palliative care unit; *Blue dots* = transfer to a nursing home.

2.4.5 Impact of Epigenetic Age Acceleration and Telomere Length on Discharge Decision-Making

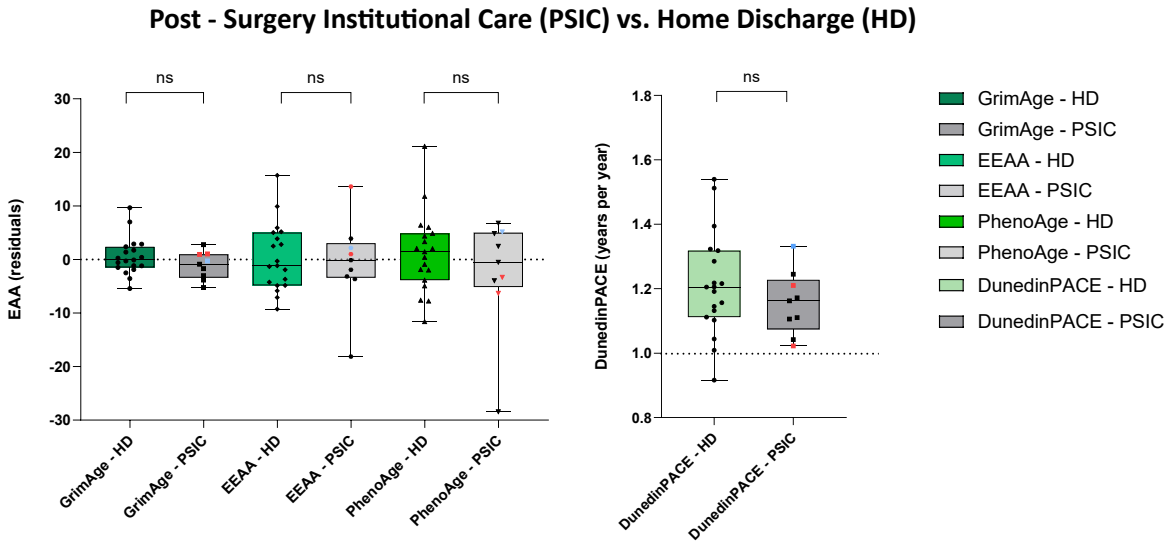

Fig. 19. *EAA* = epigenetic age acceleration based on the residual method; *EEAA* = extrinsic epigenetic age acceleration based on the residual method; *HD* = home discharge; *PSIC* = post-surgery institutional care, which includes the following: *Black dots* = transfer to an external rehabilitation clinic for follow-up treatment; *Red dots* = transfer to other hospital units, such as the intensive care unit or palliative care unit; *Blue dots* = transfer to a nursing home.

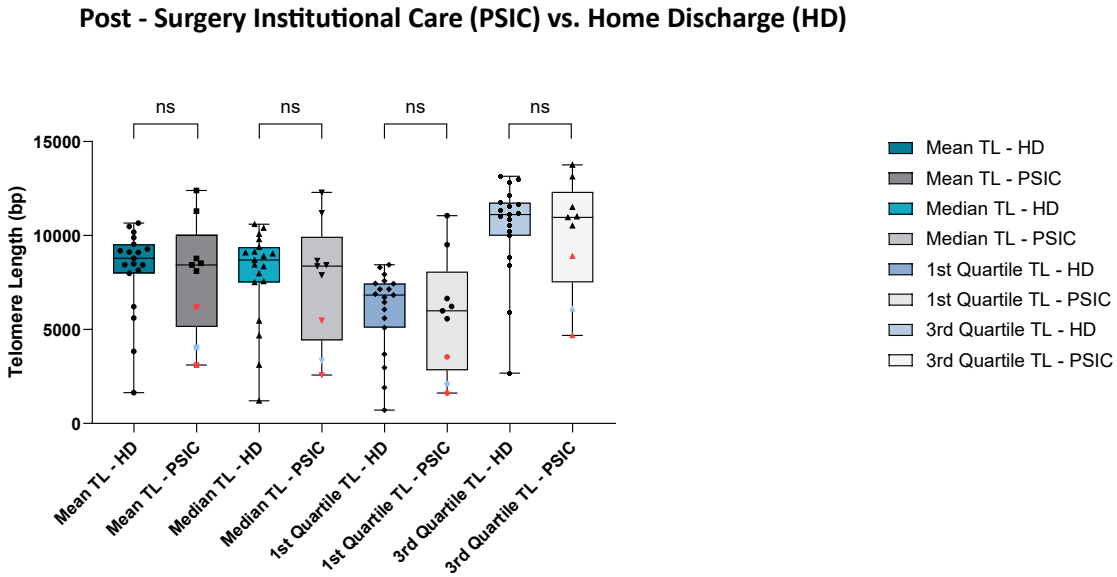

Fig. 20. *TL = telomere length (bp); HD* = home discharge; *PSIC* = post-surgery institutional care, which includes the following: *Black dots* = transfer to an external rehabilitation clinic for follow-up treatment; *Red dots* = transfer to other hospital units, such as the intensive care unit or palliative care unit; *Blue dots* = transfer to a nursing home.

Fig. 18a shows the median hospitalization duration in the Home Discharge (HD) group (10.94 days) to be slightly lower than in the Post-Surgery Institutional Care (PSIC) group (13.33 days), though this difference is not statistically significant. This suggests that patients requiring post-surgery institutional care may have more complex recovery needs contributing to longer hospital stays.

Building on this assumption, the correlation between discharge groups and their association with molecular markers was examined (Fig. 18b-20). While the findings did not reach conventional significance levels, the analysis of telomere lengths stands out (Fig. 20). High risk patients who require intensive care, palliative care, or nursing home placement (red and blue dots) exhibit the shortest mean and median telomere lengths within the PSIC group (Fig. 20). These findings emphasize the importance of further investigating the PSIC group in a larger cohort.

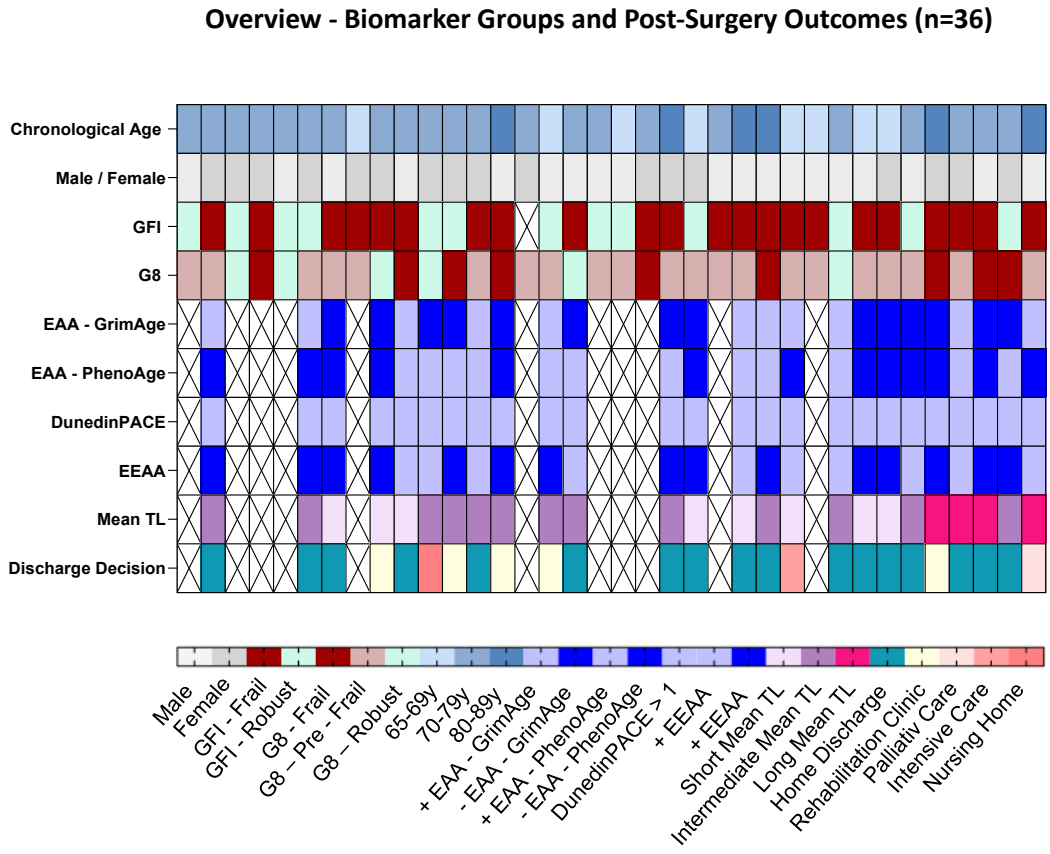

Fig. 21. *G8* = Geriatric 8 Screening Tool; *GFI* = Groningen Frailty Index; *−EAA/EEAA* = slower-than-expected age acceleration (residual method); *+EAA/EEAA* = faster-than-expected age acceleration (residual method); *Long TL* = telomere length ≥ 75th percentile; *Intermediate TL* = 25th–75th percentile; *Short TL* = ≤ 25th percentile.

2.5 Survival Analysis

2.5.1 Impact of MGMT Methylation and TERTp Mutation Status on Overall Survival (OS) and Progression-Free Survival (PFS)

Since MGMT methylation status is a key prognostic marker for overall survival in glioblastoma therapy (Drexler et al., 2023; Malmström et al., 2012b; Uno et al., 2011), the analysis initially focused on its prognostic value within the cohort. The endpoints were overall survival (OS) and progression-free survival (PFS). OS was defined as the time from recruitment to either death or the end of the observation period, while PFS was measured from recruitment to the first tumor progression.

Given its strong performance in predicting lifespan (Lu et al., 2019) and outperforming other epigenetic clocks in this regard (McCrory et al., 2021), GrimAge was evaluated as a potential prognostic biomarker beyond its established role in reflecting postoperative functional status. The analysis specifically examined whether GrimAge could provide additional stratification within MGMT-methylated and unmethylated subgroups, thereby offering further insight into survival outcomes.

Table 8. Kaplan-Meier Survival Analysis Stratified by MGMT Methylation Status (n = 39)

Group	Median OS (days)	HR (95% CI)	*p* Value*
MGMT Methylated (n = 20)	393	2.068 (1.005 - 4.259)	0.0956
MGMT Unmethylated (n = 19)	190	Reference	
	Median PFS (days)	**HR (95% CI)**	***p* Value***
MGMT Methylated (n = 20)	237.5	1.513 (0.7643 - 2.994)	0.4040
MGMT Unmethylated (n = 19)	157.0	Reference	

Notes: CI = confidence interval; *HR* = hazard ratio; *OS* = overall survival; *PFS* = progression-free survival. Statistical significance was assessed using the log-rank (Mantel–Cox) test with $\alpha = 0.05$, with statistically significant correlations indicated by an asterisk (*, $p < 0.05$).

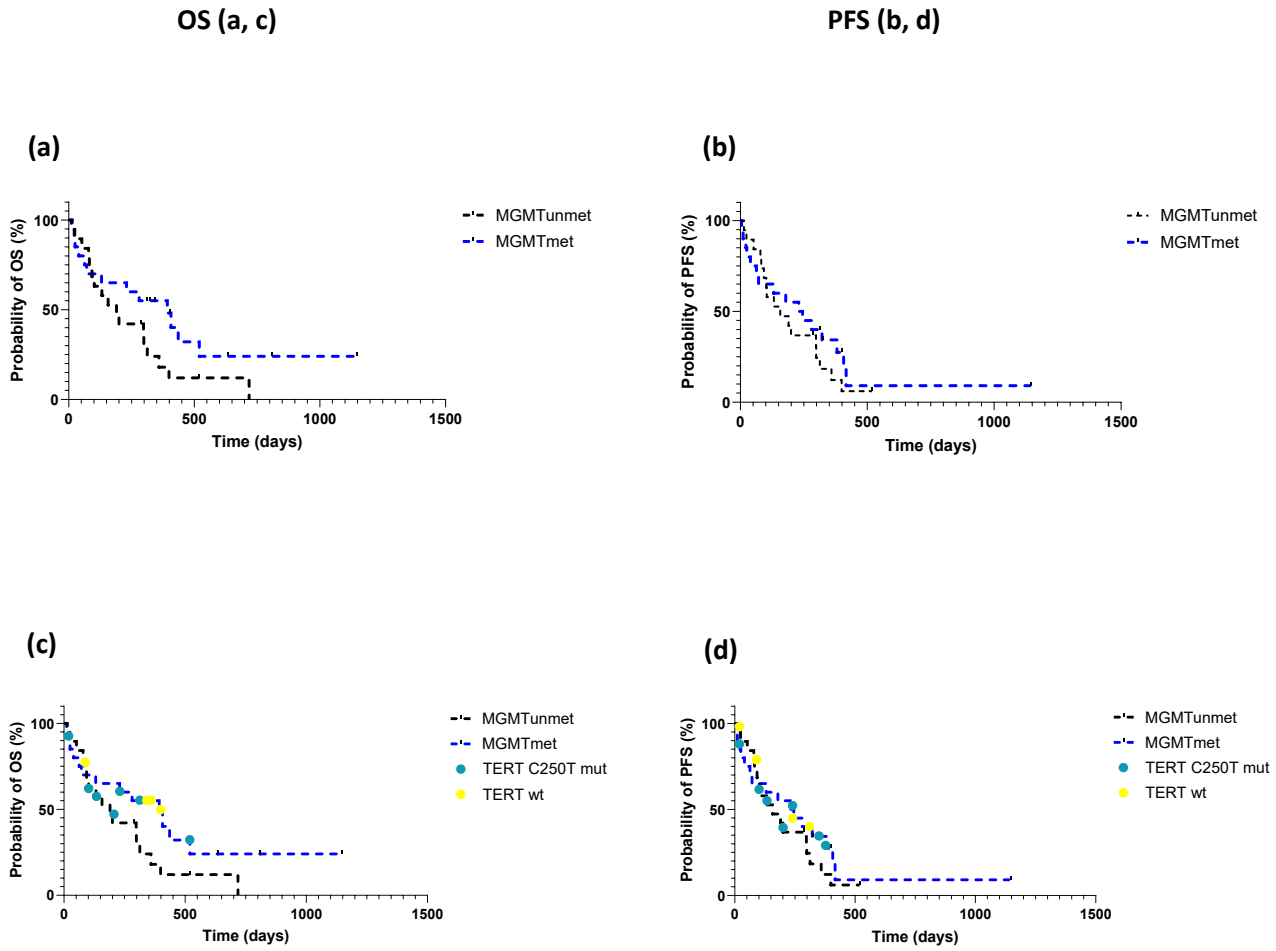

Fig. 22. *MGMTunmet* = MGMT unmethylated; *MGMTmet* = MGMT methylated; *OS* = overall survival; *PFS* = progression-free survival; *green dots* = TERT C250T mutation (mut); *yellow dots* = TERT wildtype (wt); unmarked patients carry the TERT C228T mutation. **(a)** OS by MGMT status; **(b)** PFS by MGMT status; **(c)** OS by MGMT status and TERT subclassification (green dots = TERT C250T, yellow dots = TERT wt); **(d)** PFS by MGMT status and TERT subclassification.

Table 9. Survival Data Stratified by TERTp Mutation Status and TERT Wildtype Status (Fig. 22c, Fig. 22d)

Fig. 22 (c)			**Fig. 22 (d)**		
MGMTunmet			***MGMTunmet***		
TERTp mut	**OS (days)**	**Event Status** Death; Alive; Unknown	***TERTp mut/wt***	**PFS (days)**	**Event Status** Death; Alive + TP; Alive + no TP; Unknown
C250T [1]*	102	Death	*C250T [1*]*	102	Death
C250T [2]*	190	Death	*C250T [2*]*	190	Death
C250T [3]*	132	Death	*C250T [3*]*	132	Death
TERT-wt	82	Death	*TERT-wt*	82	Death
MGMTmet			***MGMTmet***		
C250T [1]*	11	Death	*C250T [1*]*	11	Death
C250T [2]*	230	Death	*C250T [2*]*	230	Death
C250T [3]*	520	Death	*C250T [3*]*	381	Death
C250T [4]*	325	Unknown	*C250T [4*]*	325	Unknown
TERTwt [1]*	393	Death	*TERTwt [1*]*	245	Death
TERTwt [2]*	342	Alive	*TERTwt [2*]*	5	Alive+ TP
TERTwt [3]*	313	Unknown	*TERTwt [3*]*	313	unknown

Notes: MGMTunmet = MGMT unmethylated; *MGMTmet* = MGMT methylated; *OS* = overall survival; *PFS* = progression-free survival; *TERTp mut/ TERT wt* = TERT promotor mutation/TERT wild-type; *TP* = tumor progression; *C250T [1*]* = patient case 1 with a TERT C250T mutation; *TERTwt [1*]*= patient case 1 with TERT wild-type status. The superscript number (n) indicates the individual patient case, numbered sequentially.

A tendency was observed toward longer survival in the MGMT-methylated group compared to the unmethylated group (Fig. 22a,b). However, it is important to consider the heterogeneity of treatment regimens, particularly regarding the number of radiotherapy and chemotherapy cycles administered, which may limit the interpretability of these findings. Given that IDH wildtype gliomas with TERT wildtype status are associated with a more favorable prognosis (Eckel-Passow et al., 2015), an additional analysis was conducted to assess whether wildtype patients clustered at the extremes of the survival curves (Fig. 22c,d).

2.5.2 GrimAge-Based Analysis of Slow Agers in MGMT-Methylated and Unmethylated Subgroups

Table 10. Kaplan–Meier Survival Analysis Stratified by MGMT Methylation Status and Further Stratified by GrimAge-Defined Slow Agers (n = 16)

Group	**Median OS (days)**	**HR (95% CI)**	***p* Value***
MGMT Methylated (n = 8)	520.0	3.599 (1.084 – 11.95)	0.0062**
MGMT Unmethylated (n = 8)	144.5	Reference	
	Median PFS (days)	**HR (95% CI)**	***p* Value***
MGMT Methylated (n = 8)	301.5	2.087 (0.7240 – 6.014)	0.1727
MGMT Unmethylated (n = 8)	144.5	Reference	

Notes: CI = confidence interval; *HR* = hazard ratio; *OS* = overall survival; *PFS* = progression-free survival. Statistical significance was assessed using the log-rank (Mantel–Cox) test with α = 0.05, with statistically significant correlations indicated by an asterisk (*, p < 0.05).

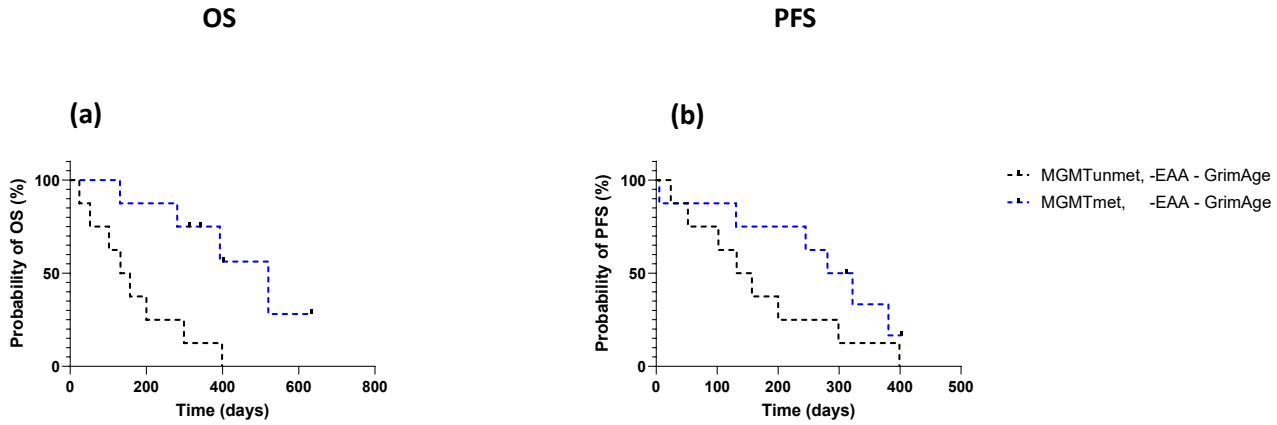

Fig. 23. *MGMTunmet* = MGMT unmethylated; *MGMTmet* = MGMT methylated; *OS* = overall survival; *PFS* = progression-free survival; *–EAA-GrimAge* = slower-than-expected age acceleration by GrimAge (residual method)

Stratification by the GrimAge clock revealed that slow agers in the MGMT-methylated group had significantly longer overall survival (520.0 days) compared to those in the unmethylated group (144.5 days; *p* = 0.0062; Table 10, Fig. 23a). While these findings are

promising, they should be interpreted with caution due to therapeutic heterogeneity within the cohort. Nonetheless, this additional layer of risk stratification underscores the relevance of assessing frailty beyond immediate postoperative function and highlights the importance of long-term frailty management throughout the entire treatment course (see Section 1.3.2).

3 Discussion

3.1 Study Design and Methodology

3.1.1.1 G8 and GFI for Risk Stratification

In this study, 27 out of 36 GBM patients classified as frail or pre-frail according to the G8 score were identified as high-risk patients (Fig. 10). In contrast, the GFI, which categorizes patients strictly as either frail or robust, identified only 22 patients as frail—five fewer than were identified with the G8 screening. This dichotomy risks underestimating high-risk patients while overestimating robust patients. As a result, some patients may be incorrectly deemed robust and therefore excluded from CGA screening, potentially leading to overlooked deficits and prolonged hospitalization. Compared to the GFI, the G8 tool enables a more nuanced risk stratification by including a pre-frail category and is thus better suited for identifying vulnerable patients in this cohort.

3.1.1.2 Predictive Value of G8 and GFI

There is no single “correct” frailty questionnaire; rather, different tools offer varying degrees of informative value. Despite the G8 screening’s superiority in risk stratification, the GFI provides valuable insights into the patient’s daily life at home, where the ability to live independently becomes critical. It focuses on self-care related questions such as “Can the patient do their own shopping?” and “Can they go to the toilet unaided?” These are essential considerations that must be taken into account before discharge, particularly for patients living alone. A gradual loss of independence in the home setting can go unnoticed and lead to serious consequences, including social isolation, declining health, and even death.

Therefore, both screenings should be incorporated into the next step of the CGA. Based on the findings indicating that polypharmacy, depressive symptoms, and difficulties in daily living reach prevalence rates of 40–70%, it is proposed that functional tests such as the Timed Get-Up-and-Go test (TGUG), Cumulative Illness Rating Scale for Geriatrics (CIRS-G), and Activities of Daily Living (ADL and IADL) be prioritized, alongside thorough medication reviews.

Interestingly, polypharmacy and psychosocial issues are not confined to high-risk patients alone. Even among patients classified as robust by both GFI and G8, polypharmacy is observed in approximately 30–40% of cases, increasing to approximately 75% in the G8 frail and GFI frail groups. Similarly, the GFI indicates that depressive symptoms affect 30–45% of robust patients, rising to 60–80% in the frail group. This suggests that frailty may initially manifest in specific domains and progressively affect others over time. It raises the question of whether robust patients might also benefit from a CGA, which warrants further investigation.

3.1.1.3 Limitations and Considerations

A critical limitation of the frailty screenings conducted in this study lies not so much in the use of questionnaire-based methods, but rather in the absence of integrated objective functional tests. For instance, Bessems et al. (2021) demonstrated that combining the Speed-Gait test with the G8 screening tool improves the precision of risk stratification.

Relying exclusively on self-reported questionnaires also carries the risk of random or systematically biased responses. Without complementary objective measurements, it remains uncertain whether the recorded information accurately reflects the patient's functional condition or is influenced by subjective perception, cognitive impairment, or social desirability bias.

3.1.2 Importance of Longitudinal Blood Analysis for Frailty Dynamics

The telomere data in Fig. 16e and Fig. 20 suggest a possible link between cellular aging and delayed recovery. It may be worthwhile to explore whether telomere length changes over time in response to surgical stress and the postoperative rehabilitation measures carried out by clinical staff.

Similarly, while the associations between epigenetic clocks and hospitalization duration were inconclusive, it remains an open question whether epigenetic age acceleration slows during postoperative recovery. Although residuals offer a snapshot of deviation from the expected epigenetic age within a cohort, a longitudinal design with repeated measurements

would be better suited to assess the individual “tick rate” of biological aging. Confirming this would require sample collection at clearly defined clinical time points: before surgery, at discharge, and prior to the start of further oncological treatment, as outlined in Section 1.3.2, Fig. 4.

The following sections provide a detailed discussion of both molecular domains, highlighting their biological significance, methodological limitations, and potential utility in frailty assessment among older GBM patients.

3.2 Telomere Length Analysis: Biological and Methodological Considerations

3.2.1 Telomere Heterogeneity Across Cell Types

Telomere length was analyzed in whole blood samples, as this approach proved more feasible within the clinical setting of the study. However, due to the high cellular heterogeneity of whole blood, peripheral blood mononuclear cells (PBMC) are generally preferred for telomere length measurements. The PBMC fraction includes lymphocytes, monocytes, $CD4^+$ and $CD8^+$ T cells, each of which displays different telomere lengths depending on their physiological characteristics. Previous studies have shown that lymphocytes, in particular, undergo more pronounced telomere shortening with age compared to granulocytes (Baerlocher et al., 2003; Rufer et al., 1999).

However, telomere length in PBMCs is influenced not only by biological aging but also by changes in the immune system. Acute inflammatory conditions, such as infections, alter the composition of leukocytes, resulting in a higher proportion of naive leukocytes in circulation (Vaiserman & Krasnienkov, 2021). Their telomere length is comparable to that of hematopoietic stem cells, while mature leukocytes have significantly shorter telomeres (Kimura et al., 2010). As these shifts cannot be clearly attributed to a specific pathological condition (Hastings et al., 2017; Krasnienkov et al., 2018) drawing conclusions about the underlying aging mechanism becomes even more challenging.

Another important factor is the cumulative immune burden, which is shaped by the patient's medical history and modulated by environmental factors (Vaiserman & Krasnienkov, 2021). $CD8^+$ T cells play a crucial role in this process. While naive $CD8^+$ T cells have relatively long telomeres, these become progressively shorter as the cells differentiate into memory $CD8^+$ T cells that have already undergone several division cycles (Chen et al., 2017). Evidence suggests that, at a given age, some individuals show a higher proportion of memory $CD8^+$ T cells in the bloodstream, which is associated with relatively shorter telomeres (Chen et al., 2017).

Given the use of whole blood in the GBM study, long-term immunological changes were partially addressed by incorporating extrinsic epigenetic age acceleration (EEAA) as a biomarker complementing telomere length. EEAA estimates biological aging while accounting for immune cell composition, particularly the proportion of $CD8^+$ T cells. Interestingly, the data revealed a slight trend toward longer hospitalization durations in GBM patients with higher EEAA values, although this finding requires validation in larger cohorts.

Beyond the role of immune cells, it remains unclear whether telomere length in PBMCs accurately reflects telomere length in other tissues (Vaiserman & Krasnienkov, 2021). Research suggests that this is not always the case, particularly in tissues with low proliferative activity, such as the central nervous system, which is essential for the aging process (Lukens et al., 2009). This raises the question of how far cognitive decline in GBM patients can be meaningfully linked to telomere length measured in blood, an important consideration given that around 40% of GBM patients in the G8 pre-frail group reported cognitive or neuropsychological impairments.

In summary, future studies should aim to combine PBMC isolation with immunophenotyping techniques such as $CD4^+$ and $CD8^+$ profiling via flow cytometry, alongside single-cell RNA sequencing, to determine whether changes in mean telomere length reflect immune cell population shifts or true shortening within specific cellular states. Integrating such analyses helps to improve the interpretability of telomere measurement methods, which will be discussed in the next subsection.

3.2.2 Limitations of Conventional Methods

The main challenge in utilizing leukocyte telomere length as a biomarker lies less in understanding telomere biology and more in the methodological aspects of its measurement and data interpretation. Standard techniques such as qPCR, Flow-FISH, and the TRF method primarily measure mean telomere length (Yu et al., 2024), thereby overlooking the inherent variability in telomere length within a single sample.

Considering that a blood sample contains between 100,000 and 200,000 leukocytes, this equates to roughly 10 million telomeres. Some of these telomeres are critically short, while others remain long even at an advanced age. The measurement of mean telomere length, therefore, provides only a one-dimensional picture. Two individuals may have the same mean telomere length, but one individual may show a relatively uniform telomere length profile, while another has a mixture of extremely short and exceptionally long telomeres. Equating these two individuals would ignore the heterogeneity of telomere length across different biological states and aging trajectories (Levine, 2022).

The TRF method used in this study is widely regarded as the gold standard for measuring telomere length, as it captures the entire distribution of telomere sizes. However, it has a detection limit of approximately 23 kb and tends to systematically overestimate true telomere length because the restriction enzymes used also cleave subtelomeric regions (Aubert et al., 2012).

Studies report overestimations of several thousand base pairs (Sanchez et al., 2024), depending on the cell type and the specific restriction enzymes used. Additionally, very short telomeres below 2 kb are difficult to detect due to low hybridization efficiency (Lai et al., 2018).

While Flow-FISH offers improved precision over TRF, it still tends to overestimate length measurements by around 1,500 base pairs, likely due to its adjustment to Southern blot data (Sanchez et al., 2024). PCR-dependent assays such as STELA and TeSLA, on the other hand, are constrained by the run length of the DNA polymerase and primarily detect shorter telomeres, failing to capture the complete telomere length distribution within a sample (Sanchez et al., 2024).

Given these complementary strengths and limitations, a combined application of TRF and TeSLA may provide a more comprehensive picture. This approach enables the

identification of GBM patients with critically short telomeres, who are likely underrepresented in the TRF data generated in this study, while still allowing for the assessment of longer telomeres.

Another relevant question is whether telomere shortening occurs uniformly across all chromosomes or whether specific chromosome arms are more affected than others. The chromosome-specific heterogeneity (Lansdorp et al., 1996) remains constant throughout the entire lifespan (Graakjaer et al., 2004). Graakjaer and his colleagues (2006) demonstrate that despite "telomerase-mediated maintenance in germ cells, allele-specific relative telomere lengths are preserved in the next generation." This conclusion is based on Q-FISH data, although the analysis was confined to a small set of polymorphic subtelomeric markers.

To further pursue questions of telomere length heritability, alongside individual influences from lifestyle and environmental factors, high-resolution sequencing is currently being implemented. Modern long-read sequencing technologies such as PacBio HiFi and Oxford Nanopore, have proven valuable for detailed telomere analysis, enabling researchers to measure telomeres at a higher resolution (Grigorev et al., 2021; Luxton et al., 2020; Sholes et al., 2022; Tham et al., 2023).

These methods are capable of capturing both short telomeres (<2 kb), which are difficult to detect using TRF, and very long telomeres (>20 kb) (Oxford Nanopore Technologies, 2024), typically using reads in the 10–20 kb range (Hon et al., 2020; Jain et al., 2018; Logsdon et al., 2020; Wang et al., 2021).

Approaches such as Telogator (Stephens et al., 2022), a bioinformatic tool that analyzes existing long-read data, and Telo-seq (Oxford Nanopore Technologies, 2023), an adapter-based sequencing protocol for capturing full-length telomeres, have contributed to major advancements in this field. Nevertheless, challenges remain, particularly in improving the accuracy of base identification (Stefan et al., 2022) and developing more effective enrichment strategies prior to sequencing (Ferrer et al., 2023).

3.3 Epigenetic Age Analysis: Biological and Methodological Considerations

3.3.1 Integrating Epigenetic Markers and Clinical Assessments in Frailty Evaluation

The epigenetic clock approach offers an alternative to the traditional strategy of selecting only a few carefully chosen biomarkers. Instead, microarray-based methods capture a broad range of molecular biomarkers simultaneously. The technical robustness of this method enables standardized measurements and enhances comparability across laboratories.

However, it is important to emphasize that epigenetic data should never be interpreted in isolation, particularly when acute clinical decision making is required. Subjective reports of deficits, such as “Does dementia cause forgetfulness in taking medication for type 2 diabetes?”, can provide critical insight into imminent health risks like hyperglycemic shock. Additionally, conventional laboratory measures, such as blood glucose levels, remain indispensable.

In frailty research, the GrimAge clock has demonstrated its superior predictive performance, as shown, for example, in the TILDA study (McCrory et al., 2020). Compared to PhenoAge and Hannum, GrimAge more accurately predicted gait speed and Fried frailty status, particularly when adjusting for age, sex, and white blood cell composition (McCrory et al., 2020). This raises the question of whether such predictive strength also applies to older glioblastoma patients in a larger cohort, or whether newer measures like DunedinPACE might yield more refined insights in this specific patient population.

3.3.2 Methodological Considerations in Statistical Analysis of Epigenetic Age Acceleration

In the present study, a simple linear regression was used to investigate the correlation between frailty scores and the epigenetic clocks (Fig. 11). A multivariate regression analysis would be methodologically preferable to include covariates such as gender, age, BMI, and

other relevant factors. However, due to the small sample size of n=28 and the age heterogeneity within the cohort, a multivariate regression analysis was not performed, as it could have led to increased multicollinearity and overfitting of the model.

With reference to Fig. 17, which illustrates the correlation between epigenetic age acceleration (EAA) and hospitalization duration, a larger cohort would allow for the subdivision of the slow and fast ager groups into "Home Discharge" and "Post-Surgery Institutional Care (PSIC)" subgroups. This would facilitate an investigation into whether and to what extent EAA influences hospitalization duration depending on whether patients are discharged home or receive post-operative institutional care. It remains uncertain whether the classification of patients into slow and fast agers provides additional predictive value for discharge decisions, thereby influencing hospitalization duration beyond the discharge decision itself.

Additionally, it is worth noting that the "Post-Surgery Institutional Care" group includes not only patients transferred to rehabilitation clinics but also those who are moved to an intensive care unit, palliative care unit, or nursing home after surgery. A further subclassification into short-term and long-term institutional care within this group would be beneficial in a larger cohort, as intensive care patients have acute, life-threatening conditions that should be distinguished from “normal” rehabilitation patients. While nursing homes and palliative care units mark the final stage of care for geriatric oncology patients, reflecting a long-term loss of independence, intensive care unit stays are usually temporary.

3.3.3 Age-Related Epigenetic Changes: Cause or Consequence?

The question of whether age-related epigenetic changes actively drive aging by regulating gene expression or whether they are merely a consequence of aging remains unresolved. In particular, longitudinal studies capturing the rate of change in DNA methylation are needed to fully address this question. It is unclear whether individuals start with different baseline levels and age at the same rate, whether aging rates vary between individuals, as reflected in their methylation levels at a given time, or whether these rates differ during development, resulting in distinct methylation levels in adulthood that eventually stabilize (Levine, 2019).

To explore these questions further, Raj (2018) introduced a theoretical framework examining the potential causal role of epigenetic modifications in aging. He suggests that inducing specific epigenetic changes in a targeted manner could help determine whether such alterations are capable of initiating the aging process. However, the technology required to implement this approach is not yet available. Moreover, this approach would fail to capture a fundamental aspect highlighted by the epigenetic clock, namely that aging is not a synchronized, coordinated process across all cells, nor does it occur uniformly within all cells. Instead, aging is followed by epigenetic alterations in a small subset of cells over an extended period of time.

The epigenetic changes that persist after the completion of physical maturation could be considered remnants of a mechanism originally required for development. In adulthood, this process continues in a diminished form, resulting in cells that have lost their original functionality but remain active (Raj, 2018).

Several researchers, including Horvath (2013) and Teschendorff et al. (2010) have demonstrated that CpGs within promoters, which are regulated by Polycomb group protein 2 (PcG2) are subject to heightened methylation as age progresses. Specifically, Teschendorff identified 69 CpGs within these regions that become hypermethylated with age (Teschendorff et al., 2010). It has also been reported that CpG sites located within bivalent chromatin domains exhibit a significant enrichment of age-associated hypermethylation. These regions are characterized by the presence of H3K4me3, as an activating mark, and H3K27me3, a repressive one (Rakyan et al., 2010).

Both loci show an increased methylation rate during development, particularly during cell proliferation. However, as cell proliferation declines in adulthood, the methylation rate of these regions decreases, leading to cellular dysfunction and ultimately compromising tissue and organ performance (Raj, 2018).

3.3.3.1 Role of age-related CpGs

Another related question is which target genes are impacted by age-related epigenetic modifications. Tissue-specific methylation changes have been identified in several notable

CpGs. Among the most well-known examples is ELOVL2, a gene involved in fatty acid metabolism, which exhibits a strong positive correlation with age (Garagnani et al., 2012; Weidner & Wagner, 2014). Other genes include GREM1, IPO8, and P2RX6 (Hannum et al., 2013; Horvath, 2013; Horvath & Raj, 2018; Levine, 2018).

As described by Levine (2019), GREM1, a bone morphogenetic protein (BMP) antagonist, is included in the Hannum clock (2013) and exhibits epigenetic drift. IPO8, a transport protein, is also part of the Horvath clock (2013) and shows moderate negative methylation trends. P2RX6, a purinergic receptor included in the Levine clock (2018), demonstrates negative methylation changes, though without an exponential decline in DNAm.

Despite the identification of these target genes, it remains challenging to provide concrete explanations for their mechanistic role in aging. As Raj (2018) argues, a strong connection between age-related methylation changes and corresponding alterations at the RNA or protein level remains challenging. Given the methylation changes across the 353 CpGs amount to only 3.2% between individuals under 35 years old and over 55 years of age, the effect on gene expression is minimal (Raj, 2018). Even if age-related methylation changes at CpGs correlate with changes in gene expression, the affected genes are likely responsible for other “normal” cellular processes rather than playing a primary role in aging. He further continues that this insight is based on the assumption that there is no “evolutionary selection mechanism for the existence of aging-specific genes" (Raj, 2018, pp. 111–112) that directly regulate aging. Instead, aging may result from the decline in cellular efficiency caused by persistent epigenetic alterations that are activated during development.

To better capture the complexity of age-related changes, single cell transcriptomic analyses have been proposed as a necessary next step, as they can resolve cellular heterogeneity that bulk tissue data tend to obscure. Since aging is not a uniform process across all cells, average gene expression values from whole tissues, expressed on a scale from 0 to 1 in microarray analyses, may fail to reveal subtle but biologically relevant differences between cell populations.

In light of the GBM clinical study, understanding cell composition and states helps contextualize aging signals from whole blood. While epigenetic clocks work effectively without detailed mechanistic insights, this knowledge might provide an additional layer of interpretation to changes in ticking rates. Specifically, in glioblastoma patients undergoing

surgery, it enables a more nuanced analysis of aging dynamics linked to systemic inflammation and their association with rehabilitation measures.

In summary, epigenetic clocks hold promise for long term risk stratification in the perioperative management of GBM. However, future longitudinal studies on larger cohorts are needed to validate their clinical utility. Based on the current findings, frailty questionnaires outperform epigenetic clocks in guiding acute interventions by enabling targeted assessment within the CGA framework.

3.4 Linking Telomere Length, Epigenetic Aging, and Cellular Senescence

3.4.1 Epigenetic Aging and Cellular Senescence

Cellular senescence is a fundamental process in aging, characterized by irreversible cell cycle arrest in mitotic cells (Burton, 2009). Over time, these cells accumulate in tissues, contributing to tissue impairment and thus age-related decline (Burton, 2009). Interestingly, studies have demonstrated that the removal of these cells in mice can slow the progression of age-related conditions, including impairments in muscle, adipose tissue and vision function (Baker et al., 2011).

While telomere shortening is a well-known trigger for a senescent state, it is not the sole cause. Other pathways, such as oncogene overexpression and the accumulation of unrepaired DNA damage, can also drive cells into a senescent state, independent of telomere attrition (Di Micco et al., 2006; von Zglinicki et al., 2000). While cellular senescence serves as a protective barrier against uncontrolled cell proliferation early in life, it may contribute to tumorigenesis at later stages (Campisi, 1997b, 1997a).

The negative impact on neighboring cells and tissues is mediated by the secretion of inflammatory cytokines, degradation of extracellular matrix components, and the release of growth factors by senescent cells (Coppé et al., 2006; Kletsas et al., 2004; West et al., 1989), ultimately leading to tissue dysfunction and associated age-related diseases (Burton et al., 2007; Campisi, 1997b, 1997a).

In the present study, GBM patients with shorter telomeres tended to experience longer hospital stays and had a higher likelihood of requiring further institutional care after discharge. These findings support the hypothesis that an increased burden of senescent cells may compromise tissue repair and enhance inflammatory responses, thereby delaying postoperative recovery and increasing complication rates. Although direct measurements of senescent cells and their SASP profiles were not performed, telomere length serves as an indirect biomarker supporting this hypothesis.

Another question that arises is whether senescent cells undergo epigenetic aging. Lowe and his colleagues (2016) studied several cell types, including primary human coronary endothelial cells, telomerase-immortalized endothelial cells, primary keratinocytes, and fibroblasts. Their findings revealed that epigenetic aging was associated with replicative and oncogene-induced senescence in endothelial cells but not with radiation-induced senescence or replicative senescence in keratinocytes and fibroblasts. These observations suggest that epigenetic aging and cellular senescence are distinct biological processes that do not always coincide (Raj, 2018).

Similarly, in clinical settings, the relationship between these two processes remains to be fully explored. The GBM cohort showed a trend toward increased extrinsic epigenetic age acceleration (EEAA) in patients with prolonged hospital stays. Given that the Hannum clock primarily reflects epigenetic changes in blood cells, this finding may indicate immune senescence as a contributing factor to impaired postoperative recovery.

Future research should aim to jointly assess senescence markers, telomere dynamics, and epigenetic aging, in relation to clinical outcomes, to better elucidate their collective impact on recovery processes.

3.4.2 Epigenetic Aging and Telomere Length

When examining telomeres specifically, it is important to note that telomere length reflects the number of cell divisions a cell has undergone. However, this does not necessarily mean that a cell ages with each division (Raj, 2018).

The potential link between telomere length and epigenetic aging was investigated by Kabacik et al. (2018). Their study analyzed hTERT-transduced fibroblasts, which were able to continue dividing without undergoing replicative senescence. Using epigenetic clocks, it was shown that these cells exhibit changes in DNA methylation despite maintaining stable telomeres. Notably, mere extension of the cells' lifespan using various hTERT mutants was enough to allow epigenetic aging to proceed, indicating that TL and epigenetic aging are addressing different aspects of aging.

In clinical contexts, the GrimAge clock, known as strongest predictor of mortality, showed only a weak association with leukocyte telomere length in the cohorts of the Framingham Heart Study, WHI BA23, and Jackson Heart Study (Lu et al., 2019). It has been suggested that the observed tendency of higher age acceleration values being associated with shorter telomere length may reflect underlying immunosenescence (Lu et al., 2019).

Nevertheless, no direct link between epigenetic aging and telomere length has been established. But interactions may still exist (Raj, 2018). The enzyme hTERT influences various cellular processes beyond its classical function and may play a role in modulating epigenetic mechanisms (Raj, 2018).

3.5 Conclusion and Future Directions

This cross-sectional study investigated the interplay between telomere length, residual-based age acceleration using the GrimAge, PhenoAge, and DunedinPACE clocks together with extrinsic epigenetic age acceleration (EEAA) derived from the Hannum clock, and clinically assessed frailty using the G8 score and the Groningen Frailty Indicator. The objective was to evaluate their prognostic value for postoperative hospital stay duration and discharge decisions in glioblastoma patients, with a particular focus on their potential as biomarkers of frailty.

Shorter telomere length and elevated EEAA showed non-significant trends toward longer hospitalization and a slightly increased probability of discharge to further institutional care. These findings suggest a potential contribution of cellular and immune senescence to postoperative recovery processes. Among the frailty screening tools, the G8 score proved more effective than the Groningen Frailty Indicator in identifying patients at high risk, as the latter tended to underestimate the number of frail GBM patients. Overall, both tools revealed key areas of concern, particularly in terms of polypharmacy, psychosocial challenges, and limitations in daily activities.

The results demonstrate that the investigated molecular biomarkers provide an additional layer to pre-screening tools, enhancing individualized risk stratification prior to surgery. Nevertheless, conventional pre-screening tools remain essential for guiding acute interventions with regard to uncovering hidden frailty risks. Based on the identified deficits, we recommend further evaluation within a Comprehensive Geriatric Assessment (CGA). This should include the Timed Get-Up-and-Go test (TGUG), the Instrumental Activities of Daily Living (IADL) questionnaire, and the Cumulative Illness Rating Scale for Geriatrics (CIRS-G) to support targeted interventions before discharge.

Future research should focus on longitudinal designs in larger, age-homogeneous glioblastoma cohorts, with samples collected before surgery, at discharge, and prior to adjuvant treatment. This approach would capture dynamic changes in telomere length and epigenetic age acceleration throughout the perioperative period.

To elucidate the link between telomere length, epigenetic aging, and cellular senescence, studies should integrate telomere and epigenetic aging data with direct measures

of senescent cell burden and senescence-associated secretory phenotypes. To better interpret telomere dynamics and epigenetic age measures, it will also be crucial to resolve cellular heterogeneity, since both cell-type composition and cellular states may confound these biomarkers. Approaches such as single-cell RNA sequencing and immunophenotyping, including the analysis of $CD4^+$ and $CD8^+$ subsets, will be important to address this complexity.

Together, these efforts are essential for translating the investigated molecular biomarkers into predictive tools for frailty in the perioperative management of glioblastoma.

4 Materials und Methods

4.1 Ethical Approval and Data Collection

Ethical approval for this study, which was conducted as part of [redacted] Biological samples and accompanying questionnaires were collected within the department and processed by the doctoral candidate in accordance with the approved study protocol.

The use of patient samples and clinical data was carried out in compliance with applicable data protection and consent regulations of the University Medical Center Mainz. As part of the application for department-specific access rights to personal data, the doctoral candidate completed a mandatory data protection training course at the responsible administrative unit. Subsequently, access to the clinical SAP (Systems, Applications, and Products in Data Processing) system was granted for viewing patient data and medical reports.

4.2 Pre-Screening Tools

GFI (Groningen Frailty Index)

	YES	NO	SOMETIMES
Mobility Can the patient perform the following tasks without assistance from another person (walking aids such as a can or a wheelchair are allowed)			
1. Grocery shopping		1	
2. Walk outside house (around house or to neighbour)		1	
3. Getting (un)dressed		1	
4. Visiting restroom		1	
Vision			
5. Does the patient encounter problems in daily life because of impaired vision?	1	0	
Hearing			
6. Does the patient encounter problems in daily life because of impaired hearing?	1	0	
Nutrition			
7. Has the patient unintentionally lost a lot of weight in the past 6 months (6kg in 6 months or 3kg in 3 months)?	1	0	
Co-morbidity			
8. Does the patient use 4 or more different types of medication?	1	0	
Cognition			
9. Does the patient have any complaints on his/her memory (or diagnosed with dementia)?	1	0	0
Psychosocial			
10. Does the patient ever experience emptiness around him? e.g. You feel so sad that you have no interest in your surroundings. Or if someone you love no longer love you, how do you feel?	1	0	1
11. Does the patient ever miss the presence of other people around him? Or do you miss anyone you love?	1	0	1
12. Does the patient ever feel left alone? e.g. You wish there is someone to go with you for something important.	1	0	1
13. Has the patient been feeling down or depressed lately?	1	0	1
14. Has the patient felt nervous or anxious lately?	1	0	1
Physical Fitness			
15. How would the patient rate his/her own physical fitness? (0–10; 0 is very bad, 10 is very good) 0–6 = 1 7–10 = 0			
TOTAL SCORE GFI			**Max. 15 points**
Cutoff for frailty according to Peters et al. (2012)**:** *GFI ≥ 4 = frail; GFI < 4 = robust*			

Notes: The numbers assigned to each answer option are used to calculate the total frailty score. The self-report version of the Groningen Frailty Indicator (GFI) was used, based on the validated structure originally developed by Steverink et al. (2001) and further examined by Schuurmans et al. (2004) and Bielderman et al. (2013). This version includes minor rewording of the psychosocial items, as described by Peters et al. (2012). The questionnaire format corresponds to a version provided by the clinical co-supervisors of this dissertation project in the Department of Neurosurgery at the University Medical Center Mainz (2021–2024).

G8 Screening Tool

	Items	**Possible answers (score)**
1	Has food intake declined over the past 3 months due to loss of appetite, digestive problems, chewing or swallowing difficulties?	0: severe decrease in food intake 1: moderate decrease in food intake 2: no decrease in food intake
2	Weight loss during the last 3 months	0: weight loss > 3 kg 1: does not know 2: weight loss between 1 and 3 kgs 3: no weight loss
3	Mobility	0: bed or chair bound 1: able to get out of bed/chair but does not go out 2: goes out
4	Neuropsychological problems	0: severe dementia or depression 1: mild dementia or depression 2: no psychological problems
5	Body Mass Index (BMI (weight in kg) / (height in m^2)	0: BMI < 19 1: BMI = 19 to BMI < 21 2: BMI = 21 to BMI < 23 3: BMI = 23 and > 23
6	Takes more than 3 medications per day	0: yes 1: no
7	In comparison with other people of the same age, how does the patient consider his/her health status?	0: not as good 0.5: does not know 1: as good 2: better
8	Age	0: >85 1: 80-85 2: <80
	TOTAL SCORE	0 – 17
	Cutoff for frailty according to Takahashi et al. (2017)**:** G8 score <11 = frail G8 score 11-14 = pre-frail G8 score >14 = robust	

Notes: The G8 score and its corresponding screening table were first introduced by Bellera et al. (2012). It was validated in a cohort of oncology patients aged 70 years and older. A three-tier classification into frail, pre-frail, and robust has since been proposed by various authors, for example by Takahashi et al. (2017). The questionnaire format used in this context corresponds to the version provided by clinical co-supervisors in the Department of Neurosurgery at the University Medical Center Mainz (2021–2024).

4.3 Molecular Pathology and Imaging

Morphological features as well as the IDH1 R132H mutation status, ATRX expression status, MGMT promoter methylation status, and Ki-67 proliferation index were obtained from the histopathological findings of the GBM patients (Table 3, Fig. 5). The TERT status mentioned in Table 3 and Fig. 5 was determined by the doctoral candidate, as methodologically described in Section 4.3.1.

For Fig. 6, a hematoxylin and eosin (H&E)-stained tissue section from formalin-fixed, paraffin-embedded (FFPE) tumor tissue of a GBM patient was used. The image was acquired using a LEICA DM5000 B microscope and the GRYPHAX® microscope camera software program (Jenoptik). A 10× objective was used for Fig. 6a, while a 40× objective was used for Fig. 6b and 6c.

Fig. 7e–h show immunohistochemical staining of FFPE tissue, which were also acquired using a 40× objective. In Fig. 7e, tumor cells harboring an IDH1 R132H mutation show a brown cytoplasmic staining due to the DAB (3,3'-diaminobenzidine) reaction, indicating the binding of the specific anti-IDH1 antibody; the nuclei are additionally counterstained blue with hematoxylin. Fig. 7f shows IDH1 R132H wild-type cells, which exhibit no brown cytoplasmic staining and only show blue-stained nuclei. In Fig. 7g, ATRX-mutated tumor cells are shown, which lack brown nuclear staining and instead display only blue counterstained nuclei, indicating absence of ATRX expression. Fig. 7h shows tumor cells with intact ATRX expression, recognizable by the brown nuclear staining caused by the DAB reaction, with the nuclei additionally counterstained in blue. Fig. 7i and 7j were generated based on the performed TERT sequencing (see Section 4.3.1) using the software program Chromas (Version 2.5.0, Technelysium Pty Ltd).

Electronic devices and software

Electronic Device / Software	**Manufacturer / Source**
LEICA DM5000 B microscope	Leica Microsystems
GRYPHAX® microscope camera software	Jenoptik
Chromas software (Version 2.5.0)	Technelysium Pty Ltd

4.3.1 TERT Promoter Sequencing

4.3.1.1 DNA Extraction from Fresh-Frozen GBM Tissue

Brain samples were collected during surgical removal of the tumor. Since tumor tissue contained both tumor cells and surrounding non-tumor tissue, an assessment of tumor cell heterogeneity was necessary. Upon receipt, the tumor tissue was washed with Dulbecco's Phosphate Buffered Saline (PBS) (Sigma-Aldrich, Cat. No. RNBJ6984) to remove blood, cut into pieces weighing 100–500 mg, placed into cryogenic storage vials (Fisher Scientific, Cat. No. 12-567-500), snap-frozen in liquid nitrogen, and stored at −80 °C. For DNA extraction, the DNA Isolation Kit for Cells and Tissues (Merck Millipore, Cat. No. 11814770001) was used. According to the instructions, the reagent volumes must be adjusted to the weighed tissue mass. The tumor masses used for extraction were between 300–400 mg on average. Thus, the volumes of reagents used for extraction, depending on the applied tumor mass, were 7.5–10 mL Cellular Lysis Buffer, 4.6–6.13 µL Proteinase K Solution, 300–400 µL RNase Solution, and 3.1–4.13 mL Protein Precipitation Solution.

Brain Tissue Weight [mg]	Cellular Lysis Buffer [ml]	Proteinase K Solution [µl]	RNase Solution [µl]	Protein Precipitation Solution [ml]
300	7.5	4.6	300	3.1
400	10	6.13	400	4.13

Notes: Description based on the DNA Isolation Kit for Cells and Tissues (Merck Millipore, Cat# 11814770001); slightly modified for clarity in this protocol.

The gentleMACS Dissociator (Miltenyi Biotec) was used with the RNA 2.0 program (Miltenyi Biotec). The MACS M Tubes (Miltenyi Biotec, Cat# 130-096-335) were filled with the appropriate amount of Cellular Lysis Buffer (see table above), which had been prewarmed for 15 minutes at 37 °C. The tumor tissue was inserted into the M Tube containing the prewarmed Cellular Lysis Buffer and was homogenized using the RNA 2.0 program. Although the program had a homogenization time of 80 seconds, homogenization was carried out only until no visible clumps remained in order to avoid unnecessary DNA degradation. The homogenized solution was transferred to a 50 mL DNase-free Eppendorf Conical Tube (Eppendorf SE, Cat# 0030122178). The appropriate amount of Proteinase K Solution was then added, and the sample was vortexed for 3 seconds. The sample was placed at 65 °C for 1 hour. Subsequently,

the sample was removed from 65 °C, and the cap was loosened to allow venting. The appropriate amount of RNase Solution was then added to each sample, followed by vortexing for 3 seconds. The sample was then incubated at 37 °C for 15 minutes.

For protein removal, the appropriate amount of Protein Precipitation Solution was added to each sample. The sample was placed on ice for 5 minutes to aid precipitation of the protein. The sample was centrifuged at 15,000 × g at 22 °C for 20 minutes. Upon centrifugation, a brown pellet was present. The transparent liquid was carefully poured into a new 50 mL DNase-free Eppendorf Conical Tube (Eppendorf SE, Cat# 0030122178) without disturbing the brown pellet. Subsequently, 0.7 volumes of Isopropanol (Fisher Chemical, Cat# 10315720) were added to the sample. The tube was gently inverted until the upper and lower phases mixed. DNA "strings" were usually visible at this stage. The sample was centrifuged at 1,400 × g for 10 minutes, and the supernatant was discarded. Cold 10 mL 70% ethanol was added to the DNA pellet. The ethanol was prepared as a 1:7 dilution of 30 mL ddH_2O (double-distilled water) and 70 mL absolute ethanol (200 proof, Molecular Biology Grade; Fisher BioReagents, Cat# 10041814). The pellet was dislodged from the bottom of the tube by gently tapping the tube. The sample was centrifuged at 1,400 × g for 5 minutes, and the supernatant was discarded. The DNA pellet was air-dried for 5 minutes. To resuspend the DNA pellet, 1.5 mL TE Buffer (pH 8.0) was added, and the sample was left overnight at 4 °C to go into solution.

Quantity and purity were measured using a NanoDrop (Thermo Fisher Scientific, Cat# ND-ONE-W). For high-quality genomic DNA, ideal purity values were a 260/280 ratio between 1.8 and 2.0 and a 260/230 ratio between 2.0 and 2.2. For calibration, TE Buffer was used. DNA integrity was assessed using the 4200 TapeStation Instrument (Model G2991A, Agilent Technologies) with the TapeStation Analysis Software (Version 4.1.1, Agilent Technologies Inc., 2021). For the analysis, Genomic DNA ScreenTape (Agilent, Cat# 5067-5365) and Genomic DNA Reagents (Agilent, Cat# 5067-5366) were used. The DNA Integrity Number (DIN) ranged between 9 and 10. Only samples with a DIN > 9 were considered for subsequent analyses. The quality-controlled DNA was distributed and aliquoted into three DNase-free reaction tubes (1.5 mL, PP, SafeSeal Reaction Tubes, Biosphere® plus, Sarstedt, Cat# 72.706.200) for each patient sample and stored at -80 °C until further use.

Prepared Solutions:

TE buffer (10 mM Tris-HCl, 1 mM EDTA, pH 8.0)

100 mL of 1× TE buffer (10 mM Tris-HCl, 1 mM EDTA, pH 8.0) was prepared by adding 200 µL of 0.5 M EDTA (pH 8.0) to 99.8 mL of 10 mM Tris-HCl (pH 8.0), as described below.

10 mM Tris (tris(hydroxymethyl)aminomethane), pH 8.0

Step	Reagent	Amount	Note
1	Tris Base, Molecular Biology Grade (Fisher BioReagents, Cat# BP1521)	121.1 mg	Dissolve in approx. 80 mL ddH_2O
2	1 M HCl	Dropwise	Adjust pH to 8.0 using Orion Star™ A215 pH/Conductivity Meter (Thermo Scientific). 1 M HCl was prepared by diluting 8.3 mL of hydrochloric acid solution, 37%, ACS reagent (Merck, Cat# 258148-500ML) with distilled water to 100 mL.
3	ddH_2O	Fill to 100 mL	After pH adjustment

0.5 M EDTA (ethylenediaminetetraacetic acid), pH 8.0

Step	Reagent	Amount	Note
1	Ethylenediaminetetraacetic Acid, Disodium Salt Dihydrate (Fisher Scientific, Cat# 10618973)	18.61 g	Dissolve in approx. 80 mL ddH_2O (may not dissolve completely)
2	1 M NaOH	Dropwise	Adjust pH to 8.0 using Orion Star™ A215 pH/Conductivity Meter (Thermo Scientific). 1 M NaOH was prepared by dissolving 4.00 g of Sodium Hydroxide Pellets (Fisher BioReagents, Cat# 10192863) in approx. 80 mL ddH_2O and filling to 100 mL after cooling.
3	ddH_2O	Fill to 100 mL	After pH adjustment; optionally sterilize

Electronic devices and software

Electronic Device / Software	Manufacturer / Source
Centrifuge 5804 R	Eppendorf
Centrifuge 5425 R	Eppendorf
Labofuge 400 R	Thermo Scientific (formerly Heraeus)
SW23 water bath	Julabo
Vortex-Genie 2	Scientific Industries
Entris® Analytical Balance	Sartorius
GentleMACS Dissociator	Miltenyi Biotec
NanoDrop ND-ONE-W	Thermo Fisher Scientific
4200 TapeStation Instrument (Model G2991A)	Agilent Technologies
TapeStation Analysis Software (Version 4.1.1)	Agilent Technologies
Orion Star™ A215 pH/Conductivity Meter	Thermo Scientific
Precision balance (SBA 32)	Scaltec
Entris precision balance	Sartorius
Entris analytical balance	Sartorius

4.3.1.2 Assessment of Tumor Cell Heterogeneity

4.3.1.2.1 Cryostat Microtomy

For sectioning, the LEICA CM1850 UV cryostat was set to -30 °C, optimized for brain tissue. A snap-frozen tumor fragment (200–500 mg) was embedded in cryo-medium (Neg-50™ Frozen Section Medium, Epredia, CAT#6502) and allowed to solidify at -30 °C within the cryostat for 10 minutes. Subsequently, tissue sections were cut at a thickness of 13 µm and mounted onto coated glass slides (Menzel-Gläser Superfrost PLUS, Thermo Scientific, CAT# J1800AMNZ). The sections were then stored at -80 °C until further use.

4.3.1.2.2 Hematoxylin and Eosin (H&E) Staining

Tissue sections were first thawed and completely air-dried. Staining was performed using Hematoxylin 7211 (Epredia, Cat# 138880) for a duration of 10 minutes. This was followed by bluing under running tap water for 5 minutes. For counterstaining, the slides were immersed in Eosin Y (Thermo Scientific, Cat# 283832) for 30 seconds.

Subsequently, dehydration was carried out by dipping the slides 3 times in isopropanol with a purity of at least 99% (Name: Isopropylalkohol Ph. Eur./USP/JP, Aug. Hedinger GmbH & Co. KG, Catalog No. 67630). For this, the slides were swirled 15 to 20 times during the first two steps, and 10 times during the third step.

Following dehydration, tissue sections were treated with Roti®Histol (Carl Roth GmbH, Cat# 6640.1). Slides were first gently swirled 15 to 20 times, then incubated in fresh Roti®Histol for 2 minutes. Finally, the samples were mounted using Eukitt® mounting medium (O. Kindler GmbH, Cat# D0814) and covered with 24 × 50 mm Menzel cover glasses (Thermo Scientific).

Tumor heterogeneity assessment was performed by neuropathology personnel at the University Medical Center Mainz. Tumor content was visually estimated from the tissue sections based on cell density and the presence of necrotic areas.

For TERT analysis, only samples with a tumor content exceeding 50% were selected. For the remaining patients whose tumor content was lower than 50%, DNA was isolated from FFPE tissue blocks (see Section 4.3.1.3) that were requested from the Neuropathology Department

in Mainz. The rationale for requesting FFPE tissue was that it allowed for a more targeted removal of tumor cells compared to fresh-frozen tissue. However, multiple DNA extractions from FFPE tissue are often required to obtain a sufficient quantity of high-quality DNA for TERT sequencing. Therefore, DNA was initially isolated from fresh-frozen tissue, prioritizing the assessment of tumor heterogeneity. Ultimately, the aim was to ensure that detectable tumor DNA was available from each patient.

4.3.1.3 DNA Extraction from FFPE GBM Tissue

DNA was extracted using the QIAamp DNA FFPE Tissue Kit® (Qiagen, Cat# 56404). A total of 90 µL ATL buffer (QIAamp DNA FFPE Tissue Kit, Qiagen, Cat# 56404) was added to a 1.5 mL microcentrifuge tube (QIAamp DNA FFPE Tissue Kit, Qiagen, Cat# 56404). Tumor tissue was manually isolated from an FFPE section by outlining the region of interest, moistening it with ATL buffer, and scraping it off with a sterile scalpel. The tissue was then transferred to the ATL-containing tube.

Subsequently, 10 µL of proteinase K (QIAamp DNA FFPE Tissue Kit, Qiagen, Cat# 56404) was added, and the sample was mixed by vortexing. The sample was incubated at 56 °C for 1 hour, followed by incubation at 90 °C for 1 hour to reverse formalin cross-linking. After a brief centrifugation to collect condensation, 100 µL Buffer AL and 100 µL absolute ethanol (200 Proof, Molecular Biology Grade; Fisher BioReagents, Cat. No. 10041814) were added sequentially, with vortexing after each addition.

The lysate was loaded onto a QIAamp MinElute column (QIAamp DNA FFPE Tissue Kit, Qiagen, Cat# 56404), avoiding contact with the rim. The column was centrifuged at 6000 × g for 1 minute, placed into a clean 2 mL collection tube (QIAamp DNA FFPE Tissue Kit, Qiagen, Cat# 56404), and the flow-through was discarded. This step was followed by sequential washes with 500 µL Buffer AW1 (QIAamp DNA FFPE Tissue Kit, Qiagen, Cat# 56404) and 500 µL Buffer AW2 (QIAamp DNA FFPE Tissue Kit, Qiagen, Cat# 56404), each followed by centrifugation at 6000 × g for 1 minute. To ensure complete drying of the membrane, the column was centrifuged at 20,000 × g for 3 minutes.

For elution, the column was transferred to a clean 1.5 mL microcentrifuge tube. A volume of 25 µL Buffer ATE (QIAamp DNA FFPE Tissue Kit, Qiagen, Cat# 56404) was applied

directly to the center of the membrane, followed by a 5-minute incubation at room temperature. DNA was then eluted by centrifugation at 20,000 × g for 1 minute.

The concentration of the eluted DNA was measured using a NanoDrop spectrophotometer (Thermo Fisher Scientific). DNA concentrations typically ranged between 20 and 200 ng/µL. Ideal purity values were a 260/280 ratio between 1.8 and 2.0 and a 260/230 ratio between 2.0 and 2.2, which were met in all samples.

4.3.1.4 PCR Amplification and Sanger Sequencing

Genomic DNA extracted from fresh-frozen brain tissue and from FFPE tissue were prepared in the previous step. The following mastermix was prepared in a DNase-free reaction tube (1.5 mL, PP, SafeSeal Reaction Tubes, Biosphere® plus, Sarstedt, Cat# 72.706.200) for a total of 13 reactions.

Components (Kit: FastStart Taq DNA Polymerase, dNTPack, Cat# 04 738 381 001, Roche/Merck)	**Mastermix for 13 Reactions**	**Mastermix for 1 Reaction**
H2O	206 µl	15.7 µl
10x Buffer	32.5 µl	2.5 µl
GC-rich 5x	39 µl	3 µl
dNTP	6.5 µl	0.5 µl
Taq Polymerase	3.9 µl	0.3 µl
Magnesium Chloride (25 mM)	3 µl	included in buffer
Primers		
Primer 0.2 µM (forward) **Sequence:** 'TGTAAACGACGGCCAGTCCGTCCTGCCCCTTCACC' (Eurofins Genomics)	13 µl	1 µl
Primer 0.2 µM (reverse) **Sequence:** 'CAGGAAACAGCTATGACCGGGCCGCGGAAAGGAAG' (Eurofins Genomics)	13 µl	1 µl

Notes: The PCR primers used for amplification contained a 5'-overhang with the M13 sequence to enable subsequent Sanger sequencing using standard M13 primers.

For amplification, an 8-well PCR strip (200 µL, PCR Performance Tested, transparent, PP, flat lid; Sarstedt, Cat# 72.991.002) was used, with each well prepared and labeled with the

respective patient number. In addition, two more PCR tubes were prepared to serve as positive and negative controls.

For each patient sample, 24 µL of the prepared master mix were pipetted into a PCR tube, followed by the addition of 1 µL of gDNA extracted from FFPE tissue or fresh frozen tissue. For the positive control, 24 µL of master mix were combined with 1 µL of high-quality genomic DNA isolated from whole blood, which provides a better DNA quality compared to FFPE tissue. For the negative control, 24 µL of master mix were mixed with 1 µL of nuclease-free water (Invitrogen, Cat# AM9939) instead of DNA.

PCR Program:

Cycles	**Temperature (°C)**	**Duration**
10×	60°C	15 sec
	59°C	15 sec
	58°C	15 sec
	57°C	15 sec
	56°C	15 sec
30×	58°C	15 sec
	72°C	15 sec
1×	72°C	5 min
Hold	8°C	

1. **Gel Electrophoresis to verify PCR Products**

The PCR product was mixed with bromophenol blue at a ratio of 5 µL PCR product to 1 µL bromophenol blue (1:6 dilution, Thermo Scientific, Cat# LT-02241). A 20-well comb and a 2% agarose gel, prepared from LE Agarose (Biozym, Cat# 840004) and 0.5X TBE buffer, were used. The 0.5X TBE buffer was prepared by a 1:10 dilution from TBE 5X (Hycultec, Cat# EC-861-4L). The gel was run at 140 V. The GeneRuler DNA Ladder, Low Range (25–700 bp) (Thermo Fisher Scientific, Cat# SM1191) was used as the molecular weight marker. A volume of 6 µL was loaded into each well, and the gel was run for 20 minutes. The gel was visualized using the Gel IX Imager (Intas).

2. Purification of PCR Products

For digestion, Shrimp Alkaline Phosphatase (rSAP, New England Biolabs, Cat# M0371S) and Exonuclease I (E. coli, New England Biolabs, Cat# M0293S) were used. The following volumes were pipetted to prepare the ExoSAP mix: 4.275 µL nuclease-free water, 0.6 µL 10× SAP buffer (rSAP, New England Biolabs, Cat# M0371S), 0.9 µL rSAP (rSAP, New England Biolabs, Cat# M0371S), and 0.225 µL Exonuclease I (E. coli, New England Biolabs, Cat# M0293S). Subsequently, 6 µL of the PCR product was added to the mix. The reaction was incubated at 37 °C for 20 minutes, followed by incubation at 72 °C for 10 minutes to inactivate the enzymes.

3. Sequencing Reaction

A sequencing reaction was prepared by combining 3 µL of DTCS Quick Start Mix (GenomeLab DTCS Quick Start Kit 30®, Cat# 10399649), 1 µL of primer (GenomeLab DTCS Quick Start Kit 30®, Cat# 10399649), 4 µL of nuclease-free water (GenomeLab DTCS Quick Start Kit 30®, Cat# 10399649), and 2 µL of the digested PCR product. The forward and reverse primers used in this step were sequences derived from the M13 phage.

4. Purification of Sequencing Products

10 µL magnetic beads from MagSi-DT-Removal (Magtivio B.V., Cat# MDKT00040050) and 42 µL of 85% ethanol (made from Ethanol, Absolute, 200 Proof, Molecular Biology Grade, Fisher BioReagents, Cat# 10041814; diluted to 85% with ddH_2O) were added to each PCR tube and incubated for 1 minute. The PCR tubes were placed on the magnetic plate and incubated for 3 minutes, allowing the beads to form a solid ring at the bottom of the tube. A multichannel pipette was used to remove the supernatant, after which 100 µL of 85% ethanol (made from Ethanol, Absolute, 200 Proof, Molecular Biology Grade, Fisher BioReagents, Cat# 10041814; diluted to 85% with ddH_2O) were added to each tube and incubated for 30 seconds. 100 µL of the supernatant were removed from each tube, and the ethanol wash was repeated by adding another 100 µL of 85% ethanol, incubating for 30 seconds, and removing the supernatant. The tubes were then removed from the magnetic plate (Alpaqua® 96R Ring Magnet, Cat# A29164), revealing a brown ring. 40 µL of Genome Lab® Loading Solution (GenomeLab DTCS Quick Start Kit 30®, Cat# 10399649) were added to each PCR tube and pipetted up and down until the

brown ring dissolved. The solution was transferred to a new PCR plate (Microseal® 'A' PCR Plate and PCR Tube Sealing Film, Bio-Rad, MSA5001). Sequencing was performed on the Genome Lab GeXP (Beckman Coulter) using the program LFR1 without denaturation for 40 minutes.

Electronic devices and software

Electronic Device / Software	Manufacturer / Source
Mikro 120 centrifuge	Hettich
Biozym Mini-Centrifuge	Biozym
NanoDrop spectrophotometer	Thermo Fisher Scientific
PeqSTAR 2x Thermocycler	VWR
Genome Lab GeXP	Beckman Coulter
EV261 Electrophoresis Power Supply	Pqlab
Gel IX Imager	Intas
Thermocell Cooling and Heating Block	Biozym
Mini-Sub Cell GT w PowerPac Basic	Bio-Rad Laboratories
Vortex-Genie 2	Scientific Industries

4.4 Whole Blood Molecular Biomarker Analysis

4.4.1 Extraction of gDNA from Whole Blood

The blood was collected using PAXgene Blood DNA Tubes (Qiagen, Cat# 761115) with a BD Vacutainer Safety-Lok Blood Collection Set, 21 G, 18 cm Tube (Becton, Dickinson and Company (BD), Cat# X91029.4). Immediately prior to blood collection, the needle was inserted into the rubber stopper, and blood was drawn until the tube reached the 8.5 mL mark. The tube was then shaken 10 times. The samples were stored in the refrigerator at 4°C for several hours until they were picked up by the PhD student.

For DNA extraction, the PAXgene Blood DNA Kit (25) (Qiagen, Cat# 3766-240224) was used, which contained Buffer BG1, Buffer BG2, Buffer BG3/PreAnalytiX Protease, and Buffer BG4. All the blood from one PAXgene Blood DNA Tube was poured into a 50 mL processing tube containing 25 mL Buffer BG1. The tube was closed and mixed by inverting 5 times. The

sample was centrifuged for 5 minutes at 2500 × g, and the supernatant was carefully discarded. 5 mL Buffer BG2 were added, the tube was closed, and the pellet was washed by vortexing for 5 seconds. The sample was centrifuged for 3 minutes at 2500 × g, and the supernatant was discarded. 5 mL Buffer BG3/PreAnalytiX Protease mix (500 µL Buffer BG3 were added to the PreAnalytiX Protease bottle and mixed) were added, and the sample was vortexed for 20 seconds at high speed. The tube was placed in a water bath and incubated at 65 °C for 10 minutes. The sample changed color from light red to light green, indicating that protein digestion had occurred. The sample was vortexed again for 5 seconds at high speed. 5 mL isopropanol (Isopropylalkohol Ph. Eur./USP/JP, Aug. Hedinger GmbH & Co. KG, Catalog No. 67630) were added, and the sample was mixed by inverting the tube at least 20 times until white DNA strands clumped visibly together.

The sample was centrifuged for 3 minutes at 2500 × g. The supernatant was discarded, and the tube was left inverted on a clean piece of absorbent paper for 1 minute. 5 mL of 70% ethanol (Ethanol, Absolute (200 Proof), Molecular Biology Grade, Fisher BioReagents, Cat# 10041814; diluted to 70% with ddH_2O) were added, and the sample was vortexed for 1 second at high speed. The sample was centrifuged for 3 minutes at 2500 × g. The supernatant was discarded, and the tube was left inverted on a clean piece of absorbent paper for at least 5 minutes. The tube was carefully dabbed onto absorbent paper to remove ethanol from the rim and was left inverted for a further 5 minutes to allow the DNA pellet to dry. 1 mL of Buffer BG4 was added, and the DNA was dissolved by incubating for 1 hour at 65 °C in a water bath, followed by incubation overnight at room temperature.

Quantity and purity were measured using a NanoDrop (Thermo Fisher Scientific, Cat# ND-ONE-W). For high-quality genomic DNA, ideal purity values were a 260/280 ratio between 1.8 and 2.0 and a 260/230 ratio between 2.0 and 2.2. DNA yields ranged from 150–500 µg and depended on the number of nucleated cells present. For calibration, Buffer BG4 was used. DNA integrity was assessed using the 4200 TapeStation Instrument (Model G2991A, manufactured in 2015–2016, Agilent Technologies) with the TapeStation Analysis Software (Version 4.1.1, Agilent Technologies Inc., 2021). For the analysis, Genomic DNA ScreenTape (Agilent, Cat# 5067-5365) and Genomic DNA Reagents (Agilent, Cat# 5067-5366) were used. The DNA Integrity Number (DIN) ranged between 9 and 10. Only samples with a DIN > 9 were considered for subsequent analyses. The quality-controlled DNA was then distributed and aliquoted into

three DNase-free reaction tubes (1.5 mL, PP, SafeSeal Reaction Tubes, Biosphere® plus, Sarstedt, Cat# 72.706.200) for each patient sample.

Electronic devices and software

Electronic Device / Software	Manufacturer / Source
Labofuge 400 R	Thermo Scientific (formerly Heraeus)
SW23 water bath	Julabo
Vortex-Genie 2	Scientific Industries
NanoDrop ND-ONE-W	Thermo Fisher Scientific
4200 TapeStation Instrument (Model G2991A)	Agilent Technologies
TapeStation Analysis Software (Version 4.1.1)	Agilent Technologies

4.4.2 TRF Analysis

Day 1 - gDNA digestion

Genomic DNA was extracted from GBM whole blood samples, and 3 µg were required for digestion. DNA extracted from a healthy male donor (RDN-7347961) obtained from Research Donors Ltd, C14 Poplar Business Park, London, E14 9RL, UK, was used as a control. The digestion was performed overnight in PCR tubes (8-strip, 200 µL, PCR Performance Tested, transparent, polypropylene, flat lid; Sarstedt, Cat# 72.991.002) following the specified protocol.

For each sample, 0.75 µL RsaI (NEB, Cat# R0167L), 0.75 µL HinfI (NEB, Cat# R0155L), 3 µL CutSmart Buffer (NEB, Cat# B6004S), and x µL of gDNA (3 µg) extracted from whole blood were combined, and the volume was adjusted to 25 µL with ddH_2O. Finally, the reactions were incubated at 37 °C overnight on the Thermal Cycling Block (Eppendorf PCR Mastercycler Pro S).

Day 2 - Gel electrophoresis run

Each gel could accommodate a maximum of 13 samples plus one control; therefore, a total of four gels was required to run 28 gDNA samples.

In the first step, a digestion check was performed. 1 µL of the digested gDNA from the previous day was taken and mixed with 9 µL of ddH_2O and 2 µL of 6× Orange DNA Loading Dye (Fisher Scientific, Cat# 11551575; 1:6 dilution with ddH_2O). For all gDNA patient samples, this process was repeated. For the ladder, 1 µL of the 1 kb Plus DNA Ladder, 1000 µg/mL, 100 µL (NEB, Cat# N3200S) was taken and mixed with 9 µL of ddH_2O. For the control, gDNA extracted from the healthy donor mentioned in Day 1 was used.

A 1% agarose gel was prepared by dissolving 1 g of NuSieve® Genetic Technology Grade™ Agarose (VWR, Cat# 733-1543) in 100 mL of 0.5× TBE buffer. The 0.5× TBE buffer was prepared by a 1:10 dilution from TBE 5× (Hycultec, Cat# EC-861-4L). Once the gel was poured into the gel tray belonging to the Mini-Sub Cell GT with PowerPac Basic (Bio-Rad Laboratories, Cat# 041BR159221), 5 µL of ethidium bromide (10 mg/mL; VWR, Cat# SA FSE1510-10ML) was added to the warm gel and gently swirled to ensure even distribution. The gel was allowed to solidify for 30 minutes under the fume hood.

The Mini-Sub Cell GT with PowerPac Basic (Bio-Rad Laboratories, Cat# 041BR159221), combined with the PowerPac HV Power Supply (Bio-Rad), was used for gel electrophoresis. While loading the prepared digested gDNA samples into the wells, 1 µg of the respective undigested gDNA was added to one well for comparison. The gel was run at 150 V for 10 minutes. Afterward, an image was taken using the Chemidoc MP Imaging System (Bio-Rad), and the intensity of individual samples was measured using the Image Lab software version 5.2.1 (Bio-Rad). Based on the sample with the lowest intensity, all other samples were diluted accordingly so that the concentrations of the samples loaded onto the same gel were matched. Finally, the gel was run at 100 V for 40 minutes. A smear indicated successful gDNA digestion.

For the TRF assay, a 0.8% agarose gel was prepared by dissolving 0.8 g of NuSieve® Genetic Technology Grade™ Agarose (VWR, Cat# 733-1543) in 250 mL of 0.5× TBE buffer, without the addition of ethidium bromide. The gel was cast in the gel tray of the Wide Mini-Sub Cell GT with PowerPac Basic and left to solidify for 1 hour. Following the concentration adjustments performed in the previous step, the digested gDNA samples, along with the control and the DIG-labeled DNA Molecular Weight Marker II (Merck/Sigma, Cat# 11218590910), were loaded into the wells. The DNA Molecular Weight Marker II was prepared

by mixing 4 µL of DIG-labeled marker with 28 µL of 0.5× TBE and 8 µL of 6× Orange DNA Loading Dye (Fisher Scientific, Cat# 11551575). A volume of 20 µL of this mixture was then loaded into the outer wells on both the left and right sides of the gel. Electrophoresis was carried out in the Wide Mini-Sub Cell GT with PowerPac Basic (Bio-Rad Laboratories, Cat# 041BR159347) connected to a PowerPac HV Power Supply (Bio-Rad) at 60 V for 16 hours.

Day 3 – Blotting

The solutions were freshly prepared:

Denaturing Solution

	1L
Sodium Hydroxide, white pellets (Fisher Scientific, Cat# 10192863)	16g
Sodium Chloride (Merck/Sigma, Cat# S9888-2.5KG)	35.1g
ddH_2O	ad 1L

Neutralizing solution (pH 7.4)

	1L
Tris Base (Fisher Scientific, Cat# 10376743)	121.4 g
Sodium Chloride (Merck/Sigma, Cat# S9888-2.5KG)	87.75 g
dd H_2O	ad 1L

Notes: To adjust the pH to 7.4, approx. 60 mL of HCl (Hydrochloric Acid Solution, 37%) (Merck/Sigma, Cat# 258148-500ML) was needed.

20X SSC (Saline-Sodium Citrate)

	1L
Sodium Citrate, Dihydrate (Fisher Scientific, Cat# 15568154)	88.2 g
Sodium Chloride (Merck/Sigma, Cat# S9888-2.5KG)	175.3 g
dd H_2O	ad 1L

Notes: The pH was adjusted to 7.0 with a few drops of HCl (Hydrochloric Acid Solution, 37%) (Merck/Sigma, Cat# 258148-500ML).

The gel was placed for 45 minutes in 1 L of denaturing solution and then for the same duration in 1 L of neutralizing solution. One piece of Hybond®-N+ Hybridization Membrane (Cytiva, Cat# RPN303B) was cut to the size of the gel (15 cm × 25 cm). Four pieces of thin Whatman paper (Cytiva, Cat# 10199320) were cut to match the gel dimensions (e.g., 15 cm × 25 cm), and one longer piece of the same paper was prepared to fit underneath the gel (e.g., 15 cm × 40 cm). Ten pieces of thick Whatman paper (Cytiva, Cat# 11330744) were also cut to the size of the gel. In addition, 1 L of 10× SSC solution was prepared by diluting 20× SSC 1:1 with ddH_2O.

In a glass dish, the electrophoresis tray was placed upside down. A long piece of thin Whatman paper (Cytiva, Cat# 10199320) was laid on top, and the dish was filled with 1 L of 10× SSC so that the ends of the paper were immersed in the buffer. The gel was then placed face down on the paper, followed by the pre-wetted Hybond®-N+ membrane (Cytiva, Cat# RPN303B). After removing air bubbles, a stack of the prepared thin Whatman paper (Cytiva, Cat# 10199320) was placed on top of the membrane, followed by a stack of the prepared thick Whatman paper (Cytiva, Cat# 11330744) and then a stack of paper towels. The Papernet Paper Towels, W-fold, 2-ply, sheet size 20.3 × 32 cm (Hygi, Cat# 176700) were used. An inverted glass dish was positioned on top to create a sealed sandwich-like setup. The assembly was wrapped with cling film (PAPSTAR Frischhaltefolie, Büro Plus, Cat# 66088) to prevent evaporation, and a weight (e.g., a 500 mL bottle) was placed on top to improve capillary transfer efficiency. The setup was left to transfer overnight.

Day 4 – Hybridization

1 M PIPES (Piperazine-N,N'-bis(2-ethanesulfonic acid), pH 6.4)

	100mL
PIPES (Merck/Sigma, Cat# P1851-25G)	30.2g

Note: The volume was filled up to 70 mL with ddH_2O, stirred, and the pH was adjusted to pH 6.4 with sodium hydroxide, white pellets (Fisher Scientific, Cat# 10192863). The volume was then adjusted to 100 mL.

Hybridization Solution (for DIG-labeled probe)

	100mL
Formamide ≥99.5% (Merck/Sigma, Cat# 47671-250ML-F)	50mL
20× SSC (see „Day 3“)	25mL
Denhardt's Solution (50×) (Fisher Scientific, Cat# 11518616)	10mL
0.5M EDTA (see Section 1.2.1)	1mL
1M PIPES pH 6.4	1mL
Yeast RNA (5 mg/mL) (Fisher Scientific, Cat# AM7120G)	40 mg in 3mL ddH2O
10% SDS Prepared by mixing 5 mL of 20% SDS solution, RNase-free (Invitrogen, Cat# AM9820) with 5 mL of ddH_2O.	10mL

Note: The solution was heated to 65 °C to ensure everything dissolved completely.

20 mL hybridization solution were placed in the Compact-Line Hybridization Oven OV 4 (Ebenrecht, Cat# 593549) at 42.5 °C to prewarm. The Hybond®-N+ membrane (Cytiva, Cat# RPN303B) was removed from the capillary transfer setup, rinsed in ddH_2O, and air-dried for 5 minutes. The Translinker CL-1000 UV 230 V (Fisher Scientific) was set to 1200 J. It was first run without the membrane, and then run again with the membrane to crosslink the DNA. The membrane was then rolled with the crosslinked side facing inward and placed in a 300 mm

Boekel Scientific™ Hybridization Glass Bottle for the Boekel Little Shot Oven (Fisher Scientific). 20 mL of hybridization solution were added to the bottle, and the membrane was left to prehybridize in the Compact-Line Hybridization Oven OV 4 at 42.5 °C for 1 hour.

For the DIG probe, the DIG Oligonucleotide 3'-End Labeling Kit, 2nd generation (Merck/Sigma, Cat# 3353575910) was used. The kit components included reaction buffer, $CoCl_2$ solution, DIG-ddUTPs, and terminal transferase (400 U).

The 100 µM oligonucleotide 5'-TTAGGGTTAGGGTTAGGG-3' (Tm = 55.6 °C, MW = 5669; Merck) was used, and 1 µL was pipetted into a PCR tube (200 µL, 8-well PCR strip, PCR Performance Tested, transparent, PP, flat lid; Sarstedt, Cat# 72.991.002). To this, 10 µL of ddH_2O was added, and the mixture was placed on ice. Subsequently, 4 µL reaction buffer, 4 µL $CoCl_2$ solution, 1 µL DIG-ddUTPs, and 1 µL terminal transferase (400 U) were added according to the kit instructions. The reaction was gently mixed, incubated at 37 °C for 30 minutes, and immediately placed on ice. The reaction was stopped by adding 2 µL of 0.2 M EDTA, prepared by a 1:2.5 dilution of 0.5 M EDTA (see Section 4.3.1.1).

The DIG-labeled probe was then denatured for 5 minutes at 95 °C, cooled on ice for another 5 minutes, and added to the hybridization solution in the bottle. The membrane was hybridized overnight at 42.5 °C.

Day 5 - Detection

5× DIG wash buffer (digoxigenin wash buffer), pH 7.5

	1000mL
Maleic Acid (Merck/Sigma, Cat# M0375-500G)	58g
Sodium Chloride (Merck/Sigma, Cat# S9888-2.5KG)	43.8g
Tween™ 20 (Fisher Scientific, Cat# 10113103)	15mL

Maleic acid buffer, pH 7.5

	1000mL
Maleic Acid (Merck/Sigma, Cat# M0375-500G)	11.67g
Sodium Chloride (Merck/Sigma, Cat# S9888-2.5KG)	8.76g

DIG detection buffer (digoxigenin detection buffer), pH 9.5

	1000mL
Tris(hydroxymethyl)aminomethanhydrochlorid, 99+% (Merck, Cat# A11379.30)	15.8g
Sodium Chloride (Merck/Sigma, Cat# S9888-2.5KG)	5.8g

20X SSC

	1L
Sodium Citrate, Dihydrate (Fisher Scientific, Cat# 15568154)	88.2 g
Sodium Chloride (Merck/Sigma, Cat# S9888-2.5KG)	175.3 g
ddH_2O	ad 1L

Note: The pH was adjusted to 7.0 with a few drops of HCl (Hydrochloric Acid Solution, 37%) (Merck/Sigma, Cat# 258148-500ML).

In addition to the above-mentioned solutions, 2× SSC with 0.1% SDS, 0.5× SSC with 0.1% SDS, and 10× Blocking Solution were prepared. 100 mL of 2× SSC with 0.1% SDS was prepared by diluting 10 mL of 20× SSC and 0.5 mL of 20% SDS solution with 89.5 mL of ddH_2O. Similarly, 100 mL of 0.5× SSC with 0.1% SDS was prepared by diluting 2.5 mL of 20× SSC and 0.5 mL of 20% SDS solution with 97 mL of ddH_2O. A 10× Blocking Solution was prepared by dissolving 10 g of Blocking Reagent (Merck/Sigma, Cat# 11096176001) in maleic acid buffer with gentle

heating and shaking until fully dissolved. The membrane was washed twice for 5 minutes with pre-warmed 2× SSC + 0.1% SDS at room temperature while rotating the bottle, followed by two washes for 20 minutes each with pre-warmed 0.5× SSC + 0.1% SDS at 42.5 °C under rotation. Subsequently, the membrane was briefly rinsed with 1× DIG wash buffer (prepared by diluting 5× DIG wash buffer 1:5). Blocking was performed by incubating the membrane in 10 mL of 1× Blocking Solution (prepared by diluting 10× Blocking Solution 1:10 with maleic acid buffer, pH 7.5) for 30 minutes at room temperature while rotating.

Anti-Digoxigenin-AP, Fab fragments, sheep polyclonal alkaline phosphatase conjugate (Merck/Sigma, Cat# 11093274910), 200 µL, was spun down for 5 minutes at 2000 rpm and 4 °C. 4 µL of the antibody were added to 20 mL of 1× Blocking Solution (1:5000 dilution). The membrane was incubated for 30 minutes at room temperature under rotation.

After antibody incubation, the membrane was washed four times for 15 minutes each with 1× DIG wash buffer at room temperature while rotating. The membrane was then incubated with DIG detection buffer for 5 minutes at room temperature under rotation.

The membrane was placed in a plastic sheet, and 2 mL of CDP-Star® ready-to-use solution (Merck/Sigma, Cat# 12041677001) was pipetted onto it. The solution was spread evenly by sliding the plastic sheet over the membrane, air bubbles were removed, and the membrane was incubated in the dark for 5 minutes. The CDP-Star solution was drained, and the membrane was transferred to a new plastic sheet and kept in the dark for 5–10 minutes.

Chemiluminescent signals were captured using the Chemidoc MP Imaging System (Bio-Rad Laboratories) with a 4×4 binning setting and automatic exposure time. Image analysis was performed using Image Lab software version 5.2.1 (Bio-Rad). Mean telomere length was measured using the online Walter tool (Lyčka et al., 2021).

Electronic devices and software

Electronic Device / Software	Manufacturer / Source
Eppendorf PCR Mastercycler Pro S	Eppendorf
Chemidoc MP Imaging System	Bio-Rad
Image Lab 5.2.1	Bio-Rad
Online Walter tool	Lyčka et al., 2021
Translinker CL-1000 UV 230V	Fisher Scientific
Compact-Line Hybridization Oven OV 4	Ebenrecht
PowerPac Basic	Bio-Rad
Mini-Sub Cell GT	Bio-Rad
Wide Mini-Sub Cell GT	Bio-Rad
Entris precision balance	Sartorius
Entris analytical balance	Sartorius
Orion Star™ A215 pH/Conductivity Meter	Thermo Scientific
Water Bath VWB2 12L	VWR

4.4.3 DNA Methylation Analysis

DNA samples from whole blood were analyzed using the Infinium MethylationEPIC v2.0 BeadChip (Illumina). The principle is based on the predominance of DNA methylation at cytosines within CpG dinucleotides (see Section 1.6). To distinguish between methylated and unmethylated cytosines, DNA is first treated with sodium bisulfite (Pidsley et al., 2016). This treatment converts unmethylated cytosines into uracils, while methylated cytosines remain unchanged (Frommer et al., 1992). The bisulfite-converted DNA is then amplified, during which uracils (formerly unmethylated cytosines) are replaced by thymines (Frommer et al., 1992). After amplification, the DNA is fragmented and applied to the BeadChip. On the beads, oligonucleotide probes are present that are complementary to a 50-base region of the bisulfite-converted DNA, with the CpG site of interest located at the 3’ end of the probe (Bibikova et al., 2009). After hybridization, a fluorescently labeled nucleotide is incorporated at this position, indicating whether a cytosine (methylated) or a thymine (unmethylated) is present (Pidsley et al., 2016). Following measurement of the fluorescence signal, the methylation level at a CpG site is calculated as a beta value. This value represents the ratio of the methylated signal (C) to the total signal from methylated (C) and unmethylated (T) alleles. A β-value of 0 represents a completely unmethylated CpG site, whereas a value close to 1 represents a fully methylated CpG site (Pidsley et al., 2016).

The Infinium MethylationEPIC v2.0 BeadChip uses both Type I and Type II probes. In the Type I design, two separate probes are used for each CpG site, one specific to the methylated form and the other to the unmethylated form. The methylation value is thereby calculated based on the intensity of two separate signals. For Type II probes, the methylation value is determined from the ratio of the two-color signals within the same probe. Type I probes are primarily used in CpG-rich regions, such as CpG islands, where high measurement precision is required, whereas Type II probes are more commonly applied in CpG-poor regions to save space on the chip and enable the analysis of a larger number of CpG sites (Dedeurwaerder et al., 2011; Pidsley et al., 2013; Teschendorff et al., 2013; Touleimat & Tost, 2012).

Following the generation of DNA methylation data at the Institute of Human Genetics, Genomics Division, Life & Brain Research Center, University of Bonn, the data were processed in the next step in R v4.0 using the packages minfi and wateRmelon. Quality control was performed with qcReport, densityPlot, and controlStripPlot in minfi. Sex was inferred from methylation patterns using estimateSex() from wateRmelon, and samples with discordant inferred and reported sex were excluded. Data normalization was performed using stratified quantile normalization (preprocessQuantile in minfi) by sex.

The resulting quality-controlled and normalized methylation data were then used as input for the calculation of biological age with the R package dnaMethyAge (Wang et al., 2023), which included the Horvath, Hannum, PhenoAge, GrimAge, and DunedinPACE clocks. A residual analysis was subsequently performed and age acceleration/deceleration was calculated as the residuals from a linear regression of DNAm age on chronological age for each clock.

To determine the extrinsic epigenetic age acceleration (EEAA), the biological age estimated by the Hannum clock was adjusted for the proportions of $CD8^+$ naïve and $CD8^+$ memory T cells to account for immune aging. Cell-type proportions were estimated using the FlowSorted.BloodExtended.EPIC package (Salas et al., 2022), developed at Dartmouth College, available under a non-exclusive research license from Dartmouth Technology Transfer, and used solely for non-commercial academic research purposes. Reference-based deconvolution was performed with this package, which includes an expanded reference panel of peripheral blood immune cell subpopulations, enabling high-resolution estimation of cell-type proportions.

In the second step, regression beta coefficients from the meta-analysis by Chen et al. (2017) for $CD8^+$ naïve T cells ($\beta = 0.0027$) and $CD8^+$ memory T cells ($\beta = -0.030$) were applied to weight the estimated cell proportions. This weighting incorporates age-related changes in immune cell composition into the model, thereby enabling the calculation of EEAA in addition to methylation-derived age. The meta-analysis combined data from the Women's Health Initiative (WHI), the Framingham Heart Study (FHS), and the Bogalusa Heart Study (BHS) to derive robust estimates of the association between immune cell proportions and chronological age (B. H. Chen, Carty, Kimura, Kark, Chen, Li, Zhang, Kooperberg, Levy, Assimes, et al., 2017).

4.5 Acknowledgment of Conceptual Influences

Section 1.5.2 draws in part on the argumentation and thematic framework presented by Vaiserman and Krasnienkov (2021). Sections 3.3.3 and 3.4 similarly draw in part on the framework presented by Raj (2018).

5 Abbreviations

ADL	Activities of Daily Living
ALT	Alternative Lengthening of Telomeres
ATRX	Alpha Thalassemia/Mental Retardation Syndrome X-linked
ATRX mut	Alpha Thalassemia/Mental Retardation Syndrome X-linked Mutation
B2M	Beta-2-Microglobulin
BHS	Bogalusa Heart Study
BMI	Body Mass Index
BMP	Bone Morphogenetic Protein
bp	Base Pair
CDKN2A/B	Cyclin Dependent Kinase Inhibitor 2A/B
CGA	Comprehensive Geriatric Assessment
CIRS-G	Cumulative Illness Rating Scale – Geriatric
CNS	Central Nervous System
CpG	Cytosine–phosphate–Guanine dinucleotide
CSHA	Canadian Study of Health and Aging
DAB	3,3’-Diaminobenzidine
DAXX	Death-Associated Protein 6
DIG	Digoxigenin
DIN	DNA Integrity Number
DNA	Deoxyribonucleic Acid
DNAm	DNA Methylation
DNMT	DNA-Methyltransferase
DTCS	Dye Terminator Cycle Sequencing
DunedinPACE	Dunedin Pace of Aging
EAA	Epigenetic Age Acceleration
EEAA	Extrinsic Epigenetic Age Acceleration
EGFR	Epidermal Growth Factor Receptor
ELOVL2	Elongation of Very Long Chain Fatty Acids Protein 2
EORTC QLQ-C30	European Organisation for Research and Treatment of Cancer Quality of Life Questionnaire – Core 30
ETS	E26 Transformation-Specific
Fab	Fragment antigen-binding
FFPE	Formalin-Fixed, Paraffin-Embedded
FHS	Framingham Heart Study
FI	Frailty Index
Flow-FISH	Flow Cytometry Fluorescence In Situ Hybridization
G	Gauge
G8	Geriatric 8 Screening Tool

GDF-15	Growth Differentiation Factor 15
GDS	Geriatric Depression Scale
GFI	Groningen Frailty Indicator/Index
GREM1	Gremlin 1
GrimAge	GrimAge epigenetic clock
H&E	Hematoxylin and Eosin
H3	Histone H3
Hannum	Hannum epigenetic clock
HCl	Hydrochloric Acid
HD	Home Discharge
HIF-1α	Hypoxia-Inducible Factor 1-alpha
HP1	Heterochromatin Protein 1
hTERC	Human Telomerase RNA Component
hTERT	Human Telomerase Reverse Transcriptase
IADL	Instrumental Activities of Daily Living
ICU	Intensive Care Unit
IDH	Isocitrate Dehydrogenase
IDH1 R132H mut	Isocitrate Dehydrogenase 1 R132H Mutation
IPO8	Importin 8
JP	Japanese Pharmacopoeia
Ki-67	Ki-67 proliferation index
LTL	Leukocyte Telomere Length
MAPK	Mitogen-Activated Protein Kinase
MCV	Mean Corpuscular Volume
MEK	Mitogen-Activated Protein Kinase Kinase
$MgCl_2$	Magnesium Chloride
MGMT	O^6-Methylguanine-DNA Methyltransferase
MGMT met	O^6-Methylguanine-DNA Methyltransferase Methylation
MNA	Mini Nutritional Assessment
MoCA	Montreal Cognitive Assessment
MW	Molecular Weight
NaCl	Sodium Chloride
NaOH	Sodium Hydroxide
OS	Overall Survival
P2RX6	Purinergic Receptor P2X, Ligand Gated Ion Channel, 6
PAI-1	Plasminogen Activator Inhibitor-1
PBMC	Peripheral Blood Mononuclear Cells
PBS	Phosphate Buffered Saline
PcG2	Polycomb group protein 2
PCR	Polymerase Chain Reaction
PFS	Progression-Free Survival

Ph. Eur.	Pharmacopoeia Europaea
PhenoAge	Phenotypic Age Epigenetic Clock
PI3K	Phosphoinositide 3-Kinase
PIPES	Piperazine-N,N'-bis(2-ethanesulfonic acid)
POT1	Protection of Telomeres 1
PP	Polypropylene
PSIC	Post-Surgery Institutional Care
PTEN	Phosphatase and Tensin Homolog
Q-FISH	Quantitative Fluorescence In Situ Hybridization
qPCR	Quantitative Polymerase Chain Reaction
RAF	Rapidly Accelerated Fibrosarcoma
RAP1	TRF2-interacting Protein (Repressor/Activator Protein 1)
RAS	Rat Sarcoma Virus
RDW	Red Cell Distribution Width
RNase	Ribonuclease
rSAP	Recombinant Shrimp Alkaline Phosphatase
SAP	Shrimp Alkaline Phosphatase
SASP	Senescence-Associated Secretory Phenotype
SDS	Sodium Dodecyl Sulfate
SSC	Saline-Sodium Citrate
STELA	Single Telomere Length Analysis
T-loop	Telomere Loop
TBE	Tris-Borate-EDTA Buffer
Telo-seq	Telomere Sequencing Protocol
TERT	Telomerase Reverse Transcriptase
TERT C228T mut	Telomerase Reverse Transcriptase C228T Mutation
TERT C250T mut	Telomerase Reverse Transcriptase C250T Mutation
TERTp	Telomerase Reverse Transcriptase promoter
TET	Ten-Eleven Translocation
TET2	Ten-Eleven Translocation Methylcytosine Dioxygenase 2
TGUG	Timed Get-Up-and-Go Test
TILDA	The Irish Longitudinal Study on Ageing
TIMP-1	Tissue Inhibitor of Metalloproteinases 1
TL	Telomere Length
TP53	Tumor Protein p53
TRF	Terminal Restriction Fragment
TRF1	Telomeric Repeat-binding Factor 1
TRF2	Telomeric Repeat-binding Factor 2
TRST	Triage Risk Screening Tool
USP	United States Pharmacopeia
UV	Ultraviolet
VEGF	Vascular Endothelial Growth Factor

VES-13	Vulnerable Elders Survey–13
WHI	Women’s Health Initiative
WHI BA23	Women’s Health Initiative Biomarkers and Aging Study 23
WHO	World Health Organization
WT	Wild-Type
α-KG	Alpha-Ketoglutarate

6 References

Aaronson, N. K., Ahmedzai, S., Bergman, B., Bullinger, M., Cull, A., Duez, N. J., Filiberti, A., Flechtner, H., Fleishman, S. B., & Haes, J. C. J. M. de. (1993). The European Organization for Research and Treatment of Cancer QLQ-C30: a quality-of-life instrument for use in international clinical trials in oncology. *JNCI: Journal of the National Cancer Institute*, *85*(5), 365–376. https://doi.org/10.1093/jnci/85.5.365

Abreu, E., Aritonovska, E., Reichenbach, P., Cristofari, G., Culp, B., Terns, R. M., Lingner, J., & Terns, M. P. (2010). TIN2-Tethered TPP1 Recruits Human Telomerase to Telomeres *In Vivo*. *Molecular and Cellular Biology*, *30*(12), 2971–2982. https://doi.org/10.1128/MCB.00240-10

Almeida, O. P., & Almeida, S. A. (1999). Short versions of the geriatric depression scale: a study of their validity for the diagnosis of a major depressive episode according to ICD-10 and DSM-IV. *International Journal of Geriatric Psychiatry*, *14*(10), 858–865. https://doi.org/10.1002/(sici)1099-1166(199910)14:10<858::aid-gps35>3.0.co;2-8

Arai, Y., Martin-Ruiz, C. M., Takayama, M., Abe, Y., Takebayashi, T., Koyasu, S., Suematsu, M., Hirose, N., & von Zglinicki, T. (2015). Inflammation, but not telomere length, predicts successful ageing at extreme old age: a longitudinal study of semi-supercentenarians. *EBioMedicine*, *2*(10), 1549–1558. https://doi.org/10.1016/j.ebiom.2015.07.029

Arthur, A., Jagger, C., Lindesay, J., Graham, C., & Clarke, M. (1999). Using an annual over-75 health check to screen for depression: validation of the short Geriatric Depression Scale (GDS15) within general practice. *International Journal of Geriatric Psychiatry*, *14*(6), 431–439. https://doi.org/10.1002/(SICI)1099-1166(199906)14:6<431::AID-GPS937>3.0.CO;2-I

Aubert, G., Hills, M., & Lansdorp, P. M. (2012). Telomere length measurement—Caveats and a critical assessment of the available technologies and tools. *Mutation Research/Fundamental and Molecular Mechanisms of Mutagenesis*, *730*(1–2), 59–67. https://doi.org/10.1016/j.mrfmmm.2011.04.003

Babizhayev, M. A., Savel'yeva, E. L., Moskvina, S. N., & Yegorov, Y. E. (2011). Telomere length is a biomarker of cumulative oxidative stress, biologic age, and an independent predictor of survival and therapeutic treatment requirement associated with smoking behavior. *American Journal of Therapeutics*, *18*(6), e209–e226. https://doi.org/10.1097/MJT.0b013e3181cf8ebb

Baerlocher, G. M., Mak, J., Röth, A., Rice, K. S., & Lansdorp, P. M. (2003). Telomere shortening in leukocyte subpopulations from baboons. *Journal of Leucocyte Biology*, *73*(2). https://doi.org/10.1189/jlb.0702361

Baker, D. J., Wijshake, T., Tchkonia, T., LeBrasseur, N. K., Childs, B. G., Van De Sluis, B., Kirkland, J. L., & Van Deursen, J. M. (2011). Clearance of p16Ink4a-positive senescent cells delays ageing-associated disorders. *Nature*, *479*(7372), 232–236. https://doi.org/10.1038/nature10600

Baumann, P., & Cech, T. R. (2001). Pot1, the Putative Telomere End-Binding Protein in Fission Yeast and Humans. *Science*, *292*(5519), 1171–1175. https://doi.org/10.1126/science.1060036

Bell, R. J. A., Rube, H. T., Kreig, A., Mancini, A., Fouse, S. D., Nagarajan, R. P., Choi, S., Hong, C., He, D., & Pekmezci, M. (2015). The transcription factor GABP selectively binds and activates the mutant TERT promoter in cancer. *Science*, *348*(6238), 1036–1039. https://doi.org/10.1126/science.aab0015

Bellera, C. A., Rainfray, M., Mathoulin-Pélissier, S., Mertens, C., Delva, F., Fonck, M., & Soubeyran, P. L. (2012). Screening older cancer patients: first evaluation of the G-8 geriatric screening tool. *Annals of Oncology*, *23*(8), 2166–2172. https://doi.org/10.1093/annonc/mdr587

Belsky, D. W., Caspi, A., Corcoran, D. L., Sugden, K., Poulton, R., Arseneault, L., Baccarelli, A., Chamarti, K., Gao, X., & Hannon, E. (2022). DunedinPACE, a DNA methylation biomarker of the pace of aging. *Elife*, *11*, e73420. https://doi.org/10.7554/eLife.73420

Benetos, A., Kark, J. D., Susser, E., Kimura, M., Sinnreich, R., Chen, W., Steenstrup, T., Christensen, K., Herbig, U., & von Bornemann Hjelmborg, J. (2013). Tracking and fixed ranking of leukocyte telomere length across the adult life course. *Aging Cell*, *12*(4), 615–621. https://doi.org/10.1111/acel.12086

Bergen, G. (2016). Falls and fall injuries among adults aged≥ 65 years—United States, 2014. *MMWR. Morbidity and Mortality Weekly Report*, *65*. https://doi.org/10.15585/mmwr.mm6537a2

Bessems, S. A. M., & et al. (2021). Frailty screening by Geriatric-8 and 4-meter gait speed test is feasible and predicts postoperative complications in elderly colorectal cancer patients. *Journal of Geriatric Oncology*, *12*(4), 592–598. https://doi.org/10.1016/j.jgo.2020.10.012

Bestor, T. H. (2000). The DNA methyltransferases of mammals. *Human Molecular Genetics*, *9*(16), 2395–2402. https://doi.org/10.1093/hmg/9.16.2395

Bianchi, A. (1999). TRF1 binds a bipartite telomeric site with extreme spatial flexibility. *The EMBO Journal*, *18*(20), 5735–5744. https://doi.org/10.1093/emboj/18.20.5735

Bibikova, M., Le, J., Barnes, B., Saedinia-Melnyk, S., Zhou, L., Shen, R., & Gunderson, K. L. (2009). Genome-wide DNA methylation profiling using Infinium® assay. *Epigenomics*, *1*(1), 177–200. https://doi.org/10.2217/epi.09.14

Bielderman, A., van der Schans, C. P., van Lieshout, M.-R. J., de Greef, M. H., Boersma, F., Krijnen, W. P., & Steverink, N. (2013). Multidimensional structure of the Groningen Frailty Indicator in community-dwelling older people. *BMC Geriatrics*, *13*(1), 86. https://doi.org/10.1186/1471-2318-13-86

Biernat, W., Huang, H., Yokoo, H., Kleihues, P., & Ohgaki, H. (2004). Predominant expression of mutant EGFR (EGFRvIII) is rare in primary glioblastomas. *Brain Pathology*, *14*(2), 131–136. https://doi.org/10.1111/j.1750-3639.2004.tb00045.x

Bird, A. (2002). DNA methylation patterns and epigenetic memory. *Genes & Development*, *16*(1), 6–21. https://doi.org/10.1101/gad.947102

Bird, A. P., & Wolffe, A. P. (1999). Methylation-induced repression—belts, braces, and chromatin. *Cell*, *99*(5), 451–454. https://doi.org/10.1016/s0092-8674(00)81532-9

Blackburn, E. H. (2001). Switching and signaling at the telomere. *Cell*, *106*(6), 661–673. https://doi.org/10.1016/s0092-8674(01)00492-5

Blasco, M. A. (2007). Telomere length, stem cells and aging. *Nature Chemical Biology*, *3*(10), 640–649. https://doi.org/10.1038/nchembio.2007.38

Bortz, W. M. (2002). A conceptual framework of frailty: a review. *The Journals of Gerontology Series A: Biological Sciences and Medical Sciences*, *57*(5), M283–M288. https://doi.org/10.1093/gerona/57.5.M283

Bountziouka, V., Nelson, C. P., Codd, V., Wang, Q., Musicha, C., Allara, E., Kaptoge, S., Di Angelantonio, E., Butterworth, A. S., & Thompson, J. R. (2022). Association of shorter leucocyte telomere length

with risk of frailty. *Journal of Cachexia, Sarcopenia and Muscle*, *13*(3), 1741–1751. https://doi.org/10.1002/jcsm.12971

Brat, D. J., Aldape, K., Colman, H., Figrarella-Branger, D., Fuller, G. N., Giannini, C., Holland, E. C., Jenkins, R. B., Kleinschmidt-DeMasters, B., & Komori, T. (2020). cIMPACT-NOW update 5: recommended grading criteria and terminologies for IDH-mutant astrocytomas. *Acta Neuropathologica*, *139*, 603–608. https://doi.org/10.1007/s00401-020-02127-9

Broccoli, D., Smogorzewska, A., Chong, L., & de Lange, T. (1997). Human telomeres contain two distinct Myb–related proteins, TRF1 and TRF2. *Nature Genetics*, *17*(2), 231–235. https://doi.org/10.1038/ng1097-231

Bryan, T. M., & Reddel, R. R. (1997). Telomere dynamics and telomerase activity in in vitro immortalised human cells. *European Journal of Cancer*, *33*(5), 767–773. https://doi.org/10.1016/S0959-8049(97)00065-8

Burton, D. G. A. (2009). Cellular senescence, ageing and disease. *Age*, *31*(1), 1–9. https://doi.org/10.1007/s11357-008-9075-y

Burton, D. G. A., Sheerin, A. N., Ostler, E. L., Smith, K., Giles, P. J., Lowe, J., RHYS-WILLIAMS, W., Kipling, D. G., & Faragher, R. G. A. (2007). Cyclin D1 overexpression permits the reproducible detection of senescent human vascular smooth muscle cells. *Annals of the New York Academy of Sciences*, *1119*(1), 20–31. https://doi.org/10.1196/annals.1404.026

Calado, R. T., & Dumitriu, B. (2013). Telomere dynamics in mice and humans. *Seminars in Hematology*, *50*(2), 165–174. https://doi.org/10.1053/j.seminhematol.2013.03.030

Campbell, A. J., & Buchner, D. M. (1997). Unstable disability and the fluctuations of frailty. *Age and Ageing*, *26*(4), 315–318. https://doi.org/10.1093/ageing/26.4.315

Campisi, J. (1997a). Aging and cancer: the double-edged sword of replicative senescence. *Journal of the American Geriatrics Society*, *45*(4), 482–488. https://doi.org/10.1111/j.1532-5415.1997.tb05175.x

Campisi, J. (1997b). The biology of replicative senescence. *European Journal of Cancer*, *33*(5), 703–709. https://doi.org/10.1016/S0959-8049(96)00058-5

Cannon, K. T., Choi, M. M., & Zuniga, M. A. (2006). Potentially inappropriate medication use in elderly patients receiving home health care: a retrospective data analysis. *The American Journal of Geriatric Pharmacotherapy*, *4*(2), 134–143. https://doi.org/10.1016/j.amjopharm.2006.06.010

Chen, B. H., Carty, C. L., Kimura, M., Kark, J. D., Chen, W., Li, S., Zhang, T., Kooperberg, C., Levy, D., & Assimes, T. (2017). Leukocyte telomere length, T cell composition and DNA methylation age. *Aging (Albany NY)*, *9*(9), 1983. https://doi.org/10.18632/aging.101293

Chen, B. H., Carty, C. L., Kimura, M., Kark, J. D., Chen, W., Li, S., Zhang, T., Kooperberg, C., Levy, D., Assimes, T., Absher, D., Horvath, S., Reiner, A. P., & Aviv, A. (2017). Leukocyte telomere length, T cell composition and DNA methylation age. *Aging*, *9*(9), 1983–1995. https://doi.org/10.18632/aging.101293

Chen, H. P., Zhao, Y. T., & Zhao, T. C. (2015). Histone deacetylases and mechanisms of regulation of gene expression. *Critical Reviews™ in Oncogenesis*, *20*(1–2). https://doi.org/10.1615/critrevoncog.2015012997

Christians, A., Adel-Horowski, A., Banan, R., Lehmann, U., Bartels, S., Behling, F., Barrantes-Freer, A., Stadelmann, C., Rohde, V., Stockhammer, F., & Hartmann, C. (2019). The prognostic role of IDH mutations in homogeneously treated patients with anaplastic astrocytomas and glioblastomas. *Acta Neuropathologica Communications*, *7*(1), 156. https://doi.org/10.1186/s40478-019-0817-0

Christmann, M., Verbeek, B., Roos, W. P., & Kaina, B. (2011). O6-Methylguanine-DNA methyltransferase (MGMT) in normal tissues and tumors: Enzyme activity, promoter methylation and immunohistochemistry. *Biochimica et Biophysica Acta (BBA) - Reviews on Cancer*, *1816*(2), 179–190. https://doi.org/10.1016/j.bbcan.2011.06.002

Clyne, B., Cooper, J. A., Hughes, C. M., Fahey, T., Smith, S. M., & team, O.-S. study. (2016). 'Potentially inappropriate or specifically appropriate?'Qualitative evaluation of general practitioners views on prescribing, polypharmacy and potentially inappropriate prescribing in older people. *BMC Family Practice*, *17*, 1–9. https://doi.org/10.1186/s12875-016-0507-y

Coppé, J.-P., Kauser, K., Campisi, J., & Beauséjour, C. M. (2006). Secretion of vascular endothelial growth factor by primary human fibroblasts at senescence. *Journal of Biological Chemistry*, *281*(40), 29568–29574. https://doi.org/10.1074/jbc.M603307200

Costello, J. F., Futscher, B. W., Kroes, R. A., & Pieper, R. O. (1994). Methylation-related chromatin structure is associated with exclusion of transcription factors from and suppressed expression of the O-6-methylguanine DNA methyltransferase gene in human glioma cell lines. *Molecular and Cellular Biology*, *14*(10), 6515–6521. https://doi.org/10.1128/MCB.14.10.6515

Court, R., Chapman, L., Fairall, L., & Rhodes, D. (2005). How the human telomeric proteins TRF1 and TRF2 recognize telomeric DNA: a view from high-resolution crystal structures. *EMBO Reports*, *6*(1), 39–45. https://doi.org/10.1038/sj.embor.7400314

Dang, L., White, D. W., Gross, S., Bennett, B. D., Bittinger, M. A., Driggers, E. M., Fantin, V. R., Jang, H. G., Jin, S., Keenan, M. C., Marks, K. M., Prins, R. M., Ward, P. S., Yen, K. E., Liau, L. M., Rabinowitz, J. D., Cantley, L. C., Thompson, C. B., Vander Heiden, M. G., & Su, S. M. (2009). Cancer-associated IDH1 mutations produce 2-hydroxyglutarate. *Nature*, *462*(7274), 739–744. https://doi.org/10.1038/nature08617

Deckx, L., Van Abbema, D. L., Van Den Akker, M., Van Den Broeke, C., Van Driel, M., Bulens, P., Tjan-Heijnen, V. C. G., Kenis, C., De Jonge, E. T., & Houben, B. (2015). A cohort study on the evolution of psychosocial problems in older patients with breast or colorectal cancer: comparison with younger cancer patients and older primary care patients without cancer. *BMC Geriatrics*, *15*, 1–13. https://doi.org/10.1186/s12877-015-0071-7

Decoster, L., Van Puyvelde, K., Mohile, S., Wedding, U., Basso, U., Colloca, G., Rostoft, S., Overcash, J., Wildiers, H., & Steer, C. (2015). Screening tools for multidimensional health problems warranting a geriatric assessment in older cancer patients: an update on SIOG recommendations. *Annals of Oncology*, *26*(2), 288–300. https://doi.org/10.1093/annonc/mdu210

Dedeurwaerder, S., Defrance, M., Calonne, E., Denis, H., Sotiriou, C., & Fuks, F. (2011). Evaluation of the Infinium Methylation 450K technology. *Epigenomics*, *3*(6), 771–784. https://doi.org/10.2217/epi.11.105

Demanelis, K., Jasmine, F., Chen, L. S., Chernoff, M., Tong, L., Delgado, D., Zhang, C., Shinkle, J., Sabarinathan, M., & Lin, H. (2020). Determinants of telomere length across human tissues. *Science*, *369*(6509), eaaz6876. https://doi.org/10.1126/science.aaz6876

Di Micco, R., Fumagalli, M., Cicalese, A., Piccinin, S., Gasparini, P., Luise, C., Schurra, C., Garre', M., Giovanni Nuciforo, P., & Bensimon, A. (2006). Oncogene-induced senescence is a DNA damage response triggered by DNA hyper-replication. *Nature*, *444*(7119), 638–642. https://doi.org/10.1038/nature05327

Drexler, R., Schüller, U., Eckhardt, A., Filipski, K., Hartung, T. I., Harter, P. N., Divé, I., Forster, M.-T., Czabanka, M., & Jelgersma, C. (2023). DNA methylation subclasses predict the benefit from gross total tumor resection in IDH-wildtype glioblastoma patients. *Neuro-Oncology*, *25*(2), 315–325. https://doi.org/10.1093/neuonc/noac177

Drey, M., Pfeifer, K., Sieber, C. C., & Bauer, J. M. (2011). The Fried Frailty Criteria as Inclusion Criteria for a Randomized Controlled Trial: Personal Experience and Literature Review. *Gerontology*, *57*(1), 11–18. https://doi.org/10.1159/000313433

Dunham, M. A., Neumann, A. A., Fasching, C. L., & Reddel, R. R. (2000). Telomere maintenance by recombination in human cells. *Nature Genetics*, *26*(4), 447–450. https://doi.org/10.1038/82586

Eckel-Passow, J. E., Lachance, D. H., Molinaro, A. M., Walsh, K. M., Decker, P. A., Sicotte, H., Pekmezci, M., Rice, T., Kosel, M. L., & Smirnov, I. V. (2015). Glioma groups based on 1p/19q, IDH, and TERT promoter mutations in tumors. *New England Journal of Medicine*, *372*(26), 2499–2508. https://doi.org/10.1056/NEJMoa1407279

Epel, E. S., Lin, J., Wilhelm, F. H., Wolkowitz, O. M., Cawthon, R., Adler, N. E., Dolbier, C., Mendes, W. B., & Blackburn, E. H. (2006). Cell aging in relation to stress arousal and cardiovascular disease risk factors. *Psychoneuroendocrinology*, *31*(3), 277–287. https://doi.org/10.1016/j.psyneuen.2005.08.011

Eustermann, S., Yang, J.-C., Law, M. J., Amos, R., Chapman, L. M., Jelinska, C., Garrick, D., Clynes, D., Gibbons, R. J., Rhodes, D., Higgs, D. R., & Neuhaus, D. (2011). Combinatorial readout of histone H3 modifications specifies localization of ATRX to heterochromatin. *Nature Structural & Molecular Biology*, *18*(7), 777–782. https://doi.org/10.1038/nsmb.2070

Everhard, S., Tost, J., El Abdalaoui, H., Crinière, E., Busato, F., Marie, Y., Gut, I. G., Sanson, M., Mokhtari, K., Laigle-Donadey, F., Hoang-Xuan, K., Delattre, J.-Y., & Thillet, J. (2009). Identification of regions correlating MGMT promoter methylation and gene expression in glioblastomas. *Neuro-Oncology*, *11*(4), 348–356. https://doi.org/10.1215/15228517-2009-001

Extermann, M. (2000). Measuring comorbidity in older cancer patients. *European Journal of Cancer*, *36*(4), 453–471. https://doi.org/10.1016/s0959-8049(99)00319-6

Extermann, M. (2012). Integrating a geriatric evaluation in the clinical setting. *Seminars in Radiation Oncology*, *22*(4), 272–276. https://doi.org/10.1016/j.semradonc.2012.05.003

Factor-Litvak, P., & Susser, E. (2015). The importance of early life studies of telomere attrition. *Paediatric and Perinatal Epidemiology*, *29*(2), 144. https://doi.org/10.1111/ppe.12181

Fayers, P., Bottomley, A., EORTC Quality of Life Group, & Quality of Life Unit. (2002). Quality of life research within the EORTC-the EORTC QLQ-C30. European Organisation for Research and Treatment of Cancer. *European Journal of Cancer (Oxford, England : 1990)*, *38 Suppl 4*, S125-33. https://doi.org/10.1016/s0959-8049(01)00448-8

Ferrer, A., Stephens, Z. D., & Kocher, J.-P. A. (2023). Experimental and computational approaches to measure telomere length: recent advances and future directions. *Current Hematologic Malignancy Reports*, *18*(6), 284–291. https://doi.org/10.1007/s11899-023-00717-4

Figueroa, M. E., Abdel-Wahab, O., Lu, C., Ward, P. S., Patel, J., Shih, A., Li, Y., Bhagwat, N., Vasanthakumar, A., Fernandez, H. F., Tallman, M. S., Sun, Z., Wolniak, K., Peeters, J. K., Liu, W., Choe, S. E., Fantin, V. R., Paietta, E., Löwenberg, B., … Melnick, A. (2010). Leukemic IDH1 and IDH2 Mutations Result in a Hypermethylation Phenotype, Disrupt TET2 Function, and Impair Hematopoietic Differentiation. *Cancer Cell*, *18*(6), 553–567. https://doi.org/10.1016/j.ccr.2010.11.015

Florath, I., Butterbach, K., Muller, H., Bewerunge-Hudler, M., & Brenner, H. (2014). Cross-sectional and longitudinal changes in DNA methylation with age: an epigenome-wide analysis revealing over 60 novel age-associated CpG sites. *Human Molecular Genetics*, *23*(5), 1186–1201. https://doi.org/10.1093/hmg/ddt531

Flynn, R. L., Cox, K. E., Jeitany, M., Wakimoto, H., Bryll, A. R., Ganem, N. J., Bersani, F., Pineda, J. R., Suvà, M. L., & Benes, C. H. (2015). Alternative lengthening of telomeres renders cancer cells hypersensitive to ATR inhibitors. *Science*, *347*(6219), 273–277. https://doi.org/10.1126/science.1257216

Fraga, M. F. (2009). Genetic and epigenetic regulation of aging. *Current Opinion in Immunology*, *21*(4), 446–453. https://doi.org/10.1016/j.coi.2009.04.003

Frenck Jr, R. W., Blackburn, E. H., & Shannon, K. M. (1998). The rate of telomere sequence loss in human leukocytes varies with age. *Proceedings of the National Academy of Sciences*, *95*(10), 5607–5610. https://doi.org/10.1073/pnas.95.10.5607

Fried, L. P., Tangen, C. M., Walston, J., Newman, A. B., Hirsch, C., Gottdiener, J., Seeman, T., Tracy, R., Kop, W. J., & Burke, G. (2001). Frailty in older adults: evidence for a phenotype. *The Journals of Gerontology Series a: Biological Sciences and Medical Sciences*, *56*(3), M146–M157. https://doi.org/10.1093/gerona/56.3.m146

Friedrich, C., Adamietz, I., & Pientka, L. (2012). Geriatrisches Assessment. *Der Onkologe*, *18*(2), 163–172. https://doi.org/10.1007/s00761-011-2204-8

Frommer, M., McDonald, L. E., Millar, D. S., Collis, C. M., Watt, F., Grigg, G. W., Molloy, P. L., & Paul, C. L. (1992). A genomic sequencing protocol that yields a positive display of 5-methylcytosine residues in individual DNA strands. *Proceedings of the National Academy of Sciences*, *89*(5), 1827–1831. https://doi.org/10.1073/pnas.89.5.1827

Garagnani, P., Bacalini, M. G., Pirazzini, C., Gori, D., Giuliani, C., Mari, D., Di Blasio, A. M., Gentilini, D., Vitale, G., Collino, S., Rezzi, S., Castellani, G., Capri, M., Salvioli, S., & Franceschi, C. (2012). Methylation of ELOVL2 gene as a new epigenetic marker of age. *Aging Cell*, *11*(6). https://doi.org/10.1111/acel.12005

Gardiner-Garden, M., & Frommer, M. (1987). CpG Islands in vertebrate genomes. *Journal of Molecular Biology*, *196*(2), 261–282. https://doi.org/10.1016/0022-2836(87)90689-9

Gibbons, R. J., Picketts, D. J., Villard, L., & Higgs, D. R. (1995). Mutations in a putative global transcriptional regulator cause X-linked mental retardation with α-thalassemia (ATR-X syndrome). *Cell*, *80*(6), 837–845. https://doi.org/10.1016/0092-8674(95)90287-2

Gillis, C., & Wischmeyer, P. E. (2019). Pre-operative nutrition and the elective surgical patient: why, how and what? *Anaesthesia*, *74*, 27–35. https://doi.org/10.1111/anae.14506

Gompertz, B. (1820). XVII. A sketch of an analysis and notation applicable to the estimation of the value of life contingencies. *Philosophical Transactions of the Royal Society of London*, *110*, 214–294. https://doi.org/10.1098/rstl.1820.0018

Graakjaer, J., Der-Sarkissian, H., Schmitz, A., Bayer, J., Thomas, G., Kolvraa, S., & Londoño-Vallejo, J.-A. (2006). Allele-specific relative telomere lengths are inherited. *Human Genetics*, *119*, 344–350. https://doi.org/10.1007/s00439-006-0137-x

Graakjaer, J., Pascoe, L., Der-Sarkissian, H., Thomas, G., Kolvraa, S., Christensen, K., & Londoño-Vallejo, J. (2004). The relative lengths of individual telomeres are defined in the zygote and strictly maintained during life. *Aging Cell*, *3*(3), 97–102. https://doi.org/10.1111/j.1474-9728.2004.00093.x

Graf, C. (2009). The Lawton instrumental activities of daily living (IADL) scale. *Medsurg Nurs*, *18*(5), 315–316. https://doi.org/10.1097/01.NAJ.0000314810.46029.74

Greider, C. W., & Blackburn, E. H. (1985). Identification of a specific telomere terminal transferase activity in Tetrahymena extracts. *Cell*, *43*(2), 405–413. https://doi.org/10.1016/0092-8674(85)90170-9

Griffin, C. A., Burger, P., Morsberger, L., Yonescu, R., Swierczynski, S., Weingart, J. D., & Murphy, K. M. (2006). Identification of der (1; 19)(q10; p10) in five oligodendrogliomas suggests mechanism of concurrent 1p and 19q loss. *Journal of Neuropathology & Experimental Neurology*, *65*(10), 988–994. https://doi.org/10.1097/01.jnen.0000235122.98052.8f

Griffith, J. D., Comeau, L., Rosenfield, S., Stansel, R. M., Bianchi, A., Moss, H., & De Lange, T. (1999). Mammalian telomeres end in a large duplex loop. *Cell*, *97*(4), 503–514. https://doi.org/10.1016/s0092-8674(00)80760-6

Griffiths, E., Torrance, A., & Powell, S. (2015). Emergency surgery in the elderly: challenges and solutions. *Open Access Emergency Medicine*, 55. https://doi.org/10.2147/OAEM.S68324

Grigorev, K., Foox, J., Bezdan, D., Butler, D., Luxton, J. J., Reed, J., McKenna, M. J., Taylor, L., George, K. A., & Meydan, C. (2021). Haplotype diversity and sequence heterogeneity of human telomeres. *Genome Research*, *31*(7), 1269–1279. https://doi.org/10.1101/gr.274639.120

Gritsch, S., Batchelor, T. T., & Gonzalez Castro, L. N. (2022). Diagnostic, therapeutic, and prognostic implications of the 2021 World Health Organization classification of tumors of the central nervous system. *Cancer*, *128*(1), 47–58. https://doi.org/10.1002/cncr.33918

Guigoz, Y. (2006). The mini nutritional assessment (MNA®) review of the literature-what does it tell us? *Journal of Nutrition Health and Aging*, *10*(6), 466.

Guigoz, Y., Lauque, S., & Vellas, B. J. (2002). Identifying the elderly at risk for malnutrition: The Mini Nutritional Assessment. *Clinics in Geriatric Medicine*, *18*(4), 737–757. https://doi.org/10.1016/s0749-0690(02)00059-9

Gulve, N., Su, C., Deng, Z., Soldan, S. S., Vladimirova, O., Wickramasinghe, J., Zheng, H., Kossenkov, A. V., & Lieberman, Paul. M. (2022). DAXX-ATRX regulation of p53 chromatin binding and DNA damage response. *Nature Communications*, *13*(1), 5033. https://doi.org/10.1038/s41467-022-32680-8

Guo, J. U., Su, Y., Zhong, C., Ming, G., & Song, H. (2011). Hydroxylation of 5-Methylcytosine by TET1 Promotes Active DNA Demethylation in the Adult Brain. *Cell*, *145*(3), 423–434. https://doi.org/10.1016/j.cell.2011.03.022

Gutman, D., & Atzmon, G. (2019). Genomic and Epigenomic Potential With Age: Genome, Epigenome, and the Epigenetic Clock. In D. Palacios (Ed.), *Epigenetics and Regeneration* (1st ed., Vol. 11, pp. 445–459). Elsevier. https://doi.org/10.1016/b978-0-12-814879-2.00019-4

Hamerman, D. (1999). Toward an understanding of frailty. *Annals of Internal Medicine*, *130*(11), 945–950. https://doi.org/10.7326/0003-4819-130-11-199906010-00022

Hannum, G., Guinney, J., Zhao, L., Zhang, L. I., Hughes, G., Sadda, S., Klotzle, B., Bibikova, M., Fan, J.-B., & Gao, Y. (2013a). Genome-wide methylation profiles reveal quantitative views of human aging rates. *Molecular Cell*, *49*(2), 359–367. https://doi.org/10.1016/j.molcel.2012.10.016

Hannum, G., Guinney, J., Zhao, L., Zhang, L. I., Hughes, G., Sadda, S., Klotzle, B., Bibikova, M., Fan, J.-B., & Gao, Y. (2013b). Genome-wide methylation profiles reveal quantitative views of human aging rates. *Molecular Cell*, *49*(2), 359–367. https://doi.org/10.1016/j.molcel.2012.10.016

Harikumar, A., & Meshorer, E. (2015). Chromatin remodeling and bivalent histone modifications in embryonic stem cells. *EMBO Reports*, *16*(12), 1609–1619. https://doi.org/10.15252/embr.201541011

Harman, D. (1981). The aging process. *Proceedings of the National Academy of Sciences*, *78*(11), 7124–7128. https://doi.org/10.1073/pnas.78.11.7124

Hashimshony, T., Zhang, J., Keshet, I., Bustin, M., & Cedar, H. (2003). The role of DNA methylation in setting up chromatin structure during development. *Nature Genetics*, *34*(2), 187–192. https://doi.org/10.1038/ng1158

Hastings, W. J., Shalev, I., & Belsky, D. W. (2017). Translating measures of biological aging to test effectiveness of geroprotective interventions: what can we learn from research on telomeres? *Frontiers in Genetics*, *8*, 164. https://doi.org/10.3389/fgene.2017.00164

Hayflick, L., & Moorhead, P. S. (1961). The serial cultivation of human diploid cell strains. *Experimental Cell Research*, *25*(3), 585–621. https://doi.org/10.1016/0014-4827(61)90192-6

Heaphy, C. M., Subhawong, A. P., Hong, S.-M., Goggins, M. G., Montgomery, E. A., Gabrielson, E., Netto, G. J., Epstein, J. I., Lotan, T. L., & Westra, W. H. (2011). Prevalence of the alternative lengthening of telomeres telomere maintenance mechanism in human cancer subtypes. *The American Journal of Pathology*, *179*(4), 1608–1615. https://doi.org/10.1016/j.ajpath.2011.06.018

Henson, J. D., Neumann, A. A., Yeager, T. R., & Reddel, R. R. (2002). Alternative lengthening of telomeres in mammalian cells. *Oncogene*, *21*(4), 598–610. https://doi.org/10.1038/sj.onc.1205058

Herrmann, M., Pusceddu, I., März, W., & Herrmann, W. (2018). Telomere biology and age-related diseases. *Clinical Chemistry and Laboratory Medicine (CCLM)*, *56*(8), 1210–1222. https://doi.org/10.1515/cclm-2017-0870

Hertler, C., Felsberg, J., Gramatzki, D., Le Rhun, E., Clarke, J., Soffietti, R., Wick, W., Chinot, O., Ducray, F., & Roth, P. (2023). Long-term survival with IDH wildtype glioblastoma: first results from the ETERNITY Brain Tumor Funders' Collaborative Consortium (EORTC 1419). *European Journal of Cancer*, *189*, 112913. https://doi.org/10.1016/j.ejca.2023.05.002

Holliday, R., & Pugh, J. E. (1975). DNA modification mechanisms and gene activity during development. *Science (New York, N.Y.)*, *187*(4173), 226–232.

Holoch, D., & Moazed, D. (2015). RNA-mediated epigenetic regulation of gene expression. *Nature Reviews Genetics*, *16*(2), 71–84. https://doi.org/10.1038/nrg3863

Hon, T., Mars, K., Young, G., Tsai, Y.-C., Karalius, J. W., Landolin, J. M., Maurer, N., Kudrna, D., Hardigan, M. A., & Steiner, C. C. (2020). Highly accurate long-read HiFi sequencing data for five complex genomes. *Scientific Data*, *7*(1), 399. https://doi.org/10.1038/s41597-020-00743-4

Hoogendijk, E. O., Rockwood, K., Theou, O., Armstrong, J. J., Onwuteaka-Philipsen, B. D., Deeg, D. J. H., & Huisman, M. (2018). Tracking changes in frailty throughout later life: results from a 17-year longitudinal study in the Netherlands. *Age and Ageing*, *47*(5), 727–733. https://doi.org/10.1093/ageing/afy081

Hopko, D. R., Bell, J. L., Armento, M. E. A., Robertson, S. M. C., Hunt, M. K., Wolf, N. J., & Mullane, C. (2008). The phenomenology and screening of clinical depression in cancer patients. *Journal of Psychosocial Oncology*, *26*(1), 31–51. https://doi.org/10.1300/j077v26n01_03

Horvath, S. (2013). DNA methylation age of human tissues and cell types. *Genome Biology*, *14*, 1–20. https://doi.org/10.1186/gb-2013-14-10-r115

Horvath, S., & Raj, K. (2018). DNA methylation-based biomarkers and the epigenetic clock theory of ageing. *Nature Reviews Genetics*, *19*(6), 371–384. https://doi.org/10.1038/s41576-018-0004-3

International Society of Geriatric Oncology. (n.d.). *Comprehensive Geriatric Assessment*. SIOG. Retrieved April 13, 2025, from https://siog.org/educational-resources/comprehensive-geriatric-assessment/

Ito, S., D'Alessio, A. C., Taranova, O. V., Hong, K., Sowers, L. C., & Zhang, Y. (2010). Role of Tet proteins in 5mC to 5hmC conversion, ES-cell self-renewal and inner cell mass specification. *Nature*, *466*(7310), 1129–1133. https://doi.org/10.1038/nature09303

Jain, M., Koren, S., Miga, K. H., Quick, J., Rand, A. C., Sasani, T. A., Tyson, J. R., Beggs, A. D., Dilthey, A. T., & Fiddes, I. T. (2018). Nanopore sequencing and assembly of a human genome with ultra-long reads. *Nature Biotechnology*, *36*(4), 338–345. https://doi.org/10.1038/nbt.4060

Johansson, Å., Enroth, S., & Gyllensten, U. (2013). Continuous aging of the human DNA methylome throughout the human lifespan. *PloS One*, *8*(6), e67378. https://doi.org/10.1371/journal.pone.0067378

Johnson, B. E., Mazor, T., Hong, C., Barnes, M., Aihara, K., McLean, C. Y., Fouse, S. D., Yamamoto, S., Ueda, H., & Tatsuno, K. (2014). Mutational analysis reveals the origin and therapy-driven evolution of recurrent glioma. *Science*, *343*(6167), 189–193. https://doi.org/10.1126/science.1239947

Johnson, T. E. (2006). Recent results: biomarkers of aging. *Experimental Gerontology*, *41*(12), 1243–1246. https://doi.org/10.1016/j.exger.2006.09.006

Jones, M. J., Goodman, S. J., & Kobor, M. S. (2015). DNA methylation and healthy human aging. *Aging Cell*, *14*(6), 924–932. https://doi.org/10.1111/acel.12349

Kabacik, S., Horvath, S., Cohen, H., & Raj, K. (2018). Epigenetic ageing is distinct from senescence-mediated ageing and is not prevented by telomerase expression. *Aging (Albany NY)*, *10*(10), 2800. https://doi.org/10.18632/aging.101588

Katz, S., Downs, T. D., Cash, H. R., & Grotz, R. C. (1970). Progress in development of the index of ADL. *The Gerontologist*, *10*(1_Part_1), 20–30. https://doi.org/10.1093/geront/10.1_part_1.20

Katz, S., Ford, A. B., Moskowitz, R. W., Jackson, B. A., & Jaffe, M. W. (1963). Studies of illness in the aged: the index of ADL: a standardized measure of biological and psychosocial function. *Jama*, *185*(12), 914–919. https://doi.org/10.1001/jama.1963.03060120024016

Kaul, Z., Cesare, A. J., Huschtscha, L. I., Neumann, A. A., & Reddel, R. R. (2012). Five dysfunctional telomeres predict onset of senescence in human cells. *EMBO Reports*, *13*(1), 52–59. https://doi.org/10.1038/embor.2011.227

Kim, S. J., & Korc-Grodzicki, B. (2017). Falls in the Older Cancer Patient. In B. Korc-Grodzicki & W. P. Tew (Eds.), *Handbook of Geriatric Oncology: Practical Guide to Caring for the Older Cancer Patient* (1st ed.). Demos Medical Publishing. https://doi.org/10.1891/9781617052828.0006

Kimura, M., Gazitt, Y., Cao, X., Zhao, X., Lansdorp, P. M., & Aviv, A. (2010). Synchrony of telomere length among hematopoietic cells. *Experimental Hematology*, *38*(10), 854–859. https://doi.org/10.1016/j.exphem.2010.06.010

Kletsas, D., Pratsinis, H., Mariatos, G., Zacharatos, P., & Gorgoulis, V. G. (2004). The proinflammatory phenotype of senescent cells: the p53-mediated ICAM-1 expression. *Annals of the New York Academy of Sciences*, *1019*(1), 330–332. https://doi.org/10.1196/annals.1297.056

Ko, F. C.-Y. (2011). The clinical care of frail, older adults. *Clinics in Geriatric Medicine*, *27*(1), 89–100. https://doi.org/10.1016/j.cger.2010.08.007

Krasnienkov, D. S., Khalangot, M. D., Kravchenko, V. I., Kovtun, V. A., Guryanov, V. G., Chizhova, V. P., Korkushko, O. V., Shatilo, V. B., Kukharsky, V. M., & Vaiserman, A. M. (2018). Hyperglycemia

attenuates the association between telomere length and age in Ukrainian population. *Experimental Gerontology*, *110*, 247–252. https://doi.org/10.1016/j.exger.2018.06.027

Lai, T.-P., Wright, W. E., & Shay, J. W. (2018). Comparison of telomere length measurement methods. *Philosophical Transactions of the Royal Society B: Biological Sciences*, *373*(1741), 20160451. https://doi.org/10.1098/rstb.2016.0451

Lansdorp, P. M., Verwoerd, N. P., Van De Rijke, F. M., Dragowska, V., Little, M.-T., Dirks, R. W., Raap, A. K., & Tanke, H. J. (1996). Heterogeneity in telomere length of human chromosomes. *Human Molecular Genetics*, *5*(5), 685–691. https://doi.org/10.1093/hmg/5.5.685

Larsen, F., Gundersen, G., Lopez, R., & Prydz, H. (1992). CpG islands as gene markers in the human genome. *Genomics*, *13*(4), 1095–1107. https://doi.org/10.1016/0888-7543(92)90024-M

Lawton, M. P. (1969). Assesment of older people: self Maintaining and instrumental activeties of daily living. *Geroulologist*, *9*, 168–179. https://doi.org/10.1093/geront/9.3_Part_1.179

Le Saux, O., Watelet, S., Haution-Bitker, M., Murard-Reeman, F., Lecardonnel, C., Harchaoui, M., Bonnefoy, M., & Falandry, C. (2017). Physiologic Changes of Aging. In B. Korc-Grodzicki & W. P. Tew (Eds.), *Handbook of Geriatric Oncology: Practical Guide to Caring for the Older Cancer Patient* (pp. 9–22). Demos Medical Publishing. https://doi.org/10.1891/9781617052828.0002

Leeper, H. E., Caron, A. A., Decker, P. A., Jenkins, R. B., Lachance, D. H., & Giannini, C. (2015). IDH mutation, 1p19q codeletion and ATRX loss in WHO grade II gliomas. *Oncotarget*, *6*(30), 30295. https://doi.org/10.18632/oncotarget.4497

Lei, M., Podell, E. R., & Cech, T. R. (2004). Structure of human POT1 bound to telomeric single-stranded DNA provides a model for chromosome end-protection. *Nature Structural & Molecular Biology*, *11*(12), 1223–1229. https://doi.org/10.1038/nsmb867

Levine, M. E. (2019). Epigenetic biomarkers of aging. In *Biomarkers of Aging* (Moskalev, A., Vol. 10, pp. 155–171). Springer International Publishing AG. https://doi.org/10.1007/978-3-030-24970-0_11

Levine, M. E. (2022). *True Age: Cutting-Edge Research To Help Turn Back The Clock*. Yellow Kite, Hodder & Stoughton Ltd.

Levine, M. E., Lu, A. T., Quach, A., Chen, B. H., Assimes, T. L., Bandinelli, S., Hou, L., Baccarelli, A. A., Stewart, J. D., & Li, Y. (2018). An epigenetic biomarker of aging for lifespan and healthspan. *Aging (Albany NY)*, *10*(4), 573. https://doi.org/10.18632/aging.101414

Lewis, P. W., Elsaesser, S. J., Noh, K.-M., Stadler, S. C., & Allis, C. D. (2010). Daxx is an H3.3-specific histone chaperone and cooperates with ATRX in replication-independent chromatin assembly at telomeres. *Proceedings of the National Academy of Sciences*, *107*(32), 14075–14080. https://doi.org/10.1073/pnas.1008850107

Libermann, T. A., Nusbaum, H. R., Razon, N., Kris, R., Lax, I., Soreq, H., Whittle, N., Waterfield, M. D., Ullrich, A., & Schlessinger, J. (1985). Amplification, enhanced expression and possible rearrangement of EGF receptor gene in primary human brain tumours of glial origin. *Nature*, *313*(5998), 144–147. https://doi.org/10.1038/313144a0

Lin, J., Kaur, P., Countryman, P., Opresko, P. L., & Wang, H. (2014). Unraveling secrets of telomeres: one molecule at a time. *DNA Repair*, *20*, 142–153. https://doi.org/10.1016/j.dnarep.2014.01.012.

Liu, W., James, C. D., Frederick, L., Alderete, B. E., & Jenkins, R. B. (1997). PTEN/MMAC1 mutations and EGFR amplification in glioblastomas. *Cancer Research*, *57*(23), 5254–5257.

Loayza, D., & de Lange, T. (2003). POT1 as a terminal transducer of TRF1 telomere length control. *Nature*, *423*(6943), 1013–1018. https://doi.org/10.1038/nature01688

Logsdon, G. A., Vollger, M. R., & Eichler, E. E. (2020). Long-read human genome sequencing and its applications. *Nature Reviews Genetics*, *21*(10), 597–614. https://doi.org/10.1038/s41576-020-0236-x

Lopez-Gines, C., Cerda-Nicolas, M., Gil-Benso, R., Pellin, A., Lopez-Guerrero, J. A., Callaghan, R., Benito, R., Roldan, P., Piquer, J., & Llacer, J. (2005). Association of chromosome 7, chromosome 10 and EGFR gene amplification in glioblastoma multiforme. *Clinical Neuropathology*, *24*(5).

Louis, D. N., Perry, A., Reifenberger, G., Von Deimling, A., Figarella-Branger, D., Cavenee, W. K., Ohgaki, H., Wiestler, O. D., Kleihues, P., & Ellison, D. W. (2016). The 2016 World Health Organization classification of tumors of the central nervous system: a summary. *Acta Neuropathologica*, *131*, 803–820. https://doi.org/10.1007/s00401-016-1545-1

Louis, D. N., Perry, A., Wesseling, P., Brat, D. J., Cree, I. A., Figarella-Branger, D., Hawkins, C., Ng, H. K., Pfister, S. M., & Reifenberger, G. (2021). The 2021 WHO classification of tumors of the central nervous system: a summary. *Neuro-Oncology*, *23*(8), 1231–1251. https://doi.org/10.1093/neuonc/noab106

Lowe, D., Horvath, S., & Raj, K. (2016). Epigenetic clock analyses of cellular senescence and ageing. *Oncotarget*, *7*(8), 8524. https://doi.org/10.18632/oncotarget.7383

Lu, A. T., Quach, A., Wilson, J. G., Reiner, A. P., Aviv, A., Raj, K., Hou, L., Baccarelli, A. A., Li, Y., & Stewart, J. D. (2019). DNA methylation GrimAge strongly predicts lifespan and healthspan. *Aging (Albany NY)*, *11*(2), 303. https://doi.org/10.18632/aging.101684

Lukens, J. N., Van Deerlin, V., Clark, C. M., Xie, S. X., & Johnson, F. B. (2009). Comparisons of telomere lengths in peripheral blood and cerebellum in Alzheimer's disease. *Alzheimer's & Dementia*, *5*(6), 463–469. https://doi.org/10.1016/j.jalz.2009.05.666

Luxton, J. J., McKenna, M. J., Taylor, L. E., George, K. A., Zwart, S. R., Crucian, B. E., Drel, V. R., Garrett-Bakelman, F. E., Mackay, M. J., & Butler, D. (2020). Temporal telomere and DNA damage responses in the space radiation environment. *Cell Reports*, *33*(10). https://doi.org/10.1016/j.celrep.2020.108435

Lyčka, M., Peska, V., Demko, M., Spyroglou, I., Kilar, A., Fajkus, J., & Fojtová, M. (2021). WALTER: an easy way to online evaluate telomere lengths from terminal restriction fragment analysis. *BMC Bioinformatics*, *22*, 1–14. https://doi.org/10.1186/s12859-021-04064-0

Makarov, V. L., Hirose, Y., & Langmore, J. P. (1997). Long G tails at both ends of human chromosomes suggest a C strand degradation mechanism for telomere shortening. *Cell*, *88*(5), 657–666. https://doi.org/10.1016/s0092-8674(00)81908-x

Makeham, W. M. (1860). On the law of mortality and the construction of annuity tables. *The Assurance Magazine, and Journal of the Institute of Actuaries*, *8*(6), 301–310. https://doi.org/10.1017/s204616580000126x

Malmström, A., Grønberg, B. H., Marosi, C., Stupp, R., Frappaz, D., Schultz, H., Abacioglu, U., Tavelin, B., Lhermitte, B., & Hegi, M. E. (2012). Temozolomide versus standard 6-week radiotherapy versus hypofractionated radiotherapy in patients older than 60 years with glioblastoma: the Nordic randomised, phase 3 trial. *The Lancet Oncology*, *13*(9), 916–926. https://doi.org/10.1016/S1470-2045(12)70265-6

Mangélinck, A., & Mann, C. (2021). DNA methylation and histone variants in aging and cancer. In U. Weyemi & L. Galluzzi (Eds.), *International Review of Cell and Molecular Biology* (Vol. 364, pp. 1–24). Academic Press. https://doi.org/10.1016/bs.ircmb.2021.06.002

Martínez, P., & Blasco, M. A. (2015). Replicating through telomeres: a means to an end. *Trends in Biochemical Sciences*, *40*(9), 504–515. https://doi.org/10.1016/j.tibs.2015.06.003

Martinez, P., Thanasoula, M., Carlos, A. R., Gómez-López, G., Tejera, A. M., Schoeftner, S., Dominguez, O., Pisano, D. G., Tarsounas, M., & Blasco, M. A. (2010). Mammalian Rap1 controls telomere function and gene expression through binding to telomeric and extratelomeric sites. *Nature Cell Biology*, *12*(8), 768–780. https://doi.org/10.1038/ncb2081

Masnoon, N., Shakib, S., Kalisch-Ellett, L., & Caughey, G. E. (2017). What is polypharmacy? A systematic review of definitions. *BMC Geriatrics*, *17*(1), 230. https://doi.org/10.1186/s12877-017-0621-2

Mather, K. A., Jorm, A. F., Parslow, R. A., & Christensen, H. (2011). Is telomere length a biomarker of aging? A review. *Journals of Gerontology Series A: Biomedical Sciences and Medical Sciences*, *66*(2), 202–213. https://doi.org/10.1093/gerona/glq180

Mathias, S., Nayak, U. S., & Isaacs, B. (1986). Balance in elderly patients: the" get-up and go" test. *Archives of Physical Medicine and Rehabilitation*, *67*(6), 387–389.

McCrory, C., Fiorito, G., Hernandez, B., Polidoro, S., O'Halloran, A. M., Hever, A., Cheallaigh, C. N., Lu, A. T., Horvath, S., & Vineis, P. (2020). Association of 4 epigenetic clocks with measures of functional health, cognition, and all-cause mortality in The Irish Longitudinal Study on Ageing (TILDA). *BioRxiv*, 2020–2024. https://doi.org/10.1101/2020.04.27.063164

McCrory, C., Fiorito, G., Hernandez, B., Polidoro, S., O'Halloran, A. M., Hever, A., Ni Cheallaigh, C., Lu, A. T., Horvath, S., Vineis, P., & Kenny, R. A. (2021). GrimAge Outperforms Other Epigenetic Clocks in the Prediction of Age-Related Clinical Phenotypes and All-Cause Mortality. *The Journals of Gerontology: Series A*, *76*(5), 741–749. https://doi.org/10.1093/gerona/glaa286

Meckstroth, S., Tin, A. L., Downey, R. J., Korc-Grodzicki, B., Vickers, A. J., & Shahrokni, A. (2024). Preoperative frailty predicts postoperative falls in older patients with cancer. *Journal of Geriatric Oncology*, *15*(2), 101688. https://doi.org/10.1016/j.jgo.2023.101688

Miller, M. D., Paradis, C. F., Houck, P. R., Mazumdar, S., Stack, J. A., Rifai, A. H., Mulsant, B., & Reynolds, C. F. (1992). Rating chronic medical illness burden in geropsychiatric practice and research: Application of the Cumulative Illness Rating Scale. *Psychiatry Research*, *41*(3), 237–248. https://doi.org/10.1016/0165-1781(92)90005-N

Miller, M. D., & Towers, A. (1991). *A manual of guidelines for scoring the Cumulative Illness Rating Scale for Geriatrics (CIRS-G)*. https://www.anq.ch/fileadmin/redaktion/deutsch/20121211_CIRSG_Manual_E.pdf

Miller, R. A. (2001). Biomarkers of Aging: A generally optimistic but not too gullible appraisal. In *Science of Aging Knowledge Environment* (Vol. 2001, Issue 1, pp. pe2–pe2). American Association for the Advancement of Science. https://doi.org/10.1126/sageke.2001.1.pe2

Mitnitski, A. B., Mogilner, A. J., & Rockwood, K. (2001). Accumulation of deficits as a proxy measure of aging. *The Scientific World Journal*, *1*(2), 323–336. https://doi.org/10.1100/tsw.2001.58

Mitnitski, A., Howlett, S. E., & Rockwood, K. (2016). Heterogeneity of Human Aging and Its Assessment. *The Journals of Gerontology Series A: Biological Sciences and Medical Sciences*. https://doi.org/10.1093/gerona/glw089

Mitnitski, A., & Rockwood, K. (2015). Aging as a process of deficit accumulation: its utility and origin. *Interdiscip Top Gerontol*, *40*, 85–98. https://doi.org/10.1159/000364933

Mitnitski, A., & Rockwood, K. (2016). The rate of aging: the rate of deficit accumulation does not change over the adult life span. *Biogerontology*, *17*, 199–204. https://doi.org/10.1007/s10522-015-9583-y

Mitnitski, A., & Rockwood, K. (2019). The Problem of Integrating of Biological and Clinical Markers of Aging. In A. Moskalev (Ed.), *Biomarkers of Human Aging* (Vol. 10, pp. 399–416). Springer. https://doi.org/10.1007/978-3-030-24970-0_23

Modrek, A. S., Bayin, N. S., & Placantonakis, D. G. (2014). Brain stem cells as the cell of origin in glioma. *World Journal of Stem Cells*, *6*(1), 43. https://doi.org/10.4252/wjsc.v6.i1.43

Monk, M., Adams, R. L. P., & Rinaldi, A. (1991). Decrease in DNA methylase activity during preimplantation development in the mouse. *Development*, *112*(1), 189–192. https://doi.org/10.1242/dev.112.1.189

Montamat, S. C., & Cusack, B. (1992). Overcoming problems with polypharmacy and drug misuse in the elderly. *Clinics in Geriatric Medicine*, *8*(1), 143–158. https://doi.org/10.1016/S0749-0690(18)30503-2

Nan, X., Hou, J., Maclean, A., Nasir, J., Lafuente, M. J., Shu, X., Kriaucionis, S., & Bird, A. (2007). Interaction between chromatin proteins MECP2 and ATRX is disrupted by mutations that cause inherited mental retardation. *Proceedings of the National Academy of Sciences*, *104*(8), 2709–2714. https://doi.org/10.1073/pnas.0608056104

Nan, X., Ng, H.-H., Johnson, C. A., Laherty, C. D., Turner, B. M., Eisenman, R. N., & Bird, A. (1998). Transcriptional repression by the methyl-CpG-binding protein MeCP2 involves a histone deacetylase complex. *Nature*, *393*(6683), 386–389. https://doi.org/10.1038/30764

Nasreddine, Z. S., Phillips, N. A., Bédirian, V., Charbonneau, S., Whitehead, V., Collin, I., Cummings, J. L., & Chertkow, H. (2005). The Montreal Cognitive Assessment, MoCA: a brief screening tool for mild cognitive impairment. *Journal of the American Geriatrics Society*, *53*(4), 695–699. https://doi.org/10.1111/j.1532-5415.2005.53221.x

Natsume, K., Yoshida, A., Sakakima, H., Yonezawa, H., Kawamura, K., Akihiro, S., Hanaya, R., & Shimodozono, M. (2024). Age-independent benefits of postoperative rehabilitation during chemoradiotherapy on functional outcomes and survival in patients with glioblastoma. *Journal of Neuro-Oncology*, *170*(1), 129–137. https://doi.org/10.1007/s11060-024-04785-1

Niccoli, T., & Partridge, L. (2012). Ageing as a risk factor for disease. *Current Biology*, *22*(17), R741–R752. https://doi.org/10.1016/j.cub.2012.07.024

Nightingale, G., Skonecki, E., & Boparai, M. K. (2017). The impact of polypharmacy on patient outcomes in older adults with cancer. *The Cancer Journal*, *23*(4), 211–218. https://doi.org/10.1097/PPO.0000000000000277

Nikolaos Panagiotou. (2025). Aging . In A. Tsatsakis (Ed.), *Telomeres: Biomarkers of a Healthy Life and Successful Aging*. Jenny Stanford Publishing Pte. Ltd.

Njajou, O. T., Cawthon, R. M., Blackburn, E. H., Harris, T. B., Li, R., Sanders, J. L., Newman, A. B., Nalls, M., Cummings, S. R., & Hsueh, W.-C. (2012). Shorter telomeres are associated with obesity and weight gain in the elderly. *International Journal of Obesity*, *36*(9), 1176–1179. https://doi.org/10.1038/ijo.2011.196

Ohki, R., Tsurimoto, T., & Ishikawa, F. (2001). In Vitro Reconstitution of the End Replication Problem. *Molecular and Cellular Biology*, *21*(17), 5753–5766. https://doi.org/10.1128/MCB.21.17.5753-5766.2001

Okuda, K., Bardeguez, A., Gardner, J. P., Rodriguez, P., Ganesh, V., Kimura, M., Skurnick, J., Awad, G., & Aviv, A. (2002). Telomere length in the newborn. *Pediatric Research*, *52*(3), 377–381. https://doi.org/10.1203/00006450-200209000-00012

O'sullivan, R. J., & Karlseder, J. (2010). Telomeres: protecting chromosomes against genome instability. *Nature Reviews Molecular Cell Biology*, *11*(3), 171–181. https://doi.org/10.1038/nrm2848

Oxford Nanopore Technologies. (2023). *Telo-seq: Native sequencing of individual telomeres on R10 nanopores*. Oxford Nanopore Technologies. https://nanoporetech.com/resource-centre/telo-seq-native-sequencing-of-individual-telomeres-on-r10-nanopores

Oxford Nanopore Technologies. (2024). *Oxford Nanopore Sequencing Platform*. Oxford Nanopore. https://nanoporetech.com/platform/

Pal, S., & Tyler, J. K. (2016). Epigenetics and aging. *Science Advances*, *2*(7). https://doi.org/10.1126/sciadv.1600584

Parmelee, P. A., Thuras, P. D., Katz, I. R., & Lawton, M. P. (1995). Validation of the Cumulative Illness Rating Scale in a geriatric residential population. *Journal of the American Geriatrics Society*, *43*(2), 130–137. https://doi.org/10.1111/j.1532-5415.1995.tb06377.x

Pegg, A. E., Dolan, M. E., & Moschel, R. C. (1995). *Structure, Function, and Inhibition of O6-Alkylguanine-DNA Alkyltransferase* (pp. 167–223). https://doi.org/10.1016/S0079-6603(08)60879-X

Peters, L. L., Boter, H., Buskens, E., & Slaets, J. P. J. (2012). Measurement Properties of the Groningen Frailty Indicator in Home-Dwelling and Institutionalized Elderly People. *Journal of the American Medical Directors Association*, *13*(6), 546–551. https://doi.org/10.1016/j.jamda.2012.04.007

Pidsley, R., Y Wong, C. C., Volta, M., Lunnon, K., Mill, J., & Schalkwyk, L. C. (2013). A data-driven approach to preprocessing Illumina 450K methylation array data. *BMC Genomics*, *14*(1), 293. https://doi.org/10.1186/1471-2164-14-293

Pidsley, R., Zotenko, E., Peters, T. J., Lawrence, M. G., Risbridger, G. P., Molloy, P., Van Djik, S., Muhlhausler, B., Stirzaker, C., & Clark, S. J. (2016). Critical evaluation of the Illumina MethylationEPIC BeadChip microarray for whole-genome DNA methylation profiling. *Genome Biology*, *17*(1), 208. https://doi.org/10.1186/s13059-016-1066-1

Pieper, R. O., Lester, K. A., & Fanton, C. P. (1999). Confluence-induced alterations in CpG island methylation in cultured normal human fibroblasts. *Nucleic Acids Research*, *27*(15), 3229–3235. https://doi.org/10.1093/nar/27.15.3229

Pinkham, M. B., Telford, N., Whitfield, G. A., Colaco, R. J., O'Neill, F., & McBain, C. A. (2015). FISHing tips: what every clinician should know about 1p19q analysis in gliomas using fluorescence in situ hybridisation. *Clinical Oncology*, *27*(8), 445–453. https://doi.org/10.1016/j.clon.2015.04.008

Podolskiy, D. I., & Gladyshev, V. N. (2019). DNA Methylation Markers to Assess Biological Age. In A. Moskalev (Ed.), *Biomarkers of Human Aging* (Vol. 10, pp. 173–184). Springer Nature Switzerland AG. https://doi.org/10.1007/978-3-030-24970-0_12

Podsiadlo, D., & Richardson, S. (1991). The timed "Up & Go": a test of basic functional mobility for frail elderly persons. *Journal of the American Geriatrics Society*, *39*(2), 142–148. https://doi.org/10.1111/j.1532-5415.1991.tb01616.x

Raj, K. (2018). The Epigenetic Clock and Aging. In Alexey Moskalev & Alexander M. Vaiserman (Eds.), *Epigenetics of Aging and Longevity* (Vol. 4, pp. 95–118). Elsevier. https://doi.org/10.1016/B978-0-12-811060-7.00004-8

Rakyan, V. K., Down, T. A., Maslau, S., Andrew, T., Yang, T.-P., Beyan, H., Whittaker, P., McCann, O. T., Finer, S., & Valdes, A. M. (2010). Human aging-associated DNA hypermethylation occurs preferentially at bivalent chromatin domains. *Genome Research*, *20*(4), 434–439. https://doi.org/10.1101/gr.103101.109

Rattan, S. I. S. (2013). Healthy ageing, but what is health? *Biogerontology*, *14*(6), 673–677. https://doi.org/10.1007/s10522-013-9442-7

Razin, A., & Kafri, T. (1994). *DNA Methylation from Embryo to Adult* (pp. 53–81). https://doi.org/10.1016/S0079-6603(08)60853-3

Riggs, A. D. (1975). X inactivation, differentiation, and DNA methylation. *Cytogenetic and Genome Research*, *14*(1), 9–25. https://doi.org/10.1159/000130315

Robinson, T. N., Walston, J. D., Brummel, N. E., Deiner, S., Brown IV, C. H., Kennedy, M., & Hurria, A. (2015). Frailty for surgeons: review of a national institute on aging conference on frailty for specialists. *Journal of the American College of Surgeons*, *221*(6). https://doi.org/10.1016/j.jamcollsurg.2015.08.428

Rochon, P. A., & Gurwitz, J. H. (2017). The prescribing cascade revisited. *The Lancet*, *389*(10081), 1778–1780. https://doi.org/10.1016/S0140-6736(17)31188-1

Rockwood, K., Blodgett, J. M., Theou, O., Sun, M. H., Feridooni, H. A., Mitnitski, A., Rose, R. A., Godin, J., Gregson, E., & Howlett, S. E. (2017). A Frailty Index Based On Deficit Accumulation Quantifies Mortality Risk in Humans and in Mice. *Scientific Reports*, *7*(1), 43068. https://doi.org/10.1038/srep43068

Rockwood, K., Fox, R. A., Stolee, P., Robertson, D., & Beattie, B. L. (1994). Frailty in elderly people: an evolving concept. *CMAJ: Canadian Medical Association Journal*, *150*(4), 489.

Rockwood, K., Hogan, D. B., & MacKnight, C. (2000). Conceptualisation and measurement of frailty in elderly people. *Drugs & Aging*, *17*, 295–302. https://doi.org/10.2165/00002512-200017040-00005

Rockwood, K., & Mitnitski, A. (2007). Frailty in relation to the accumulation of deficits. *The Journals of Gerontology Series A: Biological Sciences and Medical Sciences*, *62*(7), 722–727. https://doi.org/10.1093/gerona/62.7.722

Rockwood, K., Song, X., MacKnight, C., Bergman, H., Hogan, D. B., McDowell, I., & Mitnitski, A. (2005). A global clinical measure of fitness and frailty in elderly people. *Cmaj*, *173*(5), 489–495. https://doi.org/10.1503/cmaj.050051

Rostoft, S., & Rønning, B. (2017). Functional Dependency. In B. Korc-Grodzicki & W. P. Tew (Eds.), *Handbook of Geriatric Oncology: Practical Guide to Caring for the Older Cancer Patient* (1st ed.). Demos Medical Publishing. https://doi.org/10.1891/9781617052828.0005

Rougier, N., Bourc'his, D., Gomes, D. M., Niveleau, A., Plachot, M., Pàldi, A., & Viegas-Péquignot, E. (1998). Chromosome methylation patterns during mammalian preimplantation development. *Genes & Development*, *12*(14), 2108–2113. https://doi.org/10.1101/gad.12.14.2108

Rubenstein, L. Z., Harker, J. O., Salvà, A., Guigoz, Y., & Vellas, B. (2001). Screening for undernutrition in geriatric practice: developing the short-form mini-nutritional assessment (MNA-SF). *The Journals of Gerontology Series A: Biological Sciences and Medical Sciences*, *56*(6), M366–M372. https://doi.org/10.1093/gerona/56.6.m366

Rubenstein, L. Z., Josephson, K. R., Wieland, G. D., English, P. A., Sayre, J. A., & Kane, R. L. (1984). Effectiveness of a geriatric evaluation unit. A randomized clinical trial. *The New England Journal of Medicine*, *311*(26), 1664–1670. https://doi.org/10.1056/NEJM198412273112604

Rubiano, E. G. O., Baldoncini, M., Cómbita, A. L., Payán-Gómez, C., Gómez-Amarillo, D. F., Hakim, F., Figueredo, L. F., Forlizzi, V., Rangel, C. C., & Luzzi, S. (2023). Understanding the molecular profiling of diffuse gliomas classification: A brief overview. *Surgical Neurology International*, *14*, 225. https://doi.org/10.25259/SNI_209_2023

Rufer, N., Brümmendorf, T. H., Kolvraa, S., Bischoff, C., Christensen, K., Wadsworth, L., Schulzer, M., & Lansdorp, P. M. (1999). Telomere fluorescence measurements in granulocytes and T lymphocyte subsets point to a high turnover of hematopoietic stem cells and memory T cells in early childhood. *Journal of Experimental Medicine*, *190*(2), 157–168. https://doi.org/10.1084/jem.190.2.157

Saadeh, F. S., Mahfouz, R., & Assi, H. I. (2018). EGFR as a clinical marker in glioblastomas and other gliomas. *The International Journal of Biological Markers*, *33*(1), 22–32. https://doi.org/10.5301/ijbm.5000301

Salas, L. A., Zhang, Z., Koestler, D. C., Butler, R. A., Hansen, H. M., Molinaro, A. M., Wiencke, J. K., Kelsey, K. T., & Christensen, B. C. (2022). Enhanced cell deconvolution of peripheral blood using DNA methylation for high-resolution immune profiling. *Nature Communications*, *13*(1), 761. https://doi.org/10.1038/s41467-021-27864-7

Sanchez, S. E., Gu, Y., Wang, Y., Golla, A., Martin, A., Shomali, W., Hockemeyer, D., Savage, S. A., & Artandi, S. E. (2024). Digital telomere measurement by long-read sequencing distinguishes healthy aging from disease. *Nature Communications*, *15*(1), 5148. https://doi.org/10.1038/s41467-024-49007-4

Sandrucci, S., Beets, G., Braga, M., Dejong, K., & Demartines, N. (2018). Perioperative nutrition and enhanced recovery after surgery in gastrointestinal cancer patients. A position paper by the ESSO task force in collaboration with the ERAS society (ERAS coalition). *European Journal of Surgical Oncology*, *44*(4), 509–514. https://doi.org/10.1016/j.ejso.2017.12.010

Schübeler, D. (2015). Function and information content of DNA methylation. *Nature*, *517*(7534), 321–326. https://doi.org/10.1038/nature14192

Schuurmans, H., Steverink, N., Lindenberg, S., Frieswijk, N., & Slaets, J. P. J. (2004). Old or frail: what tells us more? *The Journals of Gerontology. Series A, Biological Sciences and Medical Sciences*, *59*(9), M962-5. https://doi.org/10.1093/gerona/59.9.m962

Shafiee Hanjani, L., Fox, S., Hubbard, R. E., Gordon, E., Reid, N., Hilmer, S. N., Saunders, R., Gnjidic, D., & Young, A. (2024). Frailty knowledge, training and barriers to frailty management: a national cross-sectional survey of health professionals in Australia. *Australasian Journal on Ageing*, *43*(2), 271–280. https://doi.org/10.1111/ajag.13232

Shin, Y.-A. (2019). How Does Obesity and Physical Activity Affect Aging?: Focused on Telomere as a Biomarker of Aging. *Journal of Obesity & Metabolic Syndrome*, *28*(2), 92–104. https://doi.org/10.7570/jomes.2019.28.2.92

Sholes, S. L., Karimian, K., Gershman, A., Kelly, T. J., Timp, W., & Greider, C. W. (2022). Chromosome-specific telomere lengths and the minimal functional telomere revealed by nanopore sequencing. *Genome Research*, *32*(4), 616–628. https://doi.org/10.1101/gr.275868.121

Smith, Z. D., Chan, M. M., Humm, K. C., Karnik, R., Mekhoubad, S., Regev, A., Eggan, K., & Meissner, A. (2014). DNA methylation dynamics of the human preimplantation embryo. *Nature*, *511*(7511), 611–615. https://doi.org/10.1038/nature13581

Song, X., Mitnitski, A., & Rockwood, K. (2011). Nontraditional risk factors combine to predict Alzheimer disease and dementia. *Neurology*, *77*(3), 227–234. https://doi.org/10.1212/WNL.0b013e318225c6bc

Soubeyran, P., Bellera, C., Goyard, J., Heitz, D., Curé, H., Rousselot, H., Albrand, G., Servent, V., Jean, O. Saint, & van Praagh, I. (2014). Screening for vulnerability in older cancer patients: the ONCODAGE Prospective Multicenter Cohort Study. *PloS One*, *9*(12), e115060. https://doi.org/10.1371/journal.pone.0115060

Steck, P. A., Pershouse, M. A., Jasser, S. A., Yung, W. K. A., Lin, H., Ligon, A. H., Langford, L. A., Baumgard, M. L., Hattier, T., & Davis, T. (1997). Identification of a candidate tumour suppressor gene, MMAC1, at chromosome 10q23. 3 that is mutated in multiple advanced cancers. *Nature Genetics*, *15*(4), 356–362. https://doi.org/10.1038/ng0497-356

Steenstrup, T., Kark, J. D., Verhulst, S., Thinggaard, M., Hjelmborg, J. V. B., Dalgård, C., Kyvik, K. O., Christiansen, L., Mangino, M., & Spector, T. D. (2017). Telomeres and the natural lifespan limit in humans. *Aging (Albany NY)*, *9*(4), 1130. https://doi.org/10.18632/aging.101216

Stefan, C. P., Hall, A. T., Graham, A. S., & Minogue, T. D. (2022). Comparison of illumina and Oxford nanopore sequencing technologies for pathogen detection from clinical matrices using molecular inversion probes. *The Journal of Molecular Diagnostics*, *24*(4), 395–405. https://doi.org/10.1016/j.jmoldx.2021.12.005

Stephens, Z., Ferrer, A., Boardman, L., Iyer, R. K., & Kocher, J.-P. A. (2022). Telogator: a method for reporting chromosome-specific telomere lengths from long reads. *Bioinformatics*, *38*(7), 1788–1793. https://doi.org/10.1093/bioinformatics/btac005

Steverink, N., Slaets, J. P. J., Schuurmans, H., & van Lis, M. (2001). Measuring frailty: Development and testing of the Groningen Frailty Indicator (GFI). *The Gerontologist*, *41*, 236–237. https://www.researchgate.net/publication/284106943_Measuring_frailty_Developing_and_testing_the_GFI_Groningen_Frailty_Indicator

Sulangi, A. J., Husain, A., Lei, H., & Okun, J. (2024). Neuronavigation in glioma resection: current applications, challenges, and clinical outcomes. *Frontiers in Surgery*, *11*. https://doi.org/10.3389/fsurg.2024.1430567

Tahiliani, M., Koh, K. P., Shen, Y., Pastor, W. A., Bandukwala, H., Brudno, Y., Agarwal, S., Iyer, L. M., Liu, D. R., Aravind, L., & Rao, A. (2009). Conversion of 5-Methylcytosine to 5-Hydroxymethylcytosine in Mammalian DNA by MLL Partner TET1. *Science*, *324*(5929), 930–935. https://doi.org/10.1126/science.1170116

Takahashi, M., Takahashi, M., Komine, K., Yamada, H., Kasahara, Y., Chikamatsu, S., Okita, A., Ito, S., Ouchi, K., Okada, Y., Imai, H., Saijo, K., Shirota, H., Takahashi, S., Mori, T., Shimodaira, H., & Ishioka, C. (2017). The G8 screening tool enhances prognostic value to ECOG performance status in elderly cancer patients: A retrospective, single institutional study. *PLOS ONE*, *12*(6), e0179694. https://doi.org/10.1371/journal.pone.0179694

Tang, J., Wu, S., Liu, H., Stratt, R., Barak, O. G., Shiekhattar, R., Picketts, D. J., & Yang, X. (2004). A Novel Transcription Regulatory Complex Containing Death Domain-associated Protein and the ATR-X Syndrome Protein. *Journal of Biological Chemistry*, *279*(19), 20369–20377. https://doi.org/10.1074/jbc.M401321200

Tate, P. H., & Bird, A. P. (1993). Effects of DNA methylation on DNA-binding proteins and gene expression. *Current Opinion in Genetics & Development*, *3*(2), 226–231. https://doi.org/10.1016/0959-437X(93)90027-M

Taylor, J. K., Fox, J., Shah, P., Ali, A., Hanley, M., & Hyatt, R. (2017). Barriers to the identification of frailty in hospital: a survey of UK clinicians. *Future Healthcare Journal*, *4*(3), 207–212. https://doi.org/10.7861/futurehosp.4-3-207

Tejera, A. M., Stagno d'Alcontres, M., Thanasoula, M., Marion, R. M., Martinez, P., Liao, C., Flores, J. M., Tarsounas, M., & Blasco, M. A. (2010). TPP1 Is Required for TERT Recruitment, Telomere Elongation during Nuclear Reprogramming, and Normal Skin Development in Mice. *Developmental Cell*, *18*(5), 775–789. https://doi.org/10.1016/j.devcel.2010.03.011

Teo, H., Ghosh, S., Luesch, H., Ghosh, A., Wong, E. T., Malik, N., Orth, A., de Jesus, P., Perry, A. S., Oliver, J. D., Tran, N. L., Speiser, L. J., Wong, M., Saez, E., Schultz, P., Chanda, S. K., Verma, I. M., & Tergaonkar, V. (2010). Telomere-independent Rap1 is an IKK adaptor and regulates NF-κB-dependent gene expression. *Nature Cell Biology*, *12*(8), 758–767. https://doi.org/10.1038/ncb2080

Teschendorff, A. E., Marabita, F., Lechner, M., Bartlett, T., Tegner, J., Gomez-Cabrero, D., & Beck, S. (2013). A beta-mixture quantile normalization method for correcting probe design bias in Illumina Infinium 450 k DNA methylation data. *Bioinformatics*, *29*(2), 189–196. https://doi.org/10.1093/bioinformatics/bts680

Teschendorff, A. E., Menon, U., Gentry-Maharaj, A., Ramus, S. J., Weisenberger, D. J., Shen, H., Campan, M., Noushmehr, H., Bell, C. G., & Maxwell, A. P. (2010). Age-dependent DNA methylation of genes that are suppressed in stem cells is a hallmark of cancer. *Genome Research*, *20*(4), 440–446. https://doi.org/10.1101/gr.103606.109

Tham, C.-Y., Poon, L., Yan, T., Koh, J. Y. P., Ramlee, M. K., Teoh, V. S. I., Zhang, S., Cai, Y., Hong, Z., & Lee, G. S. (2023). High-throughput telomere length measurement at nucleotide resolution using the PacBio high fidelity sequencing platform. *Nature Communications*, *14*(1), 281. https://doi.org/10.1038/s41467-023-35823-7

Theeler, B. J., Ellezam, B., Sadighi, Z. S., Mehta, V., Tran, M. D., Adesina, A. M., Bruner, J. M., & Puduvalli, V. K. (2014). Adult pilocytic astrocytomas: clinical features and molecular analysis. *Neuro-Oncology*, *16*(6), 841–847. https://doi.org/10.1093/neuonc/not246

Theodorakis, N., Nikolaou, M., Hitas, C., Anagnostou, D., Kreouzi, M., Kalantzi, S., Spyridaki, A., Triantafylli, G., Metheniti, P., & Papaconstantinou, I. (2024). Comprehensive peri-operative risk assessment and management of geriatric patients. *Diagnostics*, *14*(19), 2153. https://doi.org/10.3390/diagnostics14192153

Theou, O., Squires, E., Mallery, K., Lee, J. S., Fay, S., Goldstein, J., Armstrong, J. J., & Rockwood, K. (2018). What do we know about frailty in the acute care setting? A scoping review. *BMC Geriatrics*, *18*, 1–20. https://doi.org/10.1186/s12877-018-0823-2

Tom, M. C., Park, D. Y. J., Yang, K., Leyrer, C. M., Wei, W., Jia, X., Varra, V., Yu, J. S., Chao, S. T., Balagamwala, E. H., Suh, J. H., Vogelbaum, M. A., Barnett, G. H., Prayson, R. A., Stevens, G. H. J., Peereboom, D. M., Ahluwalia, M. S., & Murphy, E. S. (2019). Malignant Transformation of Molecularly Classified Adult Low-Grade Glioma. *International Journal of Radiation Oncology*Biology*Physics*, *105*(5), 1106–1112. https://doi.org/10.1016/j.ijrobp.2019.08.025

Torp, S. H., Solheim, O., & Skjulsvik, A. J. (2022). The WHO 2021 Classification of Central Nervous System tumours: a practical update on what neurosurgeons need to know—a minireview. *Acta Neurochirurgica*, *164*(9), 2453–2464. https://doi.org/10.1007/s00701-022-05301-y

Touleimat, N., & Tost, J. (2012). Complete Pipeline for Infinium ® Human Methylation 450K BeadChip Data Processing Using Subset Quantile Normalization for Accurate DNA Methylation Estimation. *Epigenomics*, *4*(3), 325–341. https://doi.org/10.2217/epi.12.21

Uno, M., Oba-Shinjo, S. M., Camargo, A. A., Moura, R. P., de Aguiar, P. H., Cabrera, H. N., Begnami, M., Rosemberg, S., Teixeira, M. J., & Marie, S. K. N. (2011). Correlation of MGMT promoter methylation status with gene and protein expression levels in glioblastoma. *Clinics*, *66*(10), 1747–1755. https://doi.org/10.1590/S1807-59322011001000013

Vaiserman, A., & Krasnienkov, D. (2021). Telomere length as a marker of biological age: state-of-the-art, open issues, and future perspectives. *Frontiers in Genetics*, *11*, 630186. https://doi.org/10.3389/fgene.2020.630186

Van Damme, J., Neiterman, E., Oremus, M., Lemmon, K., & Stolee, P. (2020). Perspectives of older adults, caregivers, and healthcare providers on frailty screening: a qualitative study. *BMC Geriatrics*, *20*, 1–12. https://doi.org/10.1186/s12877-020-1459-6

Van Rompaey, B., Elseviers, M. M., Schuurmans, M. J., Shortridge-Baggett, L. M., Truijen, S., & Bossaert, L. (2009). Risk factors for delirium in intensive care patients: a prospective cohort study. *Critical Care*, *13*, 1–12. https://doi.org/10.1186/cc7892

Veganzones, S., de la Orden, V., Requejo, L., Mediero, B., González, M. L., del Prado, N., Rodríguez García, C., Gutiérrez-González, R., Pérez-Zamarrón, A., Martínez, A., Maestro, M. L., Zimman, H. M., González-Neira, A., Vaquero, J., & Rodríguez-Boto, G. (2017). Genetic alterations of IDH1 and Vegf in brain tumors. *Brain and Behavior*, *7*(9). https://doi.org/10.1002/brb3.718

Vellas, B., Guigoz, Y., Garry, P. J., Nourhashemi, F., Bennahum, D., Lauque, S., & Albarede, J.-L. (1999). The mini nutritional assessment (MNA) and its use in grading the nutritional state of elderly patients. *Nutrition*, *15*(2), 116–122. https://doi.org/10.1016/S0899-9007(98)00171-3

Vellas, B., Villars, H., Abellan, G., Soto, M. E., Rolland, Y., Guigoz, Y., Morley, J. E., Chumlea, W., Salva, A., & Rubenstein, L. Z. (2006). Overview of the MNA®-Its history and challenges. *Journal of Nutrition Health and Aging*, *10*(6), 456.

Venkatesh, S., & Workman, J. L. (2015). Histone exchange, chromatin structure and the regulation of transcription. *Nature Reviews Molecular Cell Biology*, *16*(3), 178–189. https://doi.org/10.1038/nrm3941

Vieira, R. A., Nunes, D. P., Lima, D. B., Rocha, G. da S., Corona, L. P., Santos-Orlandi, A. A. dos, Sampaio, E. de S., Rodrigues, P. C. de O. G., & de Brito, T. R. P. (2024). Association between telomere length and anorexia of ageing: a cross-sectional study conducted with community-dwelling older people. *Journal of Human Nutrition and Dietetics*, *37*(5), 1209–1218. https://doi.org/10.1111/jhn.13338

von Zglinicki, T., Pilger, R., & Sitte, N. (2000). Accumulation of single-strand breaks is the major cause of telomere shortening in human fibroblasts. *Free Radical Biology and Medicine*, *28*(1), 64–74. https://doi.org/10.1016/S0891-5849(99)00207-5

Waitkus, M. S., Diplas, B. H., & Yan, H. (2016). Isocitrate dehydrogenase mutations in gliomas. *Neuro-Oncology*, *18*(1), 16–26. https://doi.org/10.1093/neuonc/nov136

Wallace, M., & Shelkey, M. (2007). Katz index of independence in activities of daily living (ADL). *Urol Nurs*, *27*(1), 93–94.

Wang, Y., Grant, O. A., Zhai, X., Mcdonald-Maier, K. D., & Schalkwyk, L. C. (2023). Insights into ageing rates comparison across tissues from recalibrating cerebellum DNA methylation clock. *GeroScience*, *46*(1), 39–56. https://doi.org/10.1007/s11357-023-00871-w

Wang, Y., Zhao, Y., Bollas, A., Wang, Y., & Au, K. F. (2021). Nanopore sequencing technology, bioinformatics and applications. *Nature Biotechnology*, *39*(11), 1348–1365. https://doi.org/10.1038/s41587-021-01108-x

Ward, P. S., Patel, J., Wise, D. R., Abdel-Wahab, O., Bennett, B. D., Coller, H. A., Cross, J. R., Fantin, V. R., Hedvat, C. V., Perl, A. E., Rabinowitz, J. D., Carroll, M., Su, S. M., Sharp, K. A., Levine, R. L., & Thompson, C. B. (2010). The Common Feature of Leukemia-Associated IDH1 and IDH2 Mutations Is a Neomorphic Enzyme Activity Converting α-Ketoglutarate to 2-Hydroxyglutarate. *Cancer Cell*, *17*(3), 225–234. https://doi.org/10.1016/j.ccr.2010.01.020

Watson, J. D. (1972). Origin of concatemeric T7DNA. *Nature New Biology*, *239*(94), 197–201. https://doi.org/10.1038/newbio239197a0

Watt, F., & Molloy, P. L. (1988). Cytosine methylation prevents binding to DNA of a HeLa cell transcription factor required for optimal expression of the adenovirus major late promoter. *Genes & Development*, *2*(9), 1136–1143. https://doi.org/10.1101/gad.2.9.1136

Weidner, C. I., & Wagner, W. (2014). The epigenetic tracks of aging. *Biological Chemistry*, *395*(11), 1307–1314. https://doi.org/10.1515/hsz-2014-0180

Weller, M., Knobbe-Thomsen, C. B., Le Rhun, E., & Reifenberger, G. (2022). Die WHO-Klassifikation der Tumoren des zentralen Nervensystems 2021. *Der Onkologe*, *28*(2), 155–163. https://doi.org/10.1007/s00761-021-01083-7

Werner, C., Fürster, T., Widmann, T., Pöss, J., Roggia, C., Hanhoun, M., Scharhag, J., Büchner, N., Meyer, T., & Kindermann, W. (2009). Physical exercise prevents cellular senescence in circulating leukocytes and in the vessel wall. *Circulation*, *120*(24), 2438–2447. https://doi.org/10.1161/CIRCULATIONAHA.109.861005

West, M. D., Pereira-Smith, O. M., & Smith, J. R. (1989). Replicative senescence of human skin fibroblasts correlates with a loss of regulation and overexpression of collagenase activity. *Experimental Cell Research*, *184*(1), 138–147. https://doi.org/10.1016/0014-4827(89)90372-8

Wiestler, B., Capper, D., Holland-Letz, T., Korshunov, A., Von Deimling, A., Pfister, S. M., Platten, M., Weller, M., & Wick, W. (2013). ATRX loss refines the classification of anaplastic gliomas and identifies a subgroup of IDH mutant astrocytic tumors with better prognosis. *Acta Neuropathologica*, *126*, 443–451. https://doi.org/10.1007/s00401-013-1156-z

Wildiers, H., Heeren, P., Puts, M., Topinkova, E., Janssen-Heijnen, M. L. G., Extermann, M., Falandry, C., Artz, A., Brain, E., & Colloca, G. (2014). International Society of Geriatric Oncology consensus on geriatric assessment in older patients with cancer. *Journal of Clinical Oncology*, *32*(24), 2595–2603. https://doi.org/10.1200/JCO.2013.54.8347

Wilson, S. J., Woody, A., Padin, A. C., Lin, J., Malarkey, W. B., & Kiecolt-Glaser, J. K. (2019). Loneliness and Telomere Length: Immune and Parasympathetic Function in Associations With Accelerated Aging. *Annals of Behavioral Medicine*, *53*(6), 541–550. https://doi.org/10.1093/abm/kay064

Wong, L. H., McGhie, J. D., Sim, M., Anderson, M. A., Ahn, S., Hannan, R. D., George, A. J., Morgan, K. A., Mann, J. R., & Choo, K. H. A. (2010). ATRX interacts with H3.3 in maintaining telomere structural integrity in pluripotent embryonic stem cells. *Genome Research*, *20*(3), 351–360. https://doi.org/10.1101/gr.101477.109

World Health Organization. (2016). *ICD-10 Version:2016 – F05 Delirium, not induced by alcohol and other psychoactive substances*. https://icd.who.int/browse10/2016/en#/F05

Wu, R. A., Upton, H. E., Vogan, J. M., & Collins, K. (2017). Telomerase mechanism of telomere synthesis. *Annual Review of Biochemistry*, *86*(1), 439–460. https://doi.org/10.1146/annurev-biochem-061516-045019

Xu, W., Yang, H., Liu, Y., Yang, Y., Wang, P., Kim, S.-H., Ito, S., Yang, C., Wang, P., Xiao, M.-T., Liu, L., Jiang, W., Liu, J., Zhang, J., Wang, B., Frye, S., Zhang, Y., Xu, Y., Lei, Q., … Xiong, Y. (2011). Oncometabolite 2-Hydroxyglutarate Is a Competitive Inhibitor of α-Ketoglutarate-Dependent Dioxygenases. *Cancer Cell*, *19*(1), 17–30. https://doi.org/10.1016/j.ccr.2010.12.014

Yalaza, C., Ak, H., Cagli, M. S., Ozgiray, E., Atay, S., & Aydin, H. H. (2017). R132H Mutation in IDH1 Gene is Associated with Increased Tumor HIF1-Alpha and Serum VEGF Levels in Primary Glioblastoma Multiforme. *Annals of Clinical and Laboratory Science*, *47*(3), 362–364.

Yesavage, J. A., & Sheikh, J. I. (1986). 9/Geriatric depression scale (GDS) recent evidence and development of a shorter version. *Clinical Gerontologist*, *5*(1–2), 165–173. https://doi.org/10.1300/j018v05n01_09

Yu, H. J., Byun, Y. H., & Park, C.-K. (2024). Techniques for assessing telomere length: A methodological review. *Computational and Structural Biotechnology Journal*. https://doi.org/10.1016/j.csbj.2024.04.011

Zaug, A. J., Podell, E. R., Nandakumar, J., & Cech, T. R. (2010). Functional interaction between telomere protein TPP1 and telomerase. *Genes & Development*, *24*(6), 613–622. https://doi.org/10.1101/gad.1881810

Zenin, A., Tsepilov, Y., Sharapov, S., Getmantsev, E., Menshikov, L. I., Fedichev, P. O., & Aulchenko, Y. (2019). Identification of 12 genetic loci associated with human healthspan. *Communications Biology*, *2*(1), 1–11. https://doi.org/10.1038/s42003-019-0290-0

Zhu, H., Belcher, M., & Van Der Harst, P. (2011). Healthy aging and disease: role for telomere biology? *Clinical Science (London, England: 1979)*, *120*(Pt 10), 427. https://doi.org/10.1042/CS20100385

7 Acknowledgements

I would like to express my sincere gratitude to my primary supervisor for guidance and constructive feedback, and to my co-supervisors at the University Medical Center Mainz for their valuable insights and support. I also thank the Department of Neuropathology in Mainz for providing an excellent research environment, as well as my colleagues from all the laboratories for their collaboration. I further acknowledge the International PhD Program for its support and for fostering an inspiring scientific community.

I wish to express my heartfelt gratitude to my family, especially my parents.
I thank my father, Dr.-Ing. Yasser Abuhashem. I watched your doctoral journey unfold, walking with you as a child to the TU Staatsbibliothek after kindergarten and quietly observing you as you worked on your dissertation. Two decades later, returning to your work has revealed its deeper meaning and the lasting influence it has had on my own path. This has felt particularly relevant over the past two years, when the need to rebuild and look ahead at home has been more present than ever.

I am equally grateful to my mother, Dipl.-Ing. Mervat Abuhashem, for your patience, wise counsel, and steady support, as well as for embodying the perseverance and curiosity that have inspired my academic and personal pursuits.

I wish to thank my uncle, Dr. Mysara Abu-Hashem. I have always admired your wisdom, and I am grateful for the lessons you have shared with me beyond the lecture hall.

To my friends, thank you for your unwavering presence and the laughter we have shared over these past years. You gave me a sense of home far from my own, and I believe that as we grew older, we also grew up together along the way. I feel fortunate to have shared this journey not only with you, but also with the people who shaped me long before my PhD began.

8 Curriculum Vitae